FTD-TT- 63-755

2 of 3

199-P-$3.00

STRUCTURAL DAMPING IN PERMANENT JOINTS

By

N. G. Kalinin, Yu. A. Lebedev, et al.

FOREIGN TECHNOLOGY DIVISION

AIR FORCE SYSTEMS COMMAND

WRIGHT-PATTERSON AIR FORCE BASE

OHIO

UNEDITED ROUGH DRAFT TRANSLATION

STRUCTURAL DAMPING IN PERMANENT JOINTS

BY: N. G. Kalinin, Yu. A. Lebedev, et al.

English Pages: 191

PREPARED BY:

TRANSLATION DIVISION
FOREIGN TECHNOLOGY DIVISION
WP-AFB, OHIO.

Akademiya Nauk Latviyskoy SSR
Institut Avtomatiki i Mekhaniki

KONSTRUKTSIONNOYE DEMPFIROVANIYE V NEPODVIZHNYKH SOYEDINENIYAKH

Izdatel'stvo Akademii Nauk Latviyskoy SSR
Riga - 1960

pages 3 - 169

TABLE OF CONTENTS

FOREWORD

The great effect of the damping properties of a mechanical system on its behavior on vibrations is well known; these properties acquire particular significance in resonance conditions, when the amplitudes of oscillations become limited as a result of precisely this damping. Factors causing damping of vibrations of any system are: influence of the medium in which the vibrations are performed (aero- and hydrodynamic damping), internal friction in the material and, finally, friction in supports and couplings.

In those cases when the above types of damping do not sufficiently limit of amplitude of vibrations, special devices, called vibration dampers (or dampers), are introduced into the system; for appropriate parameters these dampers become the most effective medium for vibration damping. However, the introduction of special dampers can in no way be regarded as an universal method, if we keep in mind the large variety of possible mechanical systems; various structural or service considerations frequently prevent the installation of vibration dampers.

Therefore, in the overwhelming majority of actual structures damping is created by the action of the medium, friction in the material and friction in the supports and couplings. The first two of these factors were most thoroughly investigated. The investigation of the action of the medium on a vibrating elastic system belongs to the field of hydro- and aerodynamics; great successes achieved in this field, in particular in conjunction with important prob-

lems of aircraft wing and tail structure instability (flutter), are known. Internal friction in the material has for a long period of time been subject to continuous attention by physicists; although the mechanism of internal friction has not as yet been sufficiently investigated, extensive experimental material has been collected and a volumn of reliable information on qualitative and quantitative characteristics of various materials has been obtained as of today. We should, however, confess that the effect of this factor on the damping properties of the majority of actual structures was often overestimated.

It has at present become entirely clear that in the overwhelming majority of cases the most important role is played by friction losses in couplings of mechanical systems. Two classes of cases should be here distinctly distinguished: 1) friction in moving couplings (of the type of bearings, guides, etc.); 2) friction in permanent joints (press-fit, riveted, slotted, threaded and the like). While the problem of friction in moving joints has been studied for a long time and is rather extensively illuminated in the literature, friction in permanent joints was subjected to investigation quite recently, although it is of foremost significance in damping of dynamic processes in machinery, ship and aircraft structures and many other mechanical systems. The last type of damping is further called structural damping; we shall utilize this, possibly insufficiently exact, term for the want of a better one.

Not much time has passed from the publication of the first papers specially devoted to the problem of structural damping; however significant theoretical and experimental material, pertaining to the most varied types of joints has been collected at present. The present work represents an attempt to generalize all the results ob-

tained in this field, here the basic content of the book pertains to the theory of structural damping; problems of experimental character are illuminated only to the extent necessary for reinforcement of theoretical calculations. Alongside with a detailed presentation of materials obtained by the authors in the applied mechanics laboratory of the Automation and Mechanics Institute of the Latvian SSR Academy of Sciences works of other investigators are also illuminated.

§§ 6 and 7 were written by N.G. Kalinin, §§ 12, and 14-16 - by Yu.A. Lebedev, §§ 8 and 9 - by V.I. Lebedeva, the introduction, §§ 1, 13, 18 and the conclusion - by Ya.G. Panovko, §§ 2 and 3 - by G.I. Strakhov. Section 17 was written by N.G. Kalinin and Yu.A. Lebedev, §§ 4, 5, 10, 11, 19, 20 and 21 - by Ya.G. Panovko and G.I. Strakhov.

INTRODUCTION

As has been pointed out in the preface, a distinction should be made between the cases of friction in moving joints and cases of friction in permanent joints. The point of the matter is that in solving problems of the first type it is natural to ignore the fact that the elements making up the kinematic pair are deformable, and to consider them to be entirely rigid; in the solution of problems of the second type it is impossible to ignore deformations and it becomes necessary to simultaneously consider both the friction forces along contact areas and the deformation of the joined elements. It is understood that the term "permanent joint" should be taken conventionally, since we will everywhere assume a certain mobility, caused by small deformations and relative slip of the joint elements. The energy dissipation phenomenon in permanent joints on their cyclical loading will subsequently be called structural damping.

The importance of structural damping for dynamic processes in mechanical systems has been known for some time, but it is only recently that reliable experimental data conclusively confirming the paramount significance of structural damping in the most different structures have been obtained. This pertains mainly to mechanical systems in operation of which it is impossible to entirely eliminate resonance modes (ship and aircraft structures, turbine buckets and the like). The distinguishing feature of structural damping is the known possibility of "controlling" the frictional losses in couplings; thus, a change in the forces exerted by mutual compression

between elements making up a structure can in some cases increase energy dissipation and in others - decrease it. By virtue of the same fact the designer finds himself in a situation (at least within certain limits) where he can control the damping in the system.

In published experimental works relatively much attention was paid to experimental investigations of energy dissipation on cyclical deformation of riveted joints (mainly in conjunction with the operation of metal structures in engineering installations). In particular, the substantial influence of the degree of compression of structural elements on energy dissipation attendant to cyclical loadings has been established long ago; this influence follows directly from the dependence of dry friction developed in the joint on the normal pressure. More than thirty years ago I.M. Rabinovich [19] has proposed to estimate the state of riveted bridge joints by an experimentally determined absorption coefficient.* G.A. Shapiro's book [31], in which the methodology of determination of frictional forces is developed and the description of experimental equipment and special apparatus is given, is specially devoted to the damping properties of riveted joints.

The importance of damping created in riveted joints can also be inferred from the results of tests on hulls of river and sea vessels (Taylor [39], N.N. Babayev [1] and Kumai [34]); it has been established that riveted hulls of sea and river vessels have a considerably larger abscrption coefficient in comparison with welded hulls of the same type.

A similar phenomenon is observed in housings of gas turbines, where the utilization of riveted instead of welded joints makes it possible to significantly lower the amplitudes of vibrations. It has been established in the Reference by A.M. Soyfer and V.P. Filekin [24]

that successful damping of vibrations in gas turbine housings can be achieved by utilizing special damping welded seams. The latter differ from ordinary welded seams by the fact that some relative slip of welded components, within limits allowed by the seam strength, is possible. Comparative tests of damping seams of different designs have shown that the largest absorption coefficient is provided by seams executed by means of spot welding.

A.M Soyfer's articles [21, 22] are devoted to a systematic experimental study of structural damping in gas turbine components. It is proven in these articles that structural means are solely effective for damping of inevitably arising vibrations. The author suggests a number of design schemes; thus, application of a special wire braiding on the gas turbine pipelines has made it possible to considerably decrease the amplitude of resonance vibrations. Even more substantial results were obtained with special wire dampers.

An important question about vibration damping in banks of turbine buckets was investigated by A.D. Kovalenko [9] and a number of other authors. A.M. Soyfer in Reference [23] suggests the utilization of a special design of the working part of the bucket with a core as a damper of vibrations of a turbine or gas turbine pump bucket. A metal core is fitted with positive or negative allowance inside the hollow bucket; relative displacements of the core and the bucket occur on segments of contact on cyclical deformations of the bucket, with the result that a part of the energy is lost in overcoming the frictional force. Di Taranto, in Reference [32], has investigated the effectiveness of steel wire clusters introduced into the bucket. The energy dissipation in this case occurs not only due to friction at the surface of contact of the bucket with the core, but also at the expense of friction between individual wires within

the cluster proper.

D.N. Reshetov and Z.M. Levin [20] have, on the basis of a large number of experiments, determined the energy dissipation characteristics in flat, cylindrical and tapered machine-tool component joints and have discovered optimal dimensions of these joints from the point of view of largest energy dissipation. On the basis of analysis of experimental results the authors have established operating conditions under which the greatest energy dissipation is obtained and they have also performed a comparative estimate of the effectiveness of the different types of dampers. In particular, structural hysteresis dampers were investigated; it was also established that stacked dished dampers as well as stacked dampers with rippled spacers are the best. The dished disks are deformed when the stacks are compressed, slip takes place on the tapered contact surfaces and irreversible friction work is performed. Stacked dampers [made from] rippled plates operate similarly. The elastic properties of a rippled plate are directionally anisotropic: the plate's rigidity in the direction of the ripples is considerably greater than the rigidity in the transverse direction. The compression of a rippled spacer between rigid plates is accompanied by an expansion of the plate in a direction perpendicular to the ripples. This expansion results in the displacement of the ripples relative to the rigid plates which, in turn, results in the appearance of the work of frictional forces. According to the authors' data, the energy absorption coefficient reaches the value of 1.4 - 1.6.

V.L. Biderman, Reference [2] and I.G. Parkhilovskiy, Reference [16], have experimentally investigated energy dissipation in stacked systems of the leaf-spring type.

Energy dissipation in [railroad] car suspensions is considered

in I.V. Krasavin's dissertation [10]. It is shown in Reference [27] that the intensity of the dissipated energy in a bank of elastic cantilevered beams with mutual contact at the end sections only, depends substantially on the normal pressure at the contact surface. Only by changing the compressing force of the leaves does it become possible to obtain a several-fold lowering of the maximal magnitude of vibrational stresses. Experimental results were obtained in the work for a schematized twin-leaf spring. The work by Meyer [35] is devoted to a closely related topic.

The effect of frictional forces in collet joints was experimentally investigated by E.L. Poznyak [17] in conjunction with the phenomena of shaft rotation instability in the supercritical region. As we know, forces of internal friction in the material or couplings of the rotor can be the cause of "swingout" of vibrations; the frictional forces in these cases exert an influence opposite to that of damping and are of substantial significance, although in a different sense than for permanent joints. The effect of structural friction on shaft rotation instability is investigated also by M.I. Chayevskiy, Reference [30a].

Goodman and Klamp [33] and Pian and Hallowell [38] have experimentally investigated energy dissipation in composite beams, consisting of layers pressed tightly together; here the tangential forces of interaction between the layers on bending of the beam are realized only in the form of frictional forces. It has been established that, in structures of this type, energy dissipation resulting from friction along contact surfaces exceeds manyfold the energy dissipation due to internal friction in the material of the beam's components.

Certain new experimental data about energy dissipation in models of riveted beams and in threaded joints are described below in Chap-

ters 5 and 6.

We have touched above on experimental investigations pertaining to the problem of structural damping. Altogether, these investigations conclusively prove the paramount importance of structural damping for systems of the most different types.

Theoretical investigations of problems of structural damping also begin to appear gradually. They pertain to simplified typical schemes and are constructed upon two basic assumptions of a general character: the material of the joint components is assumed to be completely elastic and the frictional properties of contact surfaces are described by the law of dry friction.

The bending of a cantilever reinforced at the top and bottom by thin pressure plates is considered in Reference [38]; the pressure plates are pressed to the beam and take up a part of the cantilever's length, without reaching the fastening surface (Fig. 1a). It is assumed that when the cantilever is loaded by a transverse end force, only frictional forces impede the slip of the pressure plates relative to the beam. The interaction between the pressure plates and the beam is different on two segments of the pressure plate's length. Near the end of the beam the tangential forces between the pressure plates and the beam are determined by the ordinary formula of strength of materials, here the tangential forces are smaller than the limiting value $q_0 = fp$ (f is the friction coefficient and p is the specific pressure on the contact surface); the pressure plates do not slip along the beam. However, it is required for the equilibrium of the pressure plates that the direction of tangential forces in its remaining length be opposite to the direction at the first segment; the pressure plate does slip along the beam at this second segment and the tangential

forces are equal to q_0. The loading of the top pressure plate is shown in Fig. 1b; the bottom pressure plate is loaded in a like manner (the tangential forces acting on it are of opposite directions).

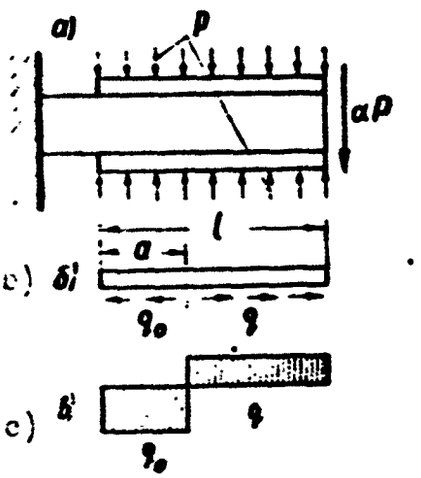

Fig. 1

It should be kept in mind that the slip zone appears for any as small as desired values of the force αP. (Here and subsequently we denote by α a dimensionless load parameter, varying between the limits $-1 \leq \alpha \leq 1$; P is the maximal magnitude of the force.)

Goodman and Klamp [33] have solved the problem of cyclical loading of a cantilevered beam, consisting of two identical layers; the latter pressed to one another by a given pressure (Fig. 2). As long as force αP is small, the tangential forces q, determined by the ordinary strength of materials formula, are smaller than

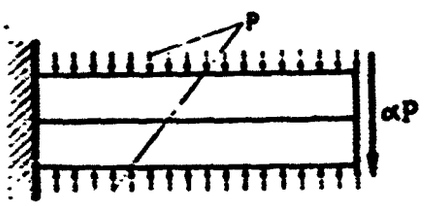

Fig. 2

the limiting value q_0; there is no relative slip between the beam layers and the cantilever bends as a beam with a monolithic cross section. No energy dissipation occurs at this stage.

When, in the process of increasing the force, the tangential forces reach the limiting value q_0, slip will occur between the beam elements and the frictional forces will perform a certain irreversible work. Goodman and Klamp have analyzed an entire symmetrical loading cycle and have found the area of the hysteresis loop. It turned out that this area depends in a peculiar manner on the given pressure p between the beam components; it was established, in particular, that

there exists a certain optimal value of the pressure for which the energy dissipated during a single cycle becomes largest. This fact can be interpreted in the following manner. When pressure p is absent, no frictional forces are developed and there is no energy dissipation. On the other hand, no energy dissipation will exist for sufficiently large values of pressure, since slip between beam layers is [then] absent. A similar problem with a composite beam in the absence of slip at the ends is solved by V.L. Filekin [30].

V.I. Feodosev [29] has solved the problem of redistribution of tangential forces in a press-fit joint, described in Fig. 3a. It is assumed that the shaft is held in the sleeve by frictional forces only and that the contact tension stress creating these frictional forces is constant along the entire length of the contact zone.

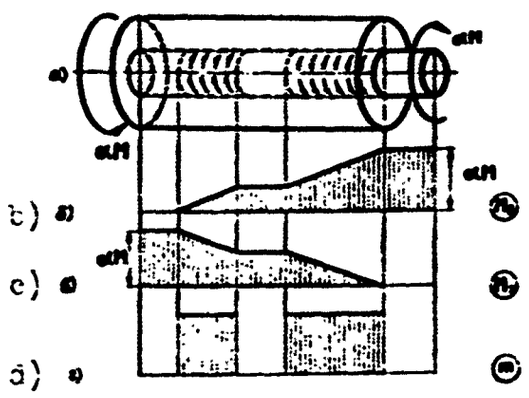

Fig. 3

The greatest value of load αM is considered to be small enough so that the shaft does not rotate at all within the sleeve. Since the sleeve and the shaft are not absolutely rigid, slip at the contact surface will begin for any, as small as desired, values of αM; here the slip zones will adjoin the end of the shaft and the end of the sleeve. The graphs of the torsional moments in the shaft and sleeve sections for the first loading stage are shown in Fig. 3b and c. The substantial peculiarity of structural hysteresis in permanent joints is distinctly seen in this case: a singlevalued determination of frictional forces is impossible without an analysis of the deformation of the mating elements.

Cyclical loading of a press-fit shaft-sleeve joint by longitu-

Fig. 4

dinal forces (Fig. 4), is systematically considered in Article [14].

The diagrams of the distribution of longitudinal forces in the shaft and sleeve sections are in this case similar to the diagrams in Fig. 3b. The Reference investigates the entire cycle, loading - unloading - loading, and determines the energy dissipated during one such cycle. The effect of transverse deformations of a shaft on the dissipated energy is investigated in Reference [25]; these deformations are unavoidable on longitudinal loading of the joint under consideration and in certain cases are of substantial significance.

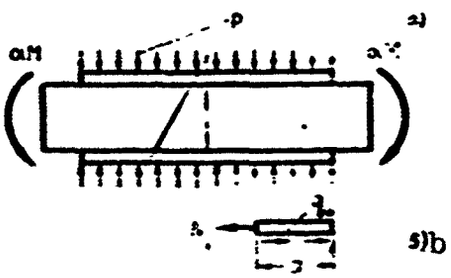

Fig. 5

Structural hysteresis resulting from slip arising between individual wires is also observed in elongation of wire cables. This problem was investigated by S.D. Ponomarev [18] (see also [4]).

The construction of the hysteresis loop for a spring was given by V.L. Biderman [2] and in Reference [27].

The case of bending of a beam with pressure plates pressed to it, described in Fig. 5, is considered in Reference [14]. The beam, at its middle segment, deforms together with the pressure plates and pure bending in the ordinary sense of the phrase is taking place; tangential forces are absent along the mating surfaces of the pressure plates and the beam. The end segments of the pressure plates are loaded in a manner shown in Fig. 5b; furthermore, the tangential forces q_0 are uniformly distributed along the length a of the end segment; they balance the force N devolving upon the middle segment of

the pressure plate. It is understood that the length a increases gradually during the process of increase of the moment αM.

The investigation of the role of frictional forces in a torsion beam, a schematic of which is presented in Fig. 6, is due to N.F. Karpachev [7]. The torsion beam represents a bank of leaves pressed to one another at their ends, which is twisted by two end couples.

The energy dissipation attendant to the compressing of a disk bank is studied in Article [26]. The bank consists of disks made of materials having different mechanical characteristics (a pair of disks is described in Fig. 7). If the friction coefficient is equal to zero and no frictional forces arise on the contact surface between the

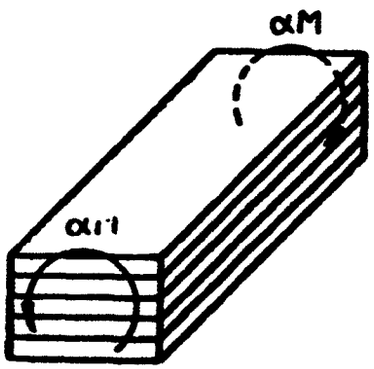

Fig. 6

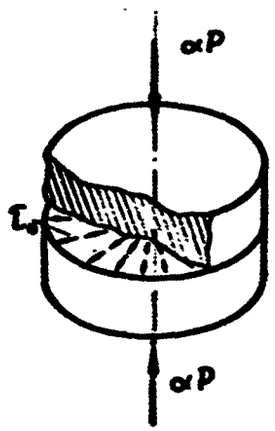

Fig. 7

disks, then the axial deformations of disks with different moduli of elasticity ε_z will also be different and, consequently, the radial deformations ε_r will also be different, even for identical Poisson's ratios. It is, therefore, obvious that if $f \neq 0$, then frictional forces will inevitably arise at the contact surface (these frictional forces are shown in Fig. 7).

The scheme of the frictional clutch, investigated in Reference [13] and represented in Fig. 8, also pertains to this class of problem. Two disks pressed one against another created a coupling, capa-

ble of transmitting, by virtue of friction, a torque not exceeding the limiting value M_{pr}, for which slip between the disks takes place. If the condition $\alpha M < M_{pr}$ is satisfied, then a certain annular slip zone the radius of which is smaller than the outside radius and which increases with the increase in the given torque, is created in the loading process. An annular zone of rigid coupling of the disks is formed on their periphery.

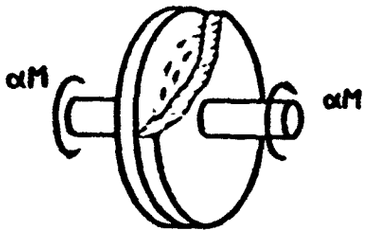

Fig. 8

Structural damping in a thin-walled beam is investigated in Reference [6]. It is assumed that the wall resists shear only and, therefore, the transverse force in each cross section of the beam is resisted by the wall, and the bending moment - by the flanges. The wall is pressed to the rods (flanges and supports) by forces of constant intensity. Only shear deformations of the wall in that zone A (Fig. 9), where the wall is pressed to the rods, are taken into account in the determination of relative slip between the wall and the flanges.

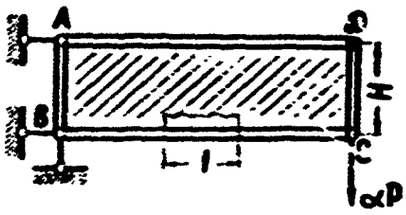

Fig. 9

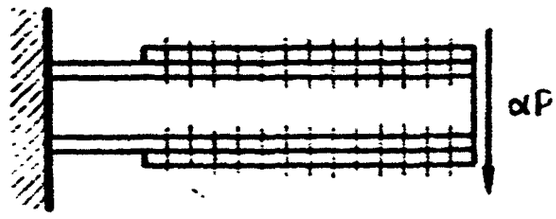

Fig. 10

In all the enumerated cases the tangential forces of interaction between the mating elements are assumed to be realized in the form of frictional forces only. Systems of this type can be called systems in which the interaction between the elements is of purely frictional character.

In addition to these systems, a series of other important schemes

in which the frictional forces of interaction between the elements are accomplished both in the form of friction as well as in the form of an elastic resistance to slip, was considered; riveted joints should primarily be counted among this type of joints. We shall call these systems systems with an elastic-frictional character of interaction between the elements.

Pian, in Reference [36], has investigated structural damping in a beam with pressure plates (Fig. 10). This scheme differs from that shown in Fig. 1 by the fact that the pressure plates are clamped to the beam by rivets, which exert an elastic resistance to the slip of the pressure plates relative to the beam.

Two types of riveted joints, represented in Fig. 11, are systematically investigated in Reference [11]. The first scheme constitutes two elastic strips, joined by a riveted seam by means of two cover plates; the connection transmits a cyclically variable longitudinal

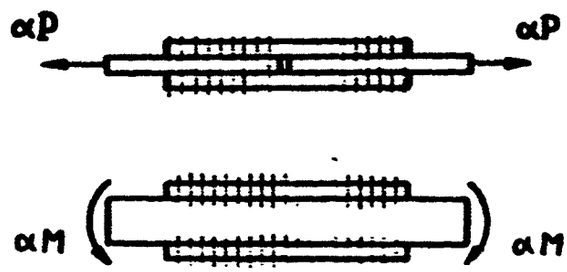

Fig. 11

force. The second scheme is a natural generalization of the scheme given in Fig. 5; a beam with two riveted pressure plates loaded by two end bending couples. As it turned out, a certain optimal value of the clamping force on the two pressure plates, ensuring greatest structural damping, exists also in this case.

The threaded joint, considered in Reference [15], also belongs among these types of systems with elastic-frictional character of

interaction. A certain relative slip of the bolt and nut threads occurs on loading of this connection; the frictional forces which are developed are the cause of the structural hysteresis.

The above gives a certain conception of the variety of the experimental and theoretical material accumulated during the last few years. However, it cannot as yet be assumed that the scope of these investigations corresponds to the great practical importance of the problem of structural damping. A multitude of problems still awaits their theoretical solution, and a series of concrete design schemes - their experimental investigation.

We subsequently present a systematic presentation of solutions pertaining to simplified typical schemes. Here almost all of the attention is paid to the construction of hysteresis loops and to the determination of the energy dissipated in the joint during a single cycle of the system's deformation. Recommendations on the taking into account of energy dissipation in the solution of problems of vibrational theory are given only in the conclusion; despite their simplicity, the recommended methods of calculation ensure sufficiently accurate results.

The law of dry friction is assumed in the entire subsequent presentation for forces of friction over contact surfaces, and the properties of the material are assumed to conform with Hooke's law. Kinematic and static hypotheses, commonly used in the methods of the strength of materials and the applied theory of elasticity are widely used in the solution of concrete problems; this makes it possible to realize substantial simplifications without serious detriment to the accuracy of results. For sake of generality asymmetrical loading cycles with an arbitrary characteristic of the cycle r:

$$r = \frac{P_{min}}{P},$$

where P and P_{min} are the largest and smallest values of the load, are considered in the majority of cases. We shall denote the current value of the external force acting on the joint in the form of αP, where α is a dimensionless load parameter. $\alpha = 1$ for a maximal load and $\alpha = \underline{r}$ for a minimal load.

Manuscript Page No.

[Footnote]

5 Let us keep in mind that by absorption coefficient we mean the ratio of energy dissipated during one cycle to the greatest potential energy of the system.

Manuscript Page No.

[List of Transliterated Symbols]

11 в = v = val = shaft

14 пр = pr = predel'nyy = limiting

Part One

SYSTEMS WITH FRICTIONAL COUPLINGS

Chapter 1

PRESS-FIT JOINTS

§1. AN ELEMENTARY SYSTEM

An example of an elementary system of the type to which the current chapter is devoted is shown in Fig. 12; certain important properties inherent to the entire class of problems considered here can be noticed in this example.

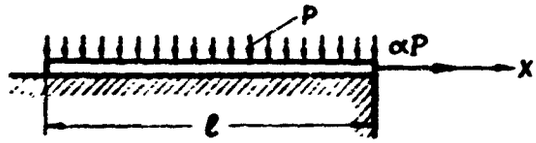

Fig. 12

Let us consider a quite thin elastic strip, pressed to an absolutely hard foundation by a constant pressure p and let us investigate the phenomena occuring as the strip is loaded by a longitudinal force αP, varying cyclically within the limits from P_{min} to P. We will assume that the greatest value of P is insufficient for causing the displacement of the entire strip along the foundation, i.e.,

$$P \leqslant fpbl = q_0 l, \qquad (1.1)$$

where f is the friction coefficient between the strip and the foundation, b and l - the width and the length of the strip and q_0 - the intensity of limiting frictional forces.

In the investigation of the distribution of frictional forces between the strip and the foundation it is important to direct one's attention to the following two peculiarities of the scheme under con-

sideration.

1. The intensity of the frictional forces (per unit of strip length) is equal to the limiting value

$$q_0 = fpb \qquad (1.2)$$

everywhere where slip of the elements of the strip along the foundation exists, i.e., on those segments where deformation of the strip is taking place; this follows directly from the assumed law of dry friction.

2. The frictional forces are entirely absent on those segments where the strip is not deformed. Actually, according to Hooke's law, the strip does not experience any load on these segments (and frictional forces would have represented such a load).

The frictional forces developed on the contact surface thus are equal either to q_0 or to zero. Assuming Hooke's and Coulomb's laws we exclude the possibility that frictional forces different from zero and at the same time smaller than q_0 act anywhere. We shall successively consider three characteristic stages of loading variation.

1. An increase of force αP from zero to the greatest value of P; $0 \leq \alpha \leq 1$ during this stage.

2. A decrease of force αP from the greatest value P, to the smallest value $P_{min} = rP$; $1 \geq \alpha \geq r$ during this stage.

3. An increase of force αP from the smallest value P_{min} to the largest value P; $r \leq \alpha \leq 1$ during this stage.

The two last stages will alternately repeat themselves during repeated cyclical loading.

The first stage. Length a of the deformation zone (slip zone) is determined by the condition of equilibrium of the strip and is equal to (Fig. 13a)

$$a_1 = \frac{\alpha P}{q_0}. \tag{1.3}$$

On gradual increase of load αP, the length of this zone will increase; according to Condition (1.1)

$$a_{1\max} = \frac{P}{q_0} \leqslant l. \tag{1.4}$$

In accordance with Hooke's law, the relative elongation of an element of the deformed zone

$$u_1' = \frac{N}{EF}, \tag{1.5}$$

where u_1 (x, α) is the displacement of an arbitrary section in the direction of the x-axis, N (x, α) is the longitudinal force in the strip cross section, EF is the strip's rigidity on stretching and F is the area of the strip's cross section. It follows from the condition of equilibrium of an element of length dx, that

$$N' = q_0. \tag{1.6}$$

Here and everywhere below, a prime denotes differentiation in respect to the x-coordinate. Substituting here (1.5), we will get

$$u_1'' = \frac{q_0}{EF}. \tag{1.7}$$

The solution of this equation

$$u_1 = A_1 + B_1 x + \frac{q_0 x^2}{2EF}. \tag{1.8}$$

Conditions pertaining to a section situated on the boundary of the deformed and undeformed zones have the form

$$u_1(l - a_1, \alpha) = 0; \quad u_1'(l - a_1, \alpha) = 0. \tag{1.9}$$

They express the absence of displacements and longitudinal force in this section. We will find from (1.9)

$$A_1 = \frac{q_0 (l - a_1)^2}{2EF}; \quad B_1 = -\frac{q_0 (l - a_1)}{EF}. \tag{1.10}$$

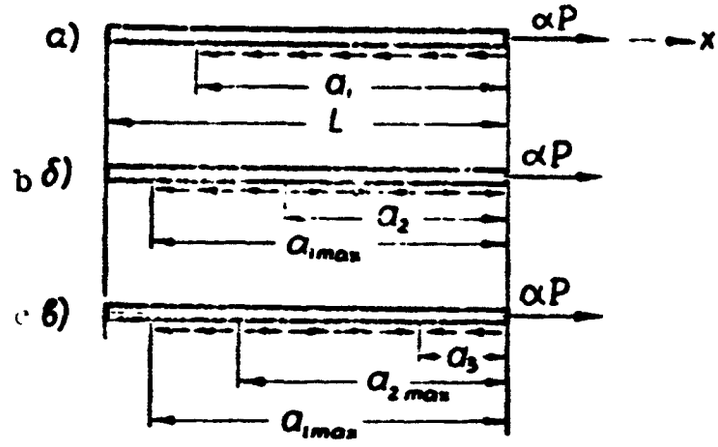

Fig. 13

Substituting this into (1.8), we will get

$$u_1 = \frac{q_0 (l - a_1 - x)^2}{2EF}, \tag{1.11}$$

where a_1 is a function of α and is determined by Expression (1.3). The following dependencies are necessary for further [discussion]:

$$u_1 (x, 1) = \frac{q_0 (l - a_{1\max} - x)^2}{2EF}. \tag{1.12}$$

$$u_1 (l, x) = \frac{x^2 p^2}{2 q_0 EF}. \tag{1.13}$$

Dependence (1.12) describes the distribution of displacements u_1 along the length of the deformed zone at the end of the first loading stage. Dependence (1.13) determines the displacement of the end section of the strip during the entire first stage.

The second stage. As soon as force αP begins decreasing, the end elements of the strip will begin to displace themselves opposite to the direction of the x-axis; frictional forces, acting in the direction of the x-axis will, correspondingly, appear. The condition of equilibrium of the strip (Fig. 13b)

$$\alpha P - q a_2 - q_0 (a_{1\max} - a_2) = 0 \tag{1.14}$$

will make it possible to find the length of the zone of "reverse"

displacements

$$u_2 = \frac{(l - x) P}{2 q_0}, \tag{1.15}$$

here

$$u_{2\max} = \frac{(l - r) P}{2 q_0}. \tag{1.16}$$

The equation of the equilibrium of an element situated anywhere within the limits of this zone has, in contrast with (1.6), the form

$$N' = -q_0. \tag{1.17}$$

Substituting here (1.5), we will arrive at the equation

$$u_2'' = -\frac{q_0}{EF}, \tag{1.18}$$

the solution of which

$$u_2 = A_2 + B_2 x - \frac{q_0 x^2}{2EF} \tag{1.19}$$

should satisfy the conditions

$$\begin{aligned} u_2 (l - a_2, a) &= u_1 (l - a_2, 1), \\ u_2' (l - a_2, a) &= u_1' (l - a_2, 1). \end{aligned} \tag{1.20}$$

These conditions express the equality of displacements and longitudinal forces in section $x = l - a_2$, where the zone of "reverse" displacements borders on the zone of "direct" displacements. Dependence (1.12) should serve as the starting point in the setting up of the right-hand sides of Expressions (1.20). From (1.20) we will get

$$\begin{aligned} A_2 &= \frac{q_0}{EF} [(l - a_{1\max})^2 - 2 (l - a_2)], \\ B_2 &= \frac{q_0}{EF} (l - 2 a_2 + a_{1\max}); \end{aligned} \tag{1.21}$$

consequently,

$$\begin{aligned} u_2 (r, x) = \frac{q_0}{2EF} [&(a_2 - a_{1\max} - r)^2 - \\ &- (l - a_2 - r)^2 - x^2 + 2 (l - a_2) (a_2 - a_{1\max})]. \end{aligned} \tag{1.22}$$

where a_2 is a function of α and is determined by Expression (1.15). Further we need the following dependencies:

$$u_2(r, r) = \frac{1 + 2r - r^2}{4q_0EF}P^2 - \frac{(l - a)r}{EF}P - \frac{q_0(l - a)^2}{2EF}. \tag{1.23}$$

$$u_2(l, \alpha) = \frac{1 + 2\alpha - \alpha^2}{4q_0EF}P^2. \tag{1.24}$$

Dependence (1.23) determines the distribution of displacements u_2 along the length of the zone of "reverse" displacements at the end of the second loading stage and Dependence (1.24) - the rule of displacement of the end section during the entire second stage.

The third stage. At the beginning of the third stage positive displacements will again arise at the ends of the strip over length a_3; the distribution of frictional forces during this stage is shown in Fig. 13c. From the conditions of equilibrium of the strip

$$\alpha P - (a_{1\max} - a_{2\max})q_0 - a_3q_0 + (a_{2\max} - a_3)q_0 = 0 \tag{1.25}$$

we will determine the length

$$a_3 = \frac{\alpha - r}{2q_0}P. \tag{1.26}$$

The differential equation again acquires the form of (1.7); its solution is

$$u_3 = A_3 + B_3x + \frac{q_0x^2}{2EF}. \tag{1.27}$$

Conditions at section $x = l - a_3$

$$\begin{aligned} u_3(l - a_3, \alpha) &= u_2(l - a_3, r), \\ u_3'(l - a_3, \alpha) &= u_2'(l - a_3, r) \end{aligned} \tag{1.28}$$

give

$$\begin{aligned} A_3 &= \frac{(1 + 2r - r^2)P^2}{4q_0EF} + \frac{q_0}{2EF}[(l - 2a_3)^2 - 2a_3^2], \\ B_3 &= \frac{q_0}{EF}\left(\frac{rP}{q} + 2a_3 - l\right). \end{aligned} \tag{1.29}$$

Consequently,

$$u_3(1, \alpha) = \frac{(1 - 2r - r^2) l^2}{4q_0 EF} - \frac{(1 - r) rl^2}{EF} - \frac{q_0 (1 - r)^2}{2EF} + \frac{q_0 (1 - u_3 - r)^2}{EF} \tag{1.30}$$

and the displacement of the end section x = 1 is determined by the dependence

$$u_3(l, \alpha) = \frac{(1 - 2\alpha r - 2r - \alpha^2) l^2}{4q_0 EF}. \tag{1.31}$$

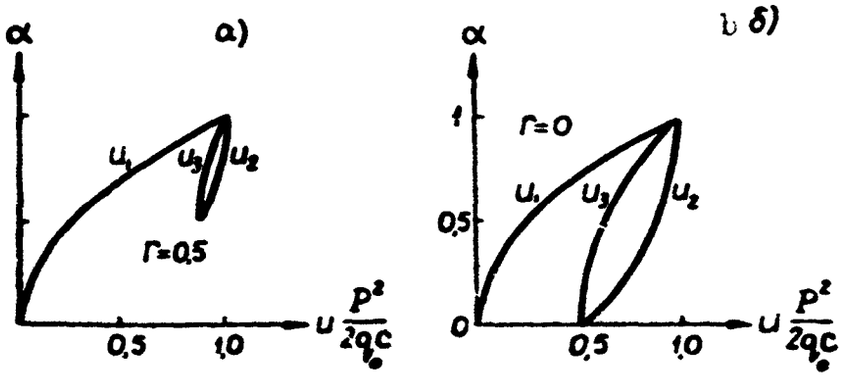

Fig. 14

Dependencies u_1 (1, α), u_2 (1, α) and u_3 (1, α) for cases r = 0.5 and r = 0 are shown in Fig. 14a and b; the closed hysteresis loops can be seen here distinctly. The area of the loop represents an irreversible part of the work, performed by the force αP. We will utilize formula

$$\Psi = \int_{P_{min}}^{P} [u_2(l, \alpha) - u_3(l, \alpha)]\, d(\alpha P) = P \int_{r}^{1} (u_2 - u_3)\, d\alpha. \tag{1.32}$$

for calculation of this work. Substituting here Expressions (1.24) and (1.31), we will find

$$\Psi = \frac{P^3 (1 - r)^3}{12 q_0 EF}. \tag{1.33}$$

The interpretation of this result will become easier if we denote the amplitude of force αP by P_v and we note that $P(1 - r) = 2P_v$. Now Formula (1.33) acquires the form

$$\Psi = \frac{2P_v^3}{3q_0 EF}. \tag{1.34}$$

It follows directly from this that the energy dissipation is independent of the mean value of the force

$$P_m = \frac{P_{min} + P}{2}$$

and is determined by the variable component P_v. The hyperbolic dependence of the dissipated energy on the intensity of pressure p (to which the limiting frictional forces q_0 are proportional) represented in Fig. 15 by a solid line corresponds to Expression (1.34); it is valid only for those sufficiently large values of p which correspond to Condition (1.1). The shorter the zone, the larger should be the corresponding minimal value of p. If the left end of the zone is fastened, the Limitation (1.1) is lifted. An investigation of this last case results in a dependence shown in Fig. 15 by a dashed line. The existence of a maximum of the area of the hysteresis loop, achieved for a certain preset value of pressure p, is noticeable.

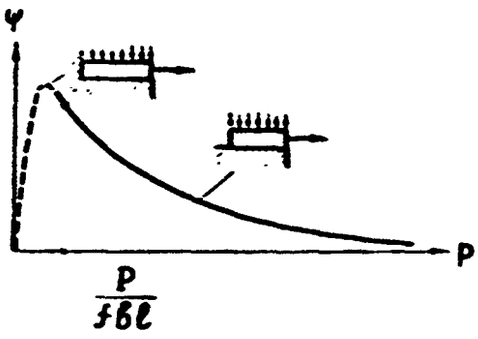

Fig. 15

§2. ENERGY DISSIPATION ON TWISTING A PRESS-FIT JOINT

Having analyzed an elementary system, let us now examine in detail the problem of energy dissipation on twisting of a purely frictional press-fit joint of the shaft-sleeve type (see Fig. 3). We shall consider three types of joints, differing in their structure and in the type of loading (Fig. 16). In the joint of the first type with the shaft cut in half (Fig. 16a), the load is in its entirety transferred to the sleeve by the frictional forces and the value of the torque M is such that the joint becomes uncoupled (the half-shafts revolve in the sleeve). In the second type of joint, with a continuous shaft (Fig. 16b), the loading is transferred to the sleeve only

in the degree permitted by the frictional forces. No torques capable of uncoupling exist for joints of the second type; furthermore, the strength of the joint is determined by the strength of the shaft and is not limited by frictional capabilities. In joints of the third type (Fig. 16c) the torques at the shaft's end sections are unequal. When a large torque M_2 is transferred to the sleeve, the sleeve may revolve on the shaft.

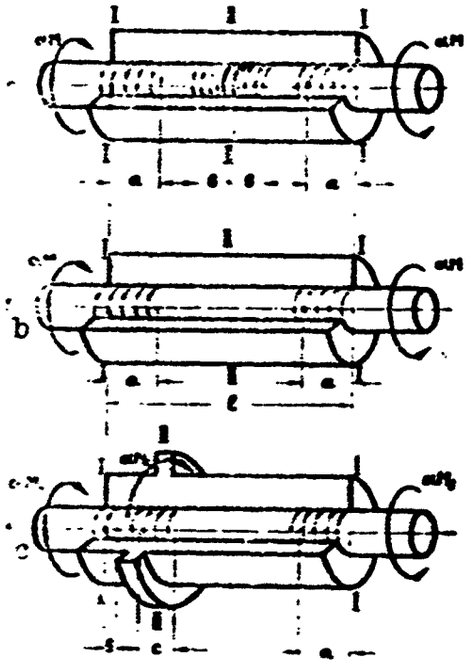

Fig. 16

Local slip of the shaft relative to the sleeve in the extreme regions of the contact surface appears in all the three cases of "permanent" joints for any as small as desired load. Joints of the first type have four local slip zones. Their length depends on the limiting frictional forces (i.e., on the stress and on the friction coefficient), the value of the load and the ratio of rigidities of the elements of the press-fit joint. However the ratio of the dimensions of the regions, a:b, is determined only by the ratio between the rigidities of the shaft GJ and of the sleeve $G_T J_T$ on twisting. If one of the elements of the joint, the shaft or the sleeve, is so rigid that it is practically possible to disregard its compliance, then the system substantially becomes analogous to an elastic strip on an absolutely rigid foundation. In the case of a totally rigid sleeve b = 0, and slip occurs only in the extreme region a; if it is the shaft which is totally rigid, then $b \neq 0$, but a = 0. Slip in two extreme regions appears in the joint of the second type on loading. When the

system is symmetrical in respect to the median cross section the dimensions of these regions will be identical; they depend, as in joints of the first type, on the load, limiting frictional forces and the relationship between the rigidities of the press-fit joint. Due to the absence of symmetry in the loading scheme of joints of the third type, the two extreme slip regions have different dimensions.

Let us start the study of quantitative relationships governing the phenomena of energy dissipation with joints of the first type. Let us assume that the system is fully symmetrical, the contact surface constitutes an annular cylinder, the pressure at all surface points is the same and the friction coefficient is the same over the entire length of the joint. Under these conditions it is sufficient to consider only one half of the shaft (Fig. 17a) and to double the thus obtained result in calculating the area of the hysteresis loop.

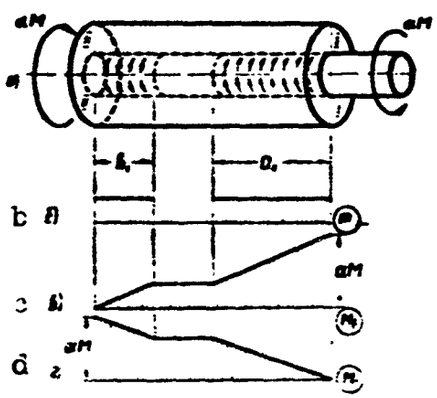

Fig. 17

Let us also assume that no frictional forces exist at the contact surface at the beginning of the first loading.

The first stage. During this stage the load αM varies between zero and the value M; we shall assume that the largest load is not sufficient for complete uncoupling of the joint. The shaft and the sleeve are deformed differently in the slip zones a and b, under the action of the torque. No slip of the shaft relative to the sleeve exists at the mid-segment of the joint, the angles of twist of their cross sections are equal to one another and, therefore, the torque is distributed between the shaft M_V, and the sleeve M_T, proportional to their rigidities

$$M_1 = \alpha k M, \tag{2.1}$$

$$M_2 = \alpha (1 - k) M, \tag{2.2}$$

where $k = \frac{GJ}{GJ + G_T J_T}$ represents the radio of the shaft's rigidity GJ, to the total rigidity of the joint; $G_T J_T$ is the torsional rigidity of the sleeve.

It can be seen from the consideration of the equilibrium of a sleeve segment of length a_1 along which slip has occurred that

$$M_T = m a_1, \tag{2.3}$$

where

$$m = 2\pi R^2 q_0 \tag{2.4}$$

represents the intensity of the torque due to frictional forces; this torque is uniformly distributed along the shaft's slip segment; R is the radius of the cylindrical surface of contact between the shaft and the sleeve.

The length of the slip region

$$a_1 = \frac{\alpha (1 - k) M}{m}. \tag{2.5}$$

is determined from Relationships (2.2) and (2.3). The length of the second slip region b_1 is determined from the consideration of the equilibrium of the shaft's end segment. We will find

$$b_1 = \frac{M_1}{m} = \frac{\alpha k M}{m}. \tag{2.6}$$

Thus, distributed torques of intensity $\underline{m}$ act on segments a_1 and b_1. Diagrams of $\underline{m}$, M_T and M_V are presented in Fig. 17.

Let us consider the angle of twist of the shaft end I - I relative to the sleeve section II — II. This angle of twist is found by adding the angles of twist of the three segments of the system. We get here

$$u_1(l, \alpha) = \frac{(1 - 3k + 3k^2)\alpha^2 M^2}{2m(1-k)GJ} + \frac{k\alpha Ml}{GJ} \qquad (2.7)$$

One's attention is attracted in this formula to the presence of a nonlinear dependence between the force and the deformation, this nonlinearity is characteristic of elastic systems with frictional couplings. Let us note that for $m \to \infty$, i.e., when the shaft and the sleeve are rigidly joined ($f \to \infty$), the first term of the formula vanishes, with only the term determining the angle of twist of a continuous shaft remaining. For $k \to 0$, (the case when the rigidity of the sleeve is considerably greater than the rigidity of the shaft $GJ \ll G_T J_T$) the structure of the last formula coincides with the analogous Formula (1.13) for a thin strip on a rigid foundation.

For the greatest value that the load can take on in the first loading stage, i.e., for $\alpha = 1$, the displacement of this section is determined by formula

$$u_1(l, 1) = \frac{M^2}{2mGJ} \cdot \frac{1 - 3k + 3k^2}{1-k} + \frac{kMl}{GJ}. \qquad (2.8)$$

Terms, corresponding to elastic twist of that part of the sleeve which is free of the shaft are absent in these formulas, since these terms do not affect the energy dissipation characteristics.

The second stage. A redistribution of frictional forces occurs in the process of unloading the joint, and regions along which slip occurs in the reverse direction appear. Let us denote the lengths of these new regions by a_2 and b_2; they are determined, as in the first stage, from the consideration of the equilibrium of shaft and sleeve segments:

$$a_2 = (1 - \alpha)\frac{kM}{2m}. \qquad (2.9)$$

$$l_{-}\ (1\ \ x)(1\ \ l)\ \frac{M}{2m} \qquad (2.10)$$

Figure 18 shows the diagrams of the torques m, M_V and M_T. By adding the angles of twist of the several segments, we can find the displacement of the same shaft section I - I in the unloading stage in the form

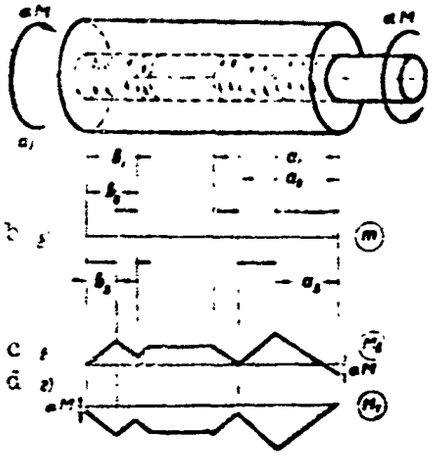

Fig. 18

$$u_2(l, \alpha) = \frac{M^2}{4mGJ}(1 + 2\alpha - \alpha^2)\left(\frac{1 - 3k + 3k^2}{1 - k}\right) + \frac{\alpha kMl}{GJ}. \qquad (2.11)$$

For $k \to 0$, the structure of this formula coincides with that of the analogous Formula (1.24) for the displacements of the end sections of the thin elastic strip along a rigid foundation during the second loading stage. If the load reaches the greatest value ($\alpha = 1$), then this formula, obviously, gives the previous result (2.8), and for a minimal value of the load, the displacement of the shaft's end section is written in the form

$$u_2(l, r) = \frac{M^2}{4mGJ}(1 + 2r - r^2)\left(\frac{1 - 3k + 3k^2}{1 - k}\right) + \frac{rkMl}{GJ}. \qquad (2.12)$$

The third stage. In contrast with the first stage, slip is already present on individual segments of the contact surface toward the beginning of the third stage under consideration and a certain system of frictional forces is in existence. The increase of the load from the minimal to the greatest value results in the appearance of still another two slip regions a_3 and b_3 (Fig. 19). The lengths of these regions are determined from the equilibrium conditions and have the values

$$a_3 = (\alpha - r)\frac{kM}{2m}. \qquad (2.13)$$

$$[illegible] \qquad (2.14)$$

The diagrams of the torques $\underline{m}$, due to frictional forces, and of M_V and M_T are shown in Fig. 19b, $\underline{c}$ and $\underline{d}$. The displacement of section I - I relative to section II - II in this loading stage is determined by the formula

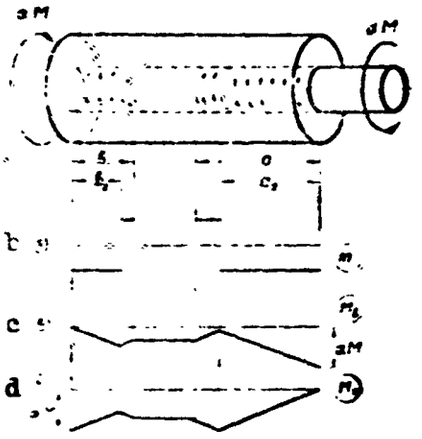

Fig. 19

$$u_3(l, \alpha) = \frac{M^2}{3mGJ}\left(1 - \frac{3k^2}{1-k}\right) - \frac{2kMl}{GJ}. \qquad (2.15)$$

For $k \to 0$ this formula coincides with the analogous Formula (1.31) of the preceding paragraph. If the load reaches its greatest and smallest values, then Formula (2.15) gives the same results as Formulas (2.8) and (2.9). Thus, when the load varies cyclically, the relationship between u ($\underline{l}$, α) and the torque αM is represented by a closed curve. forming a hysteresis loop. The shapes of the hysteresis loops are entirely similar to those shown in Fig. 14. The area of the hysteresis loop calculated by Formula (1.32) will be:

$$\Psi = \frac{2M_c^3}{3mGJ} \cdot \frac{1 - 3k - 3k^2}{1-k}. \qquad (2.16)$$

where $M_c = \frac{(1-r)M}{2}$ is the amplitude of the cycle.

This formula makes it possible to estimate the effect of design parameters of the joint and of the frictional forces distributed along the contact surface on the rate of energy dissipation attendant to cyclical loading. As can be seen, the work of the frictional force is a function of the cube of the cycle's amplitude and is related hyperbolically to the pressure $\underline{p}$ at the contact surface; this can be easily noticed if one takes into account the fact that $\underline{m}$ is determined by

Formula (2.4). It also follows from Formula (2.16) that the work of the frictional forces does not depend on the mean load of the cycle. The result obtained by Formula (2.16) should be doubled in order to determine the energy dissipation in both halves of the joint. Let us again point out that the load is insufficient for uncoupling of the joint.

Let us consider the problem of energy dissipation in a press-fit joint of the second type which was briefly characterized above. Figure 20 shows the distribution of the torque in the shaft and sleeve sections along the length of the contact surface, successively during three loading stages. Let us assume that the load applied to the end sections of the joint's shaft is smaller than the limit for which the mutual slip of the shaft and sleeve sections is propagated over the entire length of the contact surface ($M < ml$).

Formulas for the angles of twist of the end section I - I of one half of the shaft relative to the mid-section II - II (Fig. 20) during all the three loading stages have the form

$$u_1(l, \alpha) = \frac{\alpha^2 M^2}{2mGJ}(1-k)^2 + \frac{\alpha k M l}{GJ}, \tag{2.17}$$

$$u_2(l, \alpha) = \frac{M^2}{2mGJ}(1-k)^2 \cdot (1 + 2\alpha - \alpha^2) + \frac{\alpha k M l}{GJ}, \tag{2.18}$$

$$u_3(l, \alpha) = \frac{M^2}{2mGJ}(1-k)^2 \cdot (1 + 2r - 2\alpha r - \alpha^2) + \frac{\alpha k M l}{GJ}. \tag{2.19}$$

Energy dissipated in one half of the joint during a complete cycle of load variation is determined by the formula

$$\Psi = \frac{2M_0^2(1-k)^2}{3mGJ}. \tag{2.20}$$

As can be seen, energy expended on irreversible processes again in this case is independent of the mean value of the load, but depends

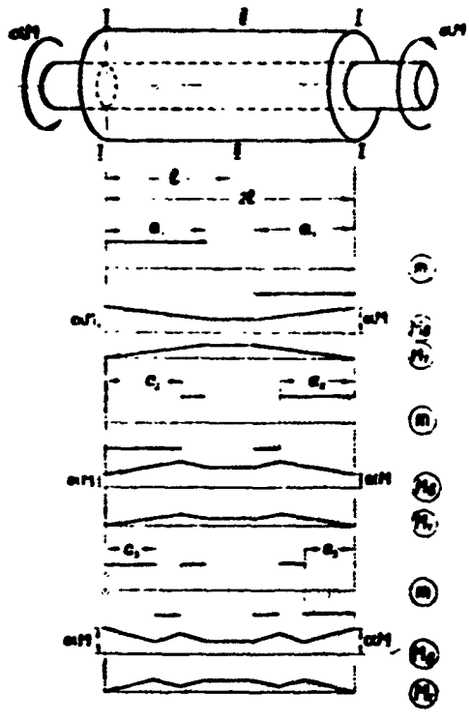

Fig. 20

on the cube of the cycle's amplitude. The hyperbolic dependence of the dissipated energy on the pressure at the contact surface is also retained.

Let us further consider the case of complete slip when the amplitude of the torque applied to the shaft exceeds the limiting value $M_v > ml$. Unidirectional slip is propagated over the entire contact surface during each stage of the cycle. Slip accumulated during the preceding stage of the cycle is "erased" and appears in a new, opposite direction

Let the greatest load of the first loading stage already exceed a value

$$\alpha_0 M = ml, \tag{2.21}$$

such that the length of the slip region becomes equal to half the length of the contact surface (Fig. 20). In this case, the loading process breaks up into two stages: during the first stage the boundary of the slip region is displaced as the load is changed; during the second stage the position of the boundary does not change.

The displacement of section I - I relative to the stationary section II - II during the first stage is determined by Formula (2.17); during the second stage, when slip is propagated over the entire length of the contact surface, the angle of twist of the same section is determined by formula

$$\varphi_1(l, x) = \frac{Ml}{2GJ}(2x - \alpha_0). \tag{2.22}$$

where α_0 is the limiting value of the dimensionless load parameter;

it can be found by Formula (2.21) from the conditions of equilibrium of the half-sleeve.

As can be seen, the presence of a stationary boundary of the slip region results in the appearance of a linear dependence of the angle of twist on the load. The function $u_1 = u_1(\underline{1}, \alpha)$ is shown graphically in Fig. 21. The nonlinear segment of the first branch of the curve shown in the graph corresponds to Dependence (2.17), the linear segment of the branch - to Dependence (2.22).

Let us now consider the unloading process. The angle of twist of section I - I relative to section II - II (slip has not as yet propagated itself over the entire contact surface) during the first stage is determined by Formula (2.18); during the second unloading stage this angle is determined by formula

$$u_2(l, \alpha) = \frac{Ml}{2GJ}(2\alpha - \alpha_0). \qquad (2.23)$$

Thus, on unloading (second branch of the hysteresis loop of Fig. 21), dependence $u_2(\underline{1}, \alpha)$ is quadratic during the first stage. This dependence becomes linear during the second stage.

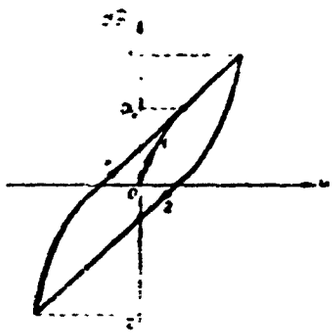

Fig. 21

The second loading causes a new change in the direction of slip. The angle of relative twist of section I - I and II - II is determined by Formula (2.19) during the first stage, and during the second stage, by Formula (2.22). The nonlinear dependence of displacement on the loading for a moving boundary of the slip region and the linear dependence for a stationary boundary of the slip region also exist during this process of repeated loading. The third branch of Fig. 21 corresponds to this process. Energy dissipated during a complete loading cycle is determined by the formula

$$\Psi = \frac{M^2}{3mGJ}\left[6\alpha_0\alpha_0^2 - 6\alpha_0^3 + 2\alpha_0^3(1 - kf^3\right]. \qquad (2.24)$$

where $\alpha_r = \frac{1}{2}(1 - r)$ is the amplitude of the variation of the dimensionless load parameter, so that the amplitude of the torque can be expressed by the dependence $M_v = \alpha_v M$.

Formula (2.24), in contrast to (2.20), is valid for small values of frictional forces, and therefore makes it possible to investigate the characteristic of energy dissipation for $m \to 0$. The dissipated energy depends on the amplitude of the load for small values of tangential frictional forces; furthermore, this energy does not depend on the mean value of the cycle's loading. The dissipated energy is parabolically related to the normal pressure on the joint's contact surface. If we take into consideration Dependence (2.21), then Formula (2.24) for the area of the hysteresis loop can be transformed to the form

$$\Psi = \frac{4\pi k^2 fl}{GJ}\left[pM_0 - \frac{2}{3}\pi R^2 fl(2 + 2k - k^2)p^2\right]. \qquad (2.25)$$

For $p = 0$, i.e., when normal pressure on the contact surface is absent, there is no friction in the joint and there is no energy dissipation. For the value $p = p_1$, which is determined by the formula

$$p_1 = \frac{3M_0}{4\pi R^2 fl(2 + 2k - k^2)}, \qquad (2.26)$$

energy dissipation reaches its highest value. In this case the area of the hysteresis loop is equal to:

$$\Psi_{max} = \frac{3M_0^2}{2GJ[3 - (1 - k)^2]}. \qquad (2.27)$$

A further increase in pressure results in a decreased energy dissipation. Under the condition $M_v = \alpha_0 M$, which determines the lower boundary of applicability of Formula (2.24), the same result is obtained as when using Formula (2.20) for which this condition is the

upper boundary of applicability. Figure 22 shows the graph of the dependence of the area of hysteresis loop on the normal pressure at the contact surface, constructed by Formulas (2.24) and (2.22). Let us note that the energy dissipation increases with an increase in the rigidity of the sleeve (i.e., for a decreasing $\underline{k}$) (compare Fig. 22 with Fig. 15).

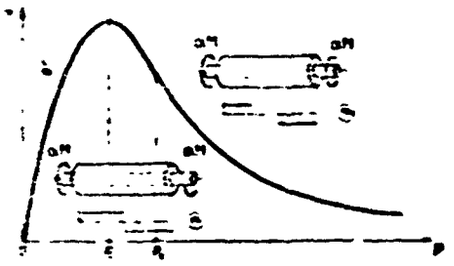

Fig. 22

The most widespread type of a press-fit torsional joint is the third type of joint. A sheave or a gear on a transmission shaft, seated with interference, is a characteristic example of this type of joint.

Due to the absence of loading symmetry (see Fig. 16) the end slip regions are of different dimensions. The presence of a torque on the step in section II - II results in the appearance of a median slip region. The dimensions of these three regions depend on the load, intensity of the moments of frictional forces and also on the ratio between the rigidities of the shaft and the sleeve.

In the limiting case, when the rigidity of the shaft is equal to infinity, slip occurs only in the end contact regions. Let us determine the energy dissipation during a cycle for this elementary and at the same time interesting for practical purposes case (since the rigidity of the step is usually by far greater than the rigidity of the shaft).*

It has already been pointed out above that for a rigid press-fit joint sleeve the problem of cyclical torsion is entirely analogous to the problem of the elastic strip on a rigid foundation. Therefore the dimensions of the extreme slip regions on first loading are determined by formulas

$$a_1 = \frac{\alpha M_1}{m}, \quad b_1 = \frac{\alpha M_3}{m} \tag{2.28}$$

which are explicitly independent of Formula (1.3).

The torques in the extreme shaft sections dM_1 and dM_3 and also the torque applied to the step dM_2, satisfy the equilibrium condition of the joint

$$\alpha (M_1 + M_2 + M_3) = 0.$$

The angles of twist of the extreme shaft sections can be determined relative to any section situated outside the slip region (sections situated in this region remain mutually stationary). For example, the angle of twist of the right end section of the shaft for the stage of first loading is determined by the formula

$$u_1 (l, \alpha) = \frac{\alpha^2 M_1^2}{2mGJ}; \tag{2.29}$$

the angle of twist of the left end section is determined by the formula

$$u_1 (-l, \alpha) = \frac{\alpha^2 M_3^2}{2mGJ}. \tag{2.30}$$

Similarly, during the unloading stage we have

$$u_2 (l, \alpha) = \frac{M_1^2}{2mGJ} (1 + 2\alpha - \alpha^2); \tag{2.31}$$

$$u_2 (-l, \alpha) = \frac{M_3^2}{2mGJ} (1 + 2\alpha - \alpha^2). \tag{2.32}$$

The angles of twist of the extreme sections during the second loading stage are determined by the formulas

$$u_3 (l, \alpha) = \frac{M_1^2}{2mGJ} (1 - 2\alpha r + 2r + \alpha^2), \tag{2.33}$$

$$u_3 (-l, \alpha) = \frac{M_3^2}{2mGJ} (1 - 2\alpha r + 2r + \alpha^2). \tag{2.34}$$

The area of the hysteresis loop for the given joint is calculated by the formula

$$\psi = \frac{2}{3\pi G J}\left(M_{1v}^3 + M_{3v}^3\right), \qquad (2.35)$$

where M_{1v} and M_{3v} are the amplitudes of torques applied to the right and the left ends of the shaft. Let us note that the last formula is valid only in the case when slip has not spread over the entire contact surface.

§3. ENERGY DISSIPATION IN A PRESS-FIT JOINT DURING TENSION – COMPRESSION

Results obtained in the preceding paragraphs can be generalized to [include] press-fit joints during cyclical tension-compression. The problem of cyclical tension-compression of a press-fit joint becomes fully analogous to the problem with cyclical torsion of a press-fit joint, if, as in the latter case, we assume that the shaft and sleeve material is subject to Hooke's law, the tangential frictional forces at the contact surface are subject to the law of dry friction and that sections which were plane before loading do not change their shape and remain plane after the load has been applied both in the slip region as well as outside this region. In addition, it is necessary to assume that the normal pressure p at the contact surface does not change either during the loading process or along the length of the joint. This assumption, obviously acceptable in torsional problems, becomes much more doubtful in problems of longitudinal loading here considered; actually, for a Poisson ratio different from zero the longitudinal loading will result in a change of effective tension and the frictional forces will lose their previous property of constancy. We shall consider this somewhat further on; at the moment we will stop at the elementary assumption, according to which the tension remains constant.

In accordance with Section 2, the following formulas can be written for areas of hysteresis loops in various types of joints (see

Fig. 16). For one half of a joint of the first type (shaft cut into halves in a sleeve), such as in Formula (2.16) we have

$$\Psi = \frac{2}{3}\frac{P_v^3}{q_0 EF}\cdot\frac{1-3k+3k^2}{1-k}. \qquad (3.1)$$

In joints of the second type (sleeve-continuous shaft) the area of the hysteresis loop for one half of the joint is determined similar to Formula (2.20)

$$\Psi = \frac{2}{3}\frac{P_v^3}{q_0 EF}(1-k)^2. \qquad (3.2)$$

The following notations are here utilized: P_v is the amplitude of the longitudinal force, q_0 - the limiting frictional force, EF - the rigidity of the shaft on tension-compression and k, as before, the ratio of the longitudinal rigidity of the shaft to the total longitudinal rigidity of the joint.

In the case of full slip over the entire contact surface the formula for the area of the hysteresis loop in the joint of the second type takes on a form similar to that of Formula (2.24):

$$\Psi = \frac{2P^3}{3q_0 EF}[3\alpha_v \alpha_0^2 - 3\alpha_0^3 + \alpha_0^3(1-k)^2], \qquad (3.3)$$

where α_v is the amplitude of the dimensionless load coefficient.

We shall examine in detail the influence of the Poisson's effect for the elementary case of a joint between a rigid sleeve and an elastic shaft (Fig. 23a).

The first stage. As before, we shall assume that no tangential forces of interaction between the shaft and the sleeve exist* at the beginning of the first loading. The initial normal pressure on the contact surface is proportional to the difference between the shaft diameter and the internal diameter of the sleeve before press-fitting

$$p_0 = \nu\delta_0, \qquad (3.4)$$

where $\delta_0 = D - D_T$, $\psi = \frac{EF}{2(1-\mu)}$ is a proportionality coefficient and D and D_T – the initial diameters of the shaft and the sleeve before pressfitting.

A change in the normal pressure p along the length of the fitted segment arises attendant to the loading of the shaft by a longitudinal force. This pressure can even disappear entirely for a sufficiently large value of the longitudinal stretching force and then a gap will appear between the sleeve and shaft surfaces. Below we shall still assume that the initial pressure p_0 is sufficiently large and a gap does not appear. Let N(x) be the current value of the longitudinal force in the shaft section and p(x) – the current value of the pressure on the contact surface; in the absence of an external load (i.e., for $\alpha = 0$) we have $N = 0$ and $p = p_0$. When the shaft elongates ($N > 0$) the pressure is diminished ($p < p_0$); when it is compressed ($N < p_0$), it increases. Under these conditions, the radial deformation of the shaft is determined by the formula

$$\varepsilon_p = -\frac{\mu N(x)}{EF} + \frac{p_0 - p(x)}{E(1-\mu)}. \quad (3.5)$$

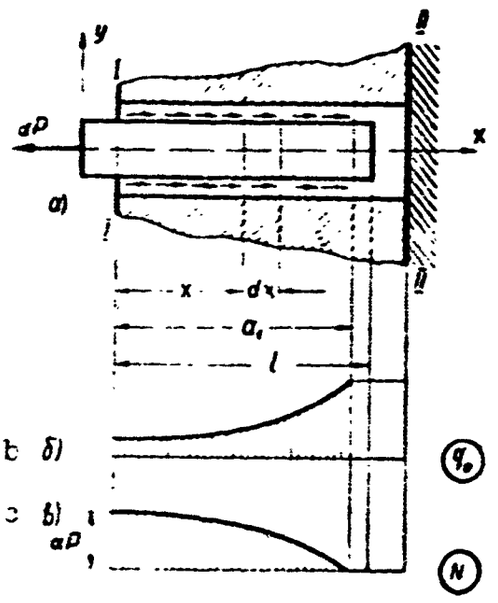

Fig. 23

Here E and μ are the modulus of elasticity of the shaft material and the Poisson's ratio and F is the cross-sectional area of the shaft.

The first term expresses the effect of the longitudinal force, the second – the effect of the pressure drop from the value p_0 to the value p (x). However, an absolutely rigid sleeve makes it impossible for the shaft to change its cross-sectional dimensions, i.e., the

radial deformation of the shaft is zero; expression (3.5) becomes the equation

$$\varepsilon_\rho = \frac{\mu N(x)}{EF} + \frac{p_0}{E(1-\mu)} - \frac{p(x)}{E(1-\mu)} = 0. \qquad (3.6)$$

We find from this equation

$$p(x) = p_0 - \frac{N(x)}{F}\mu(1-\mu). \qquad (3.7)$$

Let us introduce the notation

$$\frac{p_0 F}{\mu(1-\mu)} = N^*. \qquad (3.8)$$

Quantity N* represents the force N, for which the pressure p (x) = 0. As has already been said, $N \leq N^*$.

The relationship between pressure p (x) and force N (x) takes on the form

$$p(x) = \frac{\mu(1-\mu)}{F}[N^* - N(x)]. \qquad (3.9)$$

The intensity of the limiting frictional forces

$$q_0(x) = \pi D p f = \lambda [N^* - N(x)] \qquad (3.10)$$

varies as a function of the longitudinal force in the shaft section and is proportional to the quantity

$$\lambda = \frac{\pi \mu D f (1-\mu)}{F}. \qquad (3.11)$$

The following equation can be obtained from the equilibrium condition of a shaft element of length dx:

$$N' = -q_0. \qquad (3.12)$$

The solution of this equation under the boundary conditions

$$N(0) = \alpha P$$

has the form

$$N(x) = N^* - (N^* - \alpha P) e^{\lambda x}. \qquad (3.13)$$

The diagram of N is shown in Fig. 23c. Figure 23b gives the diagram of q_0 (x) corresponding to Dependence (3.10) if N (x) from (3.13) is substituted into it.

The boundary of slip propagation is determined from the consideration of the equilibrium of the entire shaft

$$\alpha P = \int_0^{a_1} q_0(x)\,dx. \tag{3.14}$$

Keeping in mind that q_0 (x) is determined by Dependence (3.10) and N (x) – by Expression (3.13), we will get

$$a_1 = \frac{1}{\lambda} \ln \frac{N^*}{N^* - \alpha P}. \tag{3.15}$$

When loading is absent ($\alpha = 0$) we have $a_1 = 0$. If $a_1 = l$, then the joint is uncoupled; the force necessary to bring this about is determined from (3.15)

$$\alpha_0 P = N^* (1 - e^{-\lambda l}). \tag{3.16}$$

If the load reaches its largest value $\alpha = 1$, remaining smaller than the limiting [load], then the length of the slip region is determined by the formula

$$a_{12} = \frac{1}{\lambda} \ln \frac{N^*}{N^* - P}. \tag{3.17}$$

On the basis of Hooke's law we have the equation

$$u' = \frac{N}{EF}. \tag{3.18}$$

Taking (3.13) into account, we will obtain, on integration under the conditions u_1 (a_1) = 0,

$$u_1(x, \alpha) = \frac{1}{EF}\left[N^*(x - a_1) + \frac{1}{\lambda}(N^* - \alpha P)(e^{\lambda a_1} - e^{\lambda x})\right]. \tag{3.19}$$

Correspondingly, the displacement of the end section is equal to:

$$u_1(l, \alpha) = \frac{1}{\lambda EF}[(N^* - \alpha P)(e^{\lambda a_1} - 1) - \lambda N^* a_1]. \tag{3.20}$$

If the load reaches its maximal value ($\alpha = 1$), then the displacement of this section is determined by the formula

$$u_1(0,1) = \frac{1}{\lambda EF}\left(P - N^* \ln \frac{N^*}{N^* - P}\right). \qquad (3.21)$$

Under the condition that the Poisson effect is absent ($\mu \to 0$), the latter formula, after the proper limit transition, fully coincides with the analogous Formula (1.13).

The second stage. When the loading is decreased, shaft sections are pulled into the sleeve at the extreme contact region, and reverse slip appears on a part of the contact surface. The equilibrium equation of a shaft element situated in this zone gives

$$N' = q_0(x). \qquad (3.22)$$

Substituting the expression for q_0 (x) into this equation, we will obtain a new equation for the normal force in the shaft section

$$N' - \lambda(N^* - N(x)) = 0. \qquad (3.23)$$

The solution of this equation under the condition N(0) = αP:

$$N(x) = N^* - (N^* - \alpha P)e^{-\lambda x}. \qquad (3.24)$$

If we now take the external load off completely, then residual stresses distributed according to the rule

$$N(x) = N^*(1 - e^{-\lambda x}). \qquad (3.25)$$

will appear in the pressfitted part of the shaft at the reverse slip segment. The diagrams of N (x) and q_0 (x) are shown in Fig. 24c; the boundary of the reverse slip propagation is determined from the condition of the shaft's equilibrium:

$$\alpha P = -\int_0^{a_2} q_0(x)\,dx + \int_{a_2}^{a_{22}} q_0(x)\,dx. \qquad (3.26)$$

We substitute for the integrand $q_0(x)$ its value from (3.10), taking into account that the normal force in the shaft section N (x) on the direct slip segment is determined by Formula (3.13) and on the reverse slip segment – by Formula (3.24). Then the boundary of the reverse slip region will be determined by the formula

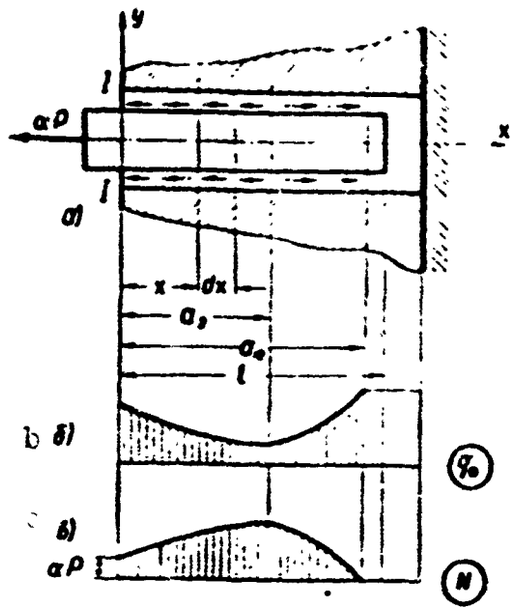

Fig. 24

$$a_2 = \frac{1}{2\lambda} \ln \frac{N^* - rP}{N^* - P}. \quad (3.27)$$

Reverse slip is absent for $\alpha = 1$ ($\alpha_2 = 0$); if the load is brought to its minimal value $\alpha = r$, then the dimensions of the reverse slip region are determined by the formula

$$a_{2r} = \frac{1}{2\lambda} \ln \frac{N^* - rP}{N^* - P}. \quad (3.28)$$

We shall determine the displacements during loading, again utilizing Dependence (3.18). After substitution of Expression (3.24) into this dependence and integrating under the condition of continuity of displacements at the boundary between direct and reverse slip segments

$$u_2(a_2) = u_{12}(a_2) \quad (3.29)$$

we will get

$$u_2(x, x) = \frac{1}{EF}\left[N^*(x - a_{12}) + \frac{1}{\lambda}(N^* - P)(e^{\lambda a_{12}} - e^{\lambda a_2}) + \right.$$
$$\left. + \frac{1}{\lambda}(N^* - \alpha P)(e^{-\lambda x} - e^{-\lambda a_2})\right]. \quad (3.30)$$

Expressing a_1 and a_2 in terms of the parameter α, we will obtain a formula for the displacement of the end section

$$u_2(x,0) \quad \frac{1}{\lambda EF}\left[2N^* - \alpha P - N^* \ln\frac{N^*}{N^*-P} - 2\sqrt{(N^*-\alpha P)(N^*-P)}\right]. \tag{3.31}$$

At the boundary of the first and second stages, i.e., for $\alpha = 1$, Formula (3.31) coincides with Formula (3.21). If the load reaches its minimal value, then the displacement of the end section is determined by the formula

$$u_2(1,0) = \frac{1}{\lambda EF}\left[2N^* - rP - N^* \ln\frac{N^*}{N^*-P} - 2\sqrt{(N^*-rP)(N^*-P)}\right]. \tag{3.32}$$

The deformation of the shaft does not disappear for $\alpha = 0$ and the shaft is loaded by a system of residual forces. The residual displacement of the end section $x = 0$ is equal to:

$$u_2(0,0) = \frac{1}{\lambda EF}\left[2N^* - N^* \ln\frac{N^*}{N^*-P} - 2\sqrt{N^*(N^*-P)}\right]. \tag{3.33}$$

Let us note that, as a result of elementary transformations and of limit transition, Formula (3.31), under the condition $\lambda \to 0$, coincides with the analogous Formula (1.24) for an elastic strip on a rigid foundation.

The third stage. On repeated loading of the shaft "erasure" of reverse slip occurs in the extreme region of the mating surfaces and a segment of direct slip a_3 again appears (Fig. 25).

The normal force N (x) is, within the limits of the direct slip segment, determined by Formula (3.13). The position of boundary a_3 is determined, as in the previous two stages, from the condition of the shaft's equilibrium

$$\alpha P = \int_0^{a_0} q_0(x)\,dx - \int_{a_0}^{a_{00}} q_0(x)\,dx + \int_{a_{00}}^{a_{000}} q_0(x)\,dx. \tag{3.34}$$

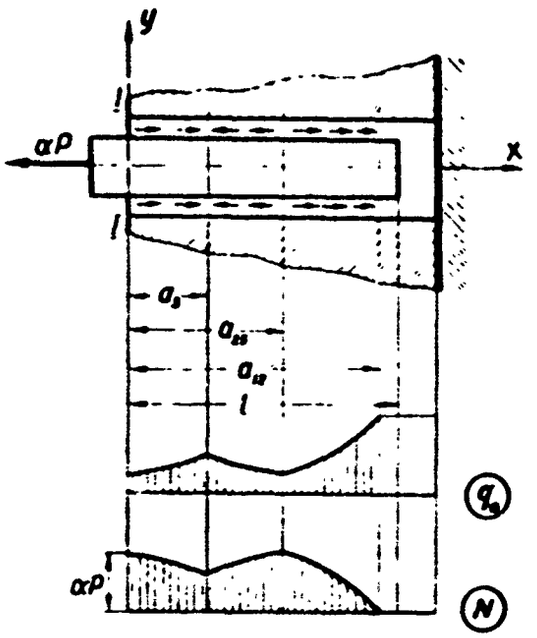

Fig. 25

From this we get

$$a_3 = \frac{1}{2\lambda} \ln \frac{N^* - rP}{N^* - \alpha P}. \quad (3.35)$$

If $\alpha = r$, then $a_3 = 0$; for $\alpha = 1$

$$a_{22} = \frac{1}{2\lambda} \ln \frac{N^* - rP}{N^* - P}. \quad (3.36)$$

The diagrams of N (x) and q (x) for the second loading stage are shown in Figs. 25b and c.

The displacement u_3 (x, α) will be determined if we integrate Eq. (3.18) under the condition of continuity of displacements on the boundary between positive and negative slip:

$$u_3(x, \alpha) = \frac{1}{\lambda EF}[\lambda N^* (x - a_{12}) + (N^* - P)(e^{\lambda a_{12}} - e^{\lambda a_{22}}) + (N^* - rP)(e^{-\lambda a_{22}} - e^{-\lambda a_{12}}) + (N^* - \alpha P)(e^{\lambda a_{22}} - e^{\lambda x})]. \quad (3.37)$$

Utilizing the above dependencies of the dimensions of slip regions a_1, a_2 and a_3 on the dimensionless load parameter α, we will determine the displacement of the end section by the formula

$$u_3(0, \alpha) = \frac{1}{\lambda EF}\left[\alpha P + 2\sqrt{(N^* - rP)(N^* - \alpha P)} - 2\sqrt{(N^* - P)(N^* - rP)} - N_0 \ln \frac{N^*}{N^* - P}\right]. \quad (3.38)$$

For $\lambda \to 0$ this formula coincides with the corresponding Formula (1.31).

If the load takes on the value rP, then the last formula coincides with (3.32); Result (3.21) is obtained for $\alpha = 1$.

The hysteresis loop for a cycle with an arbitrary characteristic is shown in Fig. 14a. Calculating its area, we obtain the formula

$$\Psi_* = \frac{2P}{\lambda EF} \int_r^1 [\sqrt{(N^* - P)(N^* - rP)} - \sqrt{(N^* - P)(N^* - \alpha P)} - \quad (3.39)$$

$$-\sqrt{(N^* - aP)(N^* - rP)} + N^* - aP\Big]\,dx. \qquad (3.39)$$

If we utilize the concepts of the mean value of load P_m and of the cycle amplitude P_v, then after performing quadratures we will have

$$\Psi_r = \frac{4P_v}{3\pi EF}\left[P_m - P_0 + \sqrt{(N^* - P)(N^* - rP)}\right]. \qquad (3.40)$$

It follows from this formula that the consideration of transverse deformations in a press-fit joint changes conclusions made earlier relative to the independence of the area of the hysteresis loop on the mean value of the load. The area of the loop depends not only on the amplitude of the cycle but also on the mean value of the load. This follows inevitably from the fact that the normal pressure depends on the shaft deformation. If we assume that p is independent of the transverse deformation of the mating elements, i.e., if we assume that $\mu = 0$, then Formula (3.40), after the proper limit transition, takes on the form

$$\Psi_{r_0} = \frac{2P_v^2}{3q_0EF} \qquad (3.41)$$

and coincides fully with the result obtained in Section 1 for an elastic strip on a rigid foundation.

Figure 26 shows graphs of Ψ_r/Ψ_{r_0} as a function of P_v/N^* for a symmetrical (lower graph) and pulsating cycles.

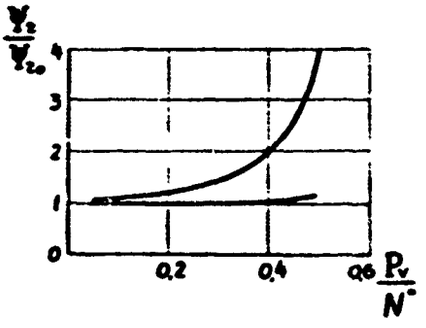

Fig. 26

As can be seen, the results of calculations by Formula (3.41) for small values of N* practically do not differ from results obtained by Formula (3.40). For a symmetrical cycle they coincide very well for large loads, even close to failure. In the case of a pulsating load the energy dissipation increases rapidly when the mean force of the cycle is

increased. The utilization of Formula (3.41) for calculation of energy dissipation for nonsymmetrical cycles gives a result on the low side. Thus, the lowering of the effective tension for a nonsymmetrical cycle results in an <u>increase</u> of the area of the hysteresis loop.

[Footnotes]

Manuscript Page No.	
36	The case of an elastic sleeve can also be investigated by similar methods; however, the computations will become much more cumbersome.
39	They can appear on pressfitting, and also as a residual effect of previous loadings.

[List of Transliterated Symbols]

Manuscript Page No.	
27	в = v = val = shaft

Chapter 2

COMPOSITE BEAMS

§4. PURE BENDING OF A BEAM WITH PRESSURE PLATES

Let us return to the scheme of a beam with a rectangular cross-section with thin pressure plates which are pressed to the beam by pressure p, described in Fig. 5. The end sections of the beam are loaded by moments αM, acting in the structure's plane of symmetry.

It should be kept in mind that it is not entirely indifferent by which method the bending moment is applied to the end: whether the corresponding surface loads are applied only to the beam proper or only to the pressure plates or, finally, to the beam as well as to the plates. The first loading version is assumed below; similar results can also be found for the conditions of the second version. However, if the loading is achieved according to the third version and the longitudinal stresses are distributed linearly over the end section. then no frictional forces will develop between the pressure plates and the beam.

And so, let us assume that the bending moments are applied only to the beam proper, and the end sections of the pressure plates are free of normal stresses. The interaction between the pressure plate and the beam will differ on different length segments. At a certain distance from the end the beam and the pressure plates act together and no slip takes place on the contact surfaces. Tangential forces are absent on these segments and the normal force in the pressure plate section will be then determined by the formula

$$N = \frac{Fh}{2J}\alpha M = \alpha\beta\frac{M}{h}. \qquad (4.1)$$

where J is the moment of inertia of the beam section (taking the pressure plates into account), h is the height of the beam cross section, F is the cross-sectional area of one pressure plate, α – the dimensionless load parameter, $\beta = Fh^2/2J$ – a constant for a given beam and M is the greatest value of the moment.

Slip of the pressure plates over the beam surfaces takes place on the end sections; the appearance of tangential forces q_0, corresponding to the law of dry friction, is related to this. Let us formulate the equations of equilibrium for a part of the upper pressure plate shown in Fig. 5b:

$$N - q_0 a = 0. \qquad (4.2)$$

The corresponding part of the lower pressure plate acts similar to the upper. Equality (4.2) makes it possible to determine the dimensions of the segment within the limits of which slip takes place:

$$a = \frac{\alpha\beta M}{q_0 h}. \qquad (4.3)$$

As can be seen, as the load increases (i.e., with increasing α) the slip is propagated in the direction of the beam's middle. Below we consider a case where the greatest value of the moment is moderate and slip does not reach the median section of the beam, i.e., when

$$a_{max} = \frac{\beta M}{q_0 h} \leq l. \qquad (4.4)$$

Let us follow the operation of the joint during various stages of the cycle; as a result of the assumed symmetry of the beam it is sufficient to consider only one half of it (Fig. 27a).

The first stage ($0 \leq \alpha \leq 1$). As the moment αM is increased, the slip is propagated from the free end of the pressure plate to the mid-

dle of the beam. The corresponding loading of the upper pressure plate is described in Fig. 27b; here the size of slip segment a_1 is determined by Formula (4.3). Considering now the deflection of the right half of the beam under the action of loads represented in Fig. 27a, we will find the angle of twist of the end section during the loading process:*

$$\varphi_1(\alpha) = \frac{\alpha(1-\beta)Ml}{EJ_0} + \frac{(\alpha\beta M)^2}{2q_0 k EJ_0}. \qquad (4.5)$$

where EJ_0 is the rigidity in bending of the beam without the pressure plates. At the end of the first stage $\alpha = 1$ and

$$\varphi_1(1) = \frac{(1-\beta)Ml}{EJ_0} + \frac{(\beta M)^2}{2qk EJ_0}. \qquad (4.6)$$

The second stage ($1 \geq \alpha \geq r$). Reverse slip appears on a part of the contact surface in the unloading process. The loading of the upper pressure plate is shown in Fig. 27c. Equating the longitudinal force (4.1) to the sum of frictional forces, we will find the length of the reverse slip segment:

$$a_2 = \frac{(1-\alpha)\beta M}{2q_0 k}. \qquad (4.7)$$

We will find the angle of twist of the beam's end section in the form

$$\varphi_2(\alpha) = \frac{\alpha(1-\beta)Ml}{EJ_0} + \frac{(1+2\alpha-\alpha^2)(\beta M)^2}{4q_0 k EJ_0}. \qquad (4.8)$$

If we substitute $\alpha = 1$ into this expression, then we will again obtain the previous result (4.6); for the end of the second stage, when $\alpha = r$:

$$\varphi_2(r) = \frac{r(1-\beta)Ml}{EJ_0} + \frac{(1+2r-r^2)(\beta M)^2}{4q_0 k EJ_0}. \qquad (4.9)$$

The third stage ($r \leq \alpha \leq 1$). The distribution of frictional forces on renewed loading is shown for the upper pressure plate in Fig. 27d. The length of the segment on which direct slip appears anew:

$$a_3 = \frac{\beta M}{2q_0 k}(\alpha - r). \qquad (4.10)$$

In accordance with the schematic described in Fig. 27a, we will find the angle of twist of the beam's end section:

$$\varphi_3(x) = \frac{\alpha(1-\beta)Ml}{EJ_0} - \frac{(1-\alpha^2+2r-2\alpha r)(\beta M)^2}{4q_0 hEJ_0}. \qquad (4.11)$$

Expressions for φ_3 and φ_2 coincide for $\alpha = r$; expressions for φ_3 and φ_1 coincide similarly for $\alpha = 1$.

The first terms of Expressions (4.5), (4.8) and (4.11) are identical. This coincidence is not accidental, since these terms

$$\frac{\alpha(1-\beta)Ml}{EJ_0} = \frac{\alpha Ml}{EJ}$$

represent angles of twist of monolithic beam, fabricated as a single entity together with the pressure plates. The second terms of these expressions show the effect of slip developed between the beam and the pressure plates. The structure of these terms does not differ from the right-hand sides of relationships found in Section 1 for the elementary problem. Therefore the character of hysteresis loops for the problem being considered will be the same as is shown in Fig. 14.

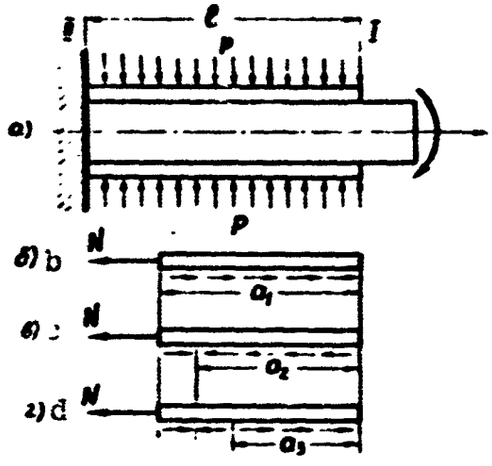

Fig. 27

For determination of energy dissipation during cyclical loading we will utilize the expression

$$\Psi = M\int_0^1 (\varphi_2 - \varphi_3)\,d\alpha. \qquad (4.12)$$

After performing quadratures we will find

$$\Psi = \frac{\beta^2 M^2 (1-r)^2}{12 q_0 h EJ_0} \qquad (4.13)$$

If we now introduce the amplitudes of the cycle

$$M_0 = \frac{(1-\alpha)M}{2}, \tag{4.14}$$

then (4.13) can be written in the form

$$\Psi = \frac{2\beta^2 M_0^3}{3q_0 hEJ_0}. \tag{4.15}$$

As can be seen, the structure of this formula coincides with those of the expressions obtained above, in §§ 1 and 2, for compression-tension cases; the energy dissipation is proportional to the cube of the amplitude of the bending moment and is inversely proportional to the clamping pressure of the pressure plates; furthermore, the mean value of the bending moment does not exert any influence on the damping properties of the system.

If condition (4.4) is not satisfied (for large values of the bending moment), then slip embraces the entire length of the beam. Without dwelling on details, which are similar to those presented in § 2, let us point out the final formula for the area of the hysteresis loop:

$$\Psi = \frac{2\beta^2 M^2 \alpha_0^2}{q_0 hEJ_0}\left(M_0 - \frac{2}{3}\alpha_0 M\right), \tag{4.16}$$

where M_v, as before, is the amplitude of the bending moment and $\alpha_0 M$ is that value of the bending moment for which slip embraces the entire length of the beam; it is easy to establish, by means of Dependence (4.4) that

$$\alpha_0 M = \frac{q_0 M}{\beta}. \tag{4.17}$$

Let us note that the region of applicability of Formula (4.16) is limited by condition $M_v \geq \alpha_0 M$, which means that slip is propagated over the entire length of the surface of contact between the beam and the pressure plates. If the load just reaches the value for which slip is propagated over the entire length of the contact surface, i.e., if

condition $M_v = \alpha_0 M$ is satisfied, then Formula (4.16) gives the result obtained above by (4.15).

Let us note that under conditions $M_v > \alpha_0 M$ the area of the hysteresis loop is proprotional to the first power of the amplitude of the moment, and not to the cube of the amplitude, as in the case for $M_v < \alpha_0 M$.

To estimate the effect of compression forces p on energy dissipation, it is sufficient to consider the effect of the quantity q_0, which is proportional to the pressure p. Substituting Expression (4.17) into Dependence (4.16), we will get

$$\Psi = \frac{2q_0 h l^2}{EJ_0}\left(M_0 - \frac{2q_0 h l}{3\beta}\right). \tag{4.18}$$

The maximal value of Ψ corresponds to a value of q_0, equal to

$$q_0 = \frac{3\beta M_0}{4hl}. \tag{4.19}$$

In general, these results coincide with the results obtained at the end of § 2 for the problem of torsion in a press-fit joint.

§5. TRANSVERSE BENDING OF CANTILEVERED BEAMS

Let us consider structural damping attendant to transverse bending of cantilevered composite beams.

We shall first of all dwell on the problem (Fig. 28) first solved by Goodman and Klamp [33]. A cantilevered beam consisting of two identical layers, pressed to one another by a distributed pressure p, is at its free end loaded by force αP, alternating within the range between − P and P. Let us find the displacements of the beam's end as a function of the magnitude of the force acting during a single loading cycle.

The first stage. As long as force αP is small and the intensity of the tangential forces q in the plane of contact between the layers

does not exceed the value $q_0 = fpb$, no slip occurs between the layers (b is the width of the beam). The system deforms as though it were a beam with a monolithic cross section and the intensity of tangential forces on the contact surface is determined by the D.I. Zhuravskiy formula

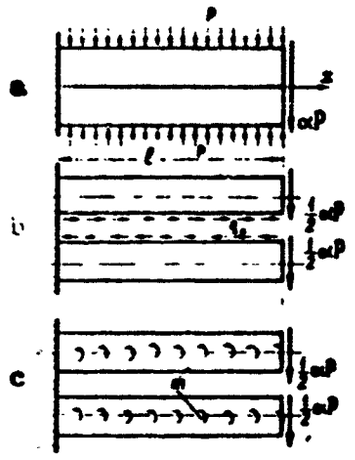

Fig. 28

$$q = \frac{3\alpha P}{4h}. \qquad (5.1)$$

The deflection of the end of the beam will be

$$u_1(\alpha) = \frac{\alpha P l^3}{24EJ}. \qquad (5.2)$$

Here h is the height and J the moment of inertia of the section of one layer.

The first stage will be terminated when the intensity of the tangential forces will reach the value $q = q_0$. According to (5.1), force

$$\alpha_0 P = \frac{4q_0 h}{3} \qquad (5.3)$$

corresponds to this case and, according to (5.2), the deflection of the end

$$u_1(\alpha_0) = \frac{\alpha_0 P l^3}{24EJ}. \qquad (5.4)$$

It is assumed that $\alpha_0 < 1$.

The second stage. After the load has reached the value $\alpha_0 P$, slip will begin at the contact surface. Since the tangential forces are everywhere the same, therefore slip will occur simultaneously along the entire beam length. On further increase in the force ($\alpha > \alpha_0$) the tangential forces on contact planes remain constant and equal to q_0. Each layer of the beam bends as an independent beam.

Figure 28b shows loads resulting in the deflection of the layer – beam: force 1/2 αP at the end and tangential forces uniformly distri-

buted over the entire beam length. Determining the deflection of the beam end it is convenient to replace the tangential forces by a uniformly distributed moment loading (Fig. 28c), the intensity of which will be

$$m = \frac{q_0 h}{2} = \frac{3\alpha_0 P}{8}. \qquad (5.5)$$

The displacement of the beam end during the second loading stage will be determined as the deflection of any layer and is expressed in the following manner:

$$u_2(\alpha) = \frac{\alpha P l^3}{6EJ} - \frac{ml^3}{3EJ} = \frac{Pl^3}{24EJ}(4\alpha - 3\alpha_0). \qquad (5.6)$$

For the beginning of the second loading stage ($\alpha = \alpha_0$) Result (5.4) is again obtained from (5.6). The second stage will be terminated when the force will reach its highest value P; here the deflection of the end amounts to

$$u_2(1) = \frac{Pl^3}{24EJ}(4 - 3\alpha_0). \qquad (5.7)$$

The third stage of the process comes at the instant when force αP begins to decrease (the coefficient α again becomes less than unity). The frictional forces at the contact surface also decrease and, since $q < q_0$, slip between layers cannot occur and the beam again bends as a beam with a monolithic cross section. The tangential forces at the contact surface will here be

$$q = q_0 - \frac{3(1-\alpha)P}{4h}. \qquad (5.8)$$

The deflection of the end of the beam will be determined by the formula

$$u_3(\alpha) = u_2(1) - \frac{(1-\alpha)Pl^3}{24EJ} = \frac{Pl^3}{24EJ}(3 - 3\alpha_0 + \alpha). \qquad (5.9)$$

As can be seen from (5.6) and (5.9), the deflections at the

beginning of the third stage and at the end of the second are identical. Let us note that on full unloading ($\alpha = 0$) the deflection is not equal to zero; the residual deflection is equal to

$$u_3(0) \quad \frac{Pl^3}{8EJ}(1 - \alpha_0). \tag{5.10}$$

The third stage will be terminated for a value of the force $\alpha_1 P$ such that the tangential forces determined by Formula (5.8) will reach the value q_0, but will be directed in a direction opposite to the one they had during the first loading stage, i.e.,

$$q_0 - \frac{3(1-\alpha_1)P}{4l} = -q_0. \tag{5.11}$$

The load coefficient, corresponding to the termination of the third and the beginning of the fourth loading stage is determined from the above:

$$\alpha_1 = 1 - 2\alpha_0. \tag{5.12}$$

The deflection of the beam's end can here be found by Formula (5.9), if we substitute in it $\alpha = \alpha_1$,

$$u_3(1) = \frac{Pl^3}{24EJ}(4 - 3\alpha_0). \tag{5.13}$$

The fourth stage. As soon as the load becomes smaller than $\alpha_1 P$, slip between the beam layers starts again, however, the direction of slip between the layers will become opposite. The deflection of the beam's end during the third stage will be determined as the deflection at the end of the third stage plus an additional deflection of one layer due to the force $\frac{\alpha_1 - \alpha}{2} P$

$$u_4(\alpha) = u_3(\alpha_1) - \frac{(\alpha_1 - \alpha)Pl^3}{6EJ} \quad \frac{Pl^3}{24EJ}(3\alpha_0 + 4\alpha). \tag{5.14}$$

At the end of the fourth stage, when the force reaches its smallest

value ($\alpha = -1$), the deflection will be equal to

$$u_4(-1) = -\frac{l^3 P}{24EJ}(4 - 3x_0). \qquad (5.15)$$

Comparing this with (5.7), we see that the deflections at the end of the second and at the end of the fourth stage are of the same magnitude but of opposite sign.

Dependencies (5.2), (5.6) and (5.14) are represented in Fig. 29 by straight lines 1, 2, 3 and 4, respectively. If we now follow the displacements of the beam's end as the load increases from the smallest to the largest value then, on considerations similar to those presented for the third and fourth stages, we can easily obtain the dependencies described in Fig. 29 by the straight lines 5 and 6. A hysteresis loop, the area of which is equal to the energy dissipation during one loading cycle and which amounts to:

$$\Psi = 4r_3(0)\, x_0 P = \frac{x_0(1-\alpha_0)P^2 l^3}{2EJ}. \qquad (5.16)$$

is thus obtained.

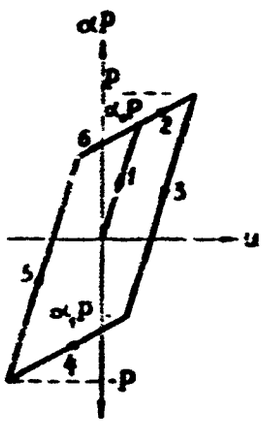

Fig. 29

For estimating the effect of different parameters of the joint, in particular of the pressure between layers, on energy dissipation in the beam, it is convenient to write the last formula in the form

$$\Psi = \frac{2q_0 h l^3 (3P - 4q_0 h)}{3EJ}. \qquad (5.17)$$

By the way, this form of writing explicity exposes the linearity of the relationship $\Psi = \Psi(P)$; Formula (5.16) can create an erroneous impression that the dissipated energy is proportional to the square of the load (actually, quantity α_0 depends on the maximal force P).

As the pressure is increased, the energy dissipation in the system increases at first. We can point out the optimal value of the pressure:

$$p_{опт} = \frac{3P}{8fbh}, \tag{5.18}$$

for which the energy dissipation becomes greatest:

$$\Psi_{max} = \frac{l^2 p}{8Ej}. \tag{5.19}$$

Accordingly, if pressure p is given, then a value of force P* such that the energy dissipation is maximal exists. It can be found from (5.13) that this value amounts to

$$P^* = \frac{8}{3} q_0 h. \tag{5.20}$$

As the load increases, when P > P*, the energy dissipation decreases.

A further increase in the interlayer pressure, above the optimal, ($p > p_{opt}$) results in a decrease in the energy dissipation. If p reaches the limiting value

$$p_{пред} = \frac{3P}{4fbh}, \tag{5.21}$$

then the twin-layered beam acts as if it were continuous for any values of the load up to the greatest loading by force P; energy dissipation due to slip disappears in this case. Accordingly, if the pressure is given, for a force $P < 4/3 q_0 h$ the composite beam acts as a beam with a monolithic cross section.

The absorption coefficient can be determined, for example, as a ratio of the dissipated energy to the greatest energy of deformation of one layer:

$$\psi = \frac{q_0 h (3P - 4q_0)}{6P^2}. \tag{5.22}$$

The absorption coefficient reaches its greatest value for a load P* calculated by Formula (5.20) and decreases sharply with a decreasing load.

The graph constructed by Goodman and Klamp showing the dependence of the absorption coefficient on the amplitude of the greatest stress in the root section as a ratio of the endurance limit is presented in Fig. 30. The graph is constructed for a beam composed of two strips of soft steel, 32.4 cm in length. The cross section of the beam was square (1.27·1.27) cm^2, the height of each layer was (0.5·1.27) cm. The layers were clamped to one another by twenty-five calibrated aluminum brackets uniformly distributed over the length of the beam with a step of 1.27 cm. The pressure with which the strips were clamped reached the value of $p = 5.62$ kg/cm^2.

The friction coefficient at the contact surface was taken as equal to $f = 0.14$. For comparison, the curve showing the variation of the energy absorption coefficient due to absorption in the material is also shown in this graph. As can be seen, energy dissipation related to the structural peculiarities of the beam considerably exceeds losses due to dissipation in the material for any loading values. As pressure p increases this difference becomes even greater. The losses in the material increase under large loads and the values of the two types of energy dissipation tend to even out.

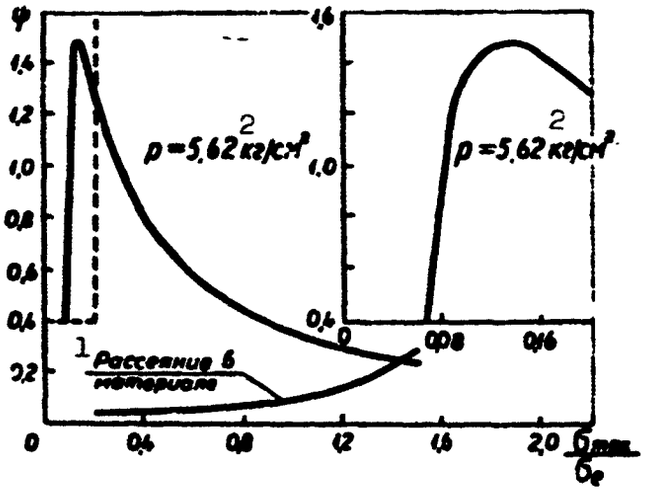

Fig. 30. 1) Dissipation in the material; 2) kg/cm^2.

The experimental investigation performed by Goodman and Klamp of a model of a twin-layered beam, the dimensions and structure of which were described in conjunction with Fig. 30, is of interest. It has been established by special investigations that the friction coefficient $\underline{f}$ depends very little on the contact pressure and remains practically constant as the number of cycles increases from 10^3 to 10^6. It has also been established that in a wide range of slip rates the friction coefficient does not effect the area of the hysteresis loop. Hysteresis loops were taken in the beginning in an almost static mode and with a velocity of 1450 cycles per second – in the second cycle of investigations.

The area of the hysteresis loop calculated by Formula (5.17) for the given beam model for a pressure $p = 5.62$ kg/cm^2 amounts to 0.243 kg-cm/cycle, while when measured in the static mode it was 0.234 kg-cm/cycle and in the dynamic mode, for a frequency of 1030 cycles per second, the area of the loop was equal to 0.241 kg-cm/cycle. These data affirm the permissibility of utilization of the law of dry friction in structural damping problems. In the experiments, alongside with changing the above parameters, the clamping pressure was also varied within the range between 1.406 kg/cm^2 and 9.842 kg/cm^2; the experiments have fully affirmed results obtained from calculations. Figure 31 presents a graph of the dependence of the absorption coefficient calculated by Formula (5.22) on the pressure at the contact surface. The calculated dependence $\psi = \psi(p)$ is shown by the solid line; the points represent the experimental results obtained under static conditions; the results of the dynamic experiments are shown by circles.

Let us now examine in detail the problem of bending of a cantilevered beam with thin pressure plates which is loaded by an end force, cyclically varying with time (Fig. 32a). As has been pointed out in

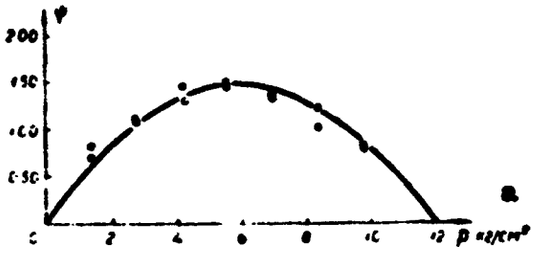

Fig. 31 a) Kg/cm^2.

the introduction, this problem was the first of the problems of the cycle under consideration, it was raised and solved in 1953 by Pian and Hollowell [38].

It is assumed that both pressure plates are clamped to the beam by a pressure p and tangential forces between the beam and the pressure plates are realized only in the form of frcitional forces. If we were to determine these frictional forces over the entire length of the pressure plate by strength of materials formulas, then the condition of the pressure plate's equilibrium (projected on the longitudinal axis) would not be satisfied. It is therefore necessary to assume that slip of pressure plates over the beam takes place at a certain segment of the contact surface. The frictional forces in this region act in the reversed direction and are determined not by the D.I. Zhuravkiy's formula, but by the law of dry friction. The dimensions of the slip region are determined from the conditions of equilibrium of the pressure plate (Fig. 32b).

$$a_1 = \frac{k \cdot Pl}{q_0 k + k \cdot P}, \qquad (5.23)$$

where $k = Fh^2/2J$ is the value of the longitudinal intensity of the frictional forces, constant for a given beam with pressure plates, F is the cross-sectional area of a pressure plate, J is the moment of inertia of the cross section of the beam and the pressure plates and b and h are the width and height of the beam cross section.

When the load increases, the dimensions of the slip region are also increased and embrace half of the contact surface for the load

$$\alpha_0 P = \frac{2qh}{k}.$$

The tangential forces in that part of the contact surface where they are determined by the D.I. Zhuravskiy's formula increase with the increase in the load. At the instant when the force will reach the value $\alpha_0 P$, determined by Formula (5.24), these tangential forces will become equal to q_0, and therefore slip will occur also on the other half of the contact surface, but it will be directed in the opposite direction. Friction forces of opposite direction thus act on each of the halves (Fig. 32c). A further increase in the load will not change the pressure plate loading conditions.

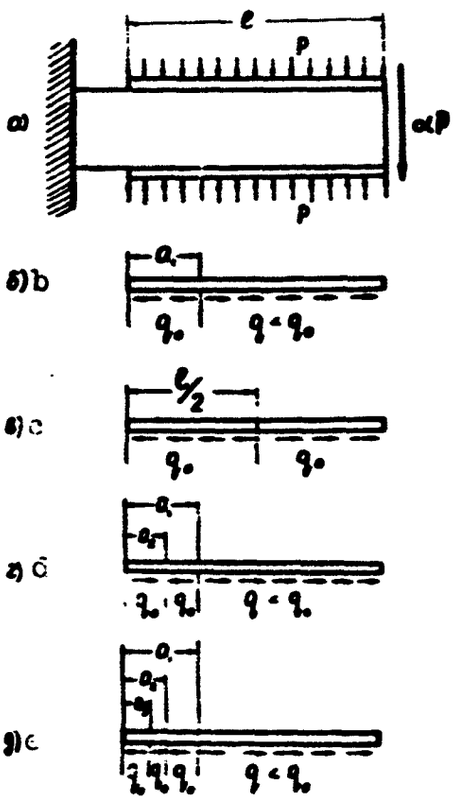

Fig. 32

It should be noted that the position of the slip zone is pointed out by Pian and Hollowell without an appropriate explanation. It is therefore useful to dwell in particular on the problem of the position of the initial slip zone. As has been pointed out, the appearance of the slip zone in the problem under consideration is necessary on static considerations; however the position of this zone cannot be determined from the equilibrium conditions only.

Slip will occur first of all namely at the left end of the pressure plates for the reason that bending moments, resulting in deformations $\varepsilon = M/EW$ in the extreme beam layers,

act on the pressure plates in the corresponding beam sections, while the pressure plates do not experience any longitudinal deformations (the longitudinal forces in these pressure plates' cross sections are zero). Slip of extreme layers of the beam relative to the pressure plates is here inevitable due to the difference in deformations; furthermore, as the loading will increase, slip will be propagated from the left pressure plate ends to their middle. The length of the slip zone is determined at any instant from the condition that the deformations of the pressure plate and the extreme beam fibers at its boundary are identical. The beam seems to have a monolithic cross section at the right sides of the pressure plates and the tangential forces on the contact surfaces are determined by Zhuravskiy's formula.

To analyze the deflections of the beam during different loading stages, it is simplest to consider the bending of the beam without pressure plates, replacing the action of the latter by corresponding tangential forces (or, in a manner of speaking – by distributed bending moments). Figure 33 describes three diagrams of bending moments, corresponding to three ordinary stages of beam loading. These diagrams pertain to a beam without pressure plates; their peculiar form is determined by the peculiarities of the action of the pressure plates over different segments of length.

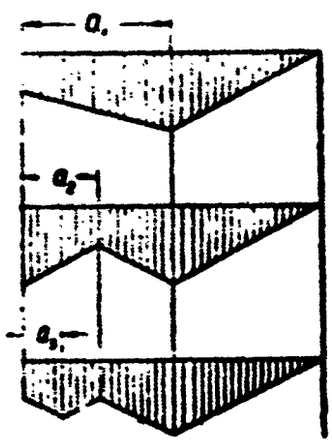

Fig. 33

Utilizing the graphico-analytic method for determination of deflections, we can find that the deflection of the beam's end during each stage amounts to:

$$u_1 = \frac{\alpha P l^3}{3EJ_0} - \frac{qh^3}{6EJ_0}\,\frac{\alpha^2 k^2 P^2 - 2k\alpha Pqk}{(\alpha Pk - qh)^2}. \qquad (5.24)$$

$$u_2 = \frac{\alpha P l^3}{3EJ_0} - \frac{qhl^3}{6EJ_0}\left[\frac{l^2k^2 + 2Pkqh}{(Pk+qh)^2} - \right.$$

$$\left. - 2\frac{(1-\alpha)^2 P^2k^2 + 4(1-\alpha)Pkqh}{[(1-\alpha)Pk+2qh]^2}\right]. \qquad (5.25)$$

$$u_3 = \frac{\alpha P l^3}{3EJ_0} - \frac{qhl^3}{6EJ_0}\left[\frac{P^2k^2 + 2Pkqh}{(Pk+qh)^2} - \right.$$

$$- 2\frac{(1-r)^2P^2k^2 + 4(1-r)Pkqh}{[(1-r)Pk+2qh]^2} +$$

$$\left. + 2\frac{(\alpha-r)^2P^2k^2 + 4(\alpha-r)Pkqh}{[(\alpha-r)Pk+2qh]^2}\right]. \qquad (5.26)$$

here the lengths a_2 and a_3 of slip segments are equal (the length of segment a_1 is given above in Formula (5.23)):

$$a_2 = \frac{(1-\alpha)Pkl}{(1-\alpha)Pk+2q}. \qquad (5.27)$$

$$a_3 = \frac{(\alpha-r)Pkl}{(\alpha-r)Pk+2qh}. \qquad (5.28)$$

A calculation of the area of the hysteresis loop gives

$$\Psi = \frac{P_0^3k^2l^2qh}{6EJ_0(4P_0+qh)^2}. \qquad (5.29)$$

The dependence of the area of the hysteresis loop on the load is close to cubic; as in the majority of previously considered cases, the area of the hysteresis loop is independent of the mean value of the cycle's load.

Experiments performed by Pian and Hollowell on a model of a beam have confirmed that the dependence between the area of the hysteresis loop and the loading amplitude is close to cubic. Figure 34 shows the graph of the dependence of the area of the hysteresis loop on the amplitude of the moment in the root section of the cantilevered beam. Experimental results are denoted by points; the solid line corresponds to the analytic dependence (5.29). Similar dependencies were obtained for three different values of clamping forces.

Let us turn to the scheme of a leaf spring with point contact between the leaves [27]. An elementary model of this system is shown in Fig. 35 and it represents a cantilevered beam built up from two leaves, rigidly inserted in the root section. Shoes are fastened to the leaves at sections close to the ends, so that contact between the leaves is possible only over small surfaces of contact between the shoes and can be considered as point contact. The leaves are held together by a clamp around the end section; this, however, does not prevent possible slip of one leaf relative to another. The clamping force between the leaves is taken as equal to P*. The external load is, in the form of a force αP, applied to the end section of the upper leaf; half of this force is transmitted to the lower leaf through the contact surface.

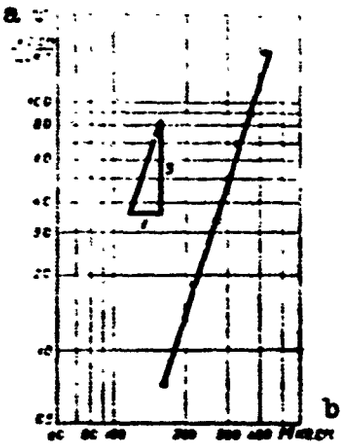

Fig. 34. a) kg-cm/cycle; b) kg-cm.

No slip occurs at the contact surfaces for relatively small values of the external load αP and the spring deforms as a channel-shaped frame with an absolutely rigid cross bar. The transverse force in the frame's cross bar in this case is:

$$Q = \frac{\alpha P l}{4h} \tag{5.30}$$

(h is the distance between the leaves' centers of gravity and l is the length of the spring); here Q is smaller than the limiting force T which is determined by the law of dry friction:

$$T = \left(P^* + \frac{1}{2}\alpha P\right) f. \tag{5.31}$$

The displacement of the end section is, during this stage, determined by the formula

$$u_1(l, \alpha) = \frac{\alpha P l^3}{24EJ}. \qquad (5.32)$$

where EJ is the rigidity in bending of one spring leaf. Segment 1 of the graph (Fig. 36a) corresponds to this loading stage.

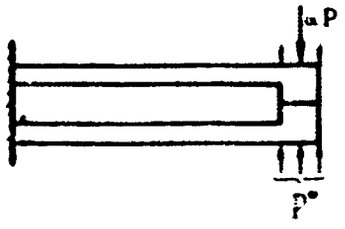

Fig. 35

The first stage of the system's elastic deformation terminates as soon as slip appears in the point of contact. The appearance of slip becomes possible if the transverse force in the cross bar, Q, reaches the value of the limiting force T. There-

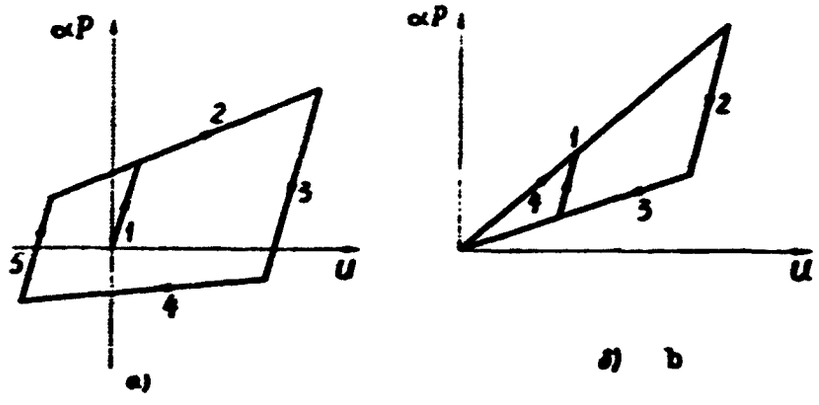

Fig. 36

after the structure begins to act as a system with friction. The load for which slip appears and the second stage begins is determined by the formula

$$\alpha_0 P = \frac{4P^* fk}{l - 2fk}. \qquad (5.33)$$

The displacements of the end section during this stage are determined by the formula

$$u_2(l, \alpha) = \frac{\alpha P l^3}{6EJ} - \frac{(\alpha P + 2P^*) fkl^2}{4EJ}. \qquad (5.34)$$

Segment 2 on the graph (Fig. 36a) corresponds to this dependence. The second term of Expression (5.33) characterizes the frictional properties

of the system. The system's rigidity during this loading stage amounts to $1/2(2 - 3fh/\underline{l})$ of the frame's rigidity $24EJ/\underline{l}^3$. After the load has reached its greatest value ($\alpha = 1$) and begun to decrease, slip ceases and the spring again deforms as a channel-shaped frame with a rigid cross bar. Dependence $u_3 = u_{3(\underline{l},\alpha)}$ on this segment of the hysteresis loop is written in the form

$$u_3(l, \alpha) = \frac{(\alpha + 3)Pl^3}{24EJ} - \frac{P + 2P^*}{4EJ} fh^2 \qquad (5.35)$$

and is represented by segment 3 in Fig. 36a. Here the rigidity is the same as during the first stage.

The third loading stage for the beam terminates when reverse slip appears on the contact surface. Thereafter, the displacement of the end section (segment 3 in Fig. 36a) is determined by the formula

$$u_4(l, \alpha) = \frac{\alpha Pl^3}{6EJ} - \frac{\alpha P + 2P^*}{4EJ} fh^2. \qquad (5.36)$$

If the external load is completely taken off, then, in the presence of initial tension $P^* \neq 0$, the end section does not return to the zero position. The residual deflection will be equal to:

$$u_0(l, \alpha) = \frac{P^* fh^2}{2EJ}. \qquad (5.37)$$

If $P^* = 0$, then the three stages which were considered acquire the character described in Fig. 36b. When the load takes on a minimal value, the third stage ends. Thereafter reverse slip ceases and the system again deforms as a channel-shaped frame on new loading. The displacement of the end section during this fifth loading stage is determined by the formula

$$u_5(l, \alpha) = \frac{(\alpha + 3r)Pl^3}{24EJ} + \frac{rP + 2P^*}{4EJ} fh^2 \qquad (5.38)$$

(segment 5 in Fig. 36a). The fifth stage terminates when direct slip

arises on the contact surface. The end of the fifth stage completes a complete loading cycle. Stages 2 – 3 – 4 – 5 are repeated during subsequent cycles.

The area of the hysteresis loop for an arbitrary characteristic of the cycle is determined by the formula

$$\Psi = \frac{l}{4EJ\sqrt{ab}}\left[Pa\left(P + 4J^{*0}\right) - r^2b\left(r^2 + 4J^{*0}\right) - 32J^{*2}\right], \qquad (5.39)$$

where

$$a = \frac{(l-2fh)^2}{fhl}, \quad b = \frac{(l+2fh)^2}{fhl}. \qquad (5.40)$$

Formula (5.38) shows the peculiar dependence of the area of the hysteresis loop on the clamping effort [applied to] the contact surfaces. As in the case of the cantilevered beam, we can point out an optimal clamping effort for which the energy dissipation in the system becomes maximal; this force is equal to:

$$P^*_{опт} = \frac{(a-rb)P}{16}. \qquad (5.41)$$

There is little energy dissipation due to friction at the contact surface for small values of P*, for P* = 0 it depends only on the external load. If the clamping effort satisfies the inequality

$$P^*_{опт} \geqslant \frac{P}{16}\left[a - rb + \sqrt{(a-rb)^2 + 8(a-r^2b)}\right], \qquad (5.42)$$

then the beam acts as an elastic channel-shaped frame for any loads up to the maximal [load] P; no slip arises on the contact area between the leaves in this case. For the given clamping force we can here point out the load

$$P_{опт} = \frac{16P^*}{a-rb}, \qquad (5.43)$$

which corresponds to maximal energy dissipation.

If the initial pressure between the leaves is absent (P* = 0),

then Formula (5.38) acquires the form

$$\Psi = \frac{fhP}{4EJ\sqrt{ab}}\left[4aP_0P_m - (P_m - P_0)(b-a)\right]. \qquad (5.44)$$

This formula shows distinctly the dependence of the energy dissipation on the mean value of the load. This dependence is a result of the existence of a relationship between the frictional forces and the external load. It is not difficult to notice that, in the absence of this relationship, when T = fP*, the limiting frictional force is independent of the external load and the second term vanishes in Formula (5.31); the Formula for the area of the hysteresis loop (5.39) acquires the form

$$\Psi = \frac{2fhl}{EJ}\left[P_0P^*l - 4P^{*2}fh\right]. \qquad (5.45)$$

Below are presented results of static and dynamic tests of a model of a two-leaf spring. The schematic of the installation is shown in Fig. 37. The spring leaves were made from spring steel, the length of the

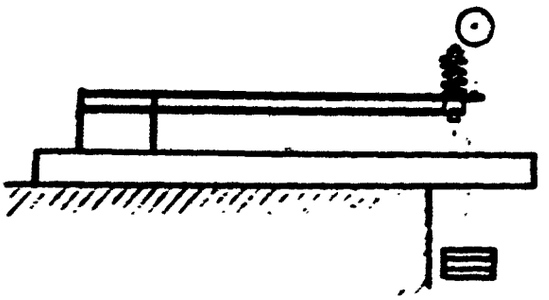

Fig. 37

leaves l = 500 mm and the dimensions of the leaf cross sections t x b = 8 x 65 mm. The contact surfaces were cleaned to remove the skin and were degreased.

The areas of the hysteresis loops were measured under static conditions (cycle length 3-4 minutes) after the joint had been properly conditioned (10^3 cycles) under dynamic conditions.

The curves of damped vibrations were recorded during the dynamic tests by a tensometer installation with wire sensors. Then the energy dissipation during one cycle was determined by the curve in the usual manner for different amplitudes.

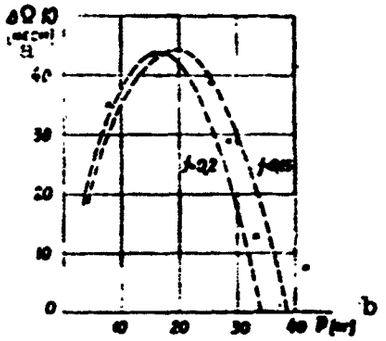

Fig. 38. a) Kg-cm;
b) kg.

Figure 38 presents a graph of the dependence of the area of the hysteresis loop on the force with which the leaves are clamped together. The results of calculations for a symmetrical cycle for two values of the friction coefficient f = 0.20 and f = 0.25, by Formula (5.39) are shown by the solid line. Experimental results are denoted by points. The experiments confirm the existence of an optimal clamping force P^*_{opt}, for which the greatest energy dissipation exists in the joint for a given external load.

For large clamping forces (considerably larger than P_{opt}) the experimental points do not agree with analytic results. This is due to the fact that the experimentally measured energy dissipation depends not only on the friction in the slip region but also on other factors (energy dissipation in the beam's fastening and in its material). Hysteresis of another type acquires dominating significance for large clamping efforts. Ratio $\Psi_{max} : \Psi_{min}$ can be utilized for estimating the relative importance of losses; as can be seen, the relationship between the two types of losses for a spring on optimal clamping P^*_{opt} fluctu-

ates between 8 and 10.

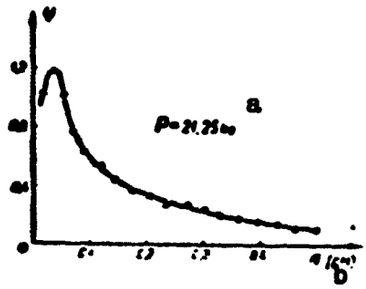

Fig. 39. a) Kg; b) [cm].

Figure 39 shows the graph of variation of the absorption coefficient as a function of the amplitude of the damped vibrations; theoretically calculated results are also presented for comparison. The experiments point to an increase of the absorption coefficient with decreasing amplitudes. However, for a preset value of the amplitude of vibrations slip vanishes from the contact surface, rigid coupling between the leaves takes over and the spring begins to act as an elastic system; in addition energy dissipation due to friction on the contact surface also ceases. The fact that cohesion takes place between the contact surfaces is also expressed by the fact that a change in the rigidity of the system, and together with this in the frequency of natural oscillations, takes place. Figure 40 presents an experimental graph of the variation of the frequency of a system's natural oscillations as a function of the amplitude of oscillations.

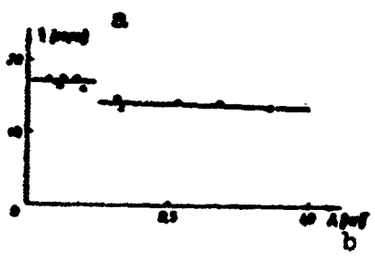

Fig. 40. a) Cycles per second; b) [mm].

Similar experimental results were obtained also in investigations of stacked joints of flat cantilevered rods (multileaf spring of the cantilever type) with point contact between them.

§6. TRANSVERSE BENDING OF A MULTILAYERED CANTILEVER

The Goodman and Klamp problem on bending of a two-layer cantilever considered in the preceding paragraph can be extended to the case when the cantilever consists of many layers (Fig. 41). Let us assume that the layers are identical (made from the same material and having iden-

tical dimensions) and the compression intensity between the layers is constant along the beam length for all contact surfaces. The cantilever is loaded at the end by a periodic force αP, the coefficient of which varies within the limits of $-1 \leq \alpha \leq 1$.

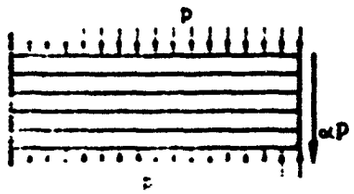

Fig. 41

Let us first turn to a three-layered beam (Fig. 42a). The first process of loading the beam ($0 \leq \alpha \leq 1$) consists of two stages. During the first stage, when the tangential forces on the contact surfaces are sufficiently small and satisfy the inequality

$$q = \frac{4\alpha P}{9h} < q_0. \qquad (6.1)$$

no slip occurs between the layers and the cantilever bends as a beam of a monolithic cross section. The deflection at the beam's end will here be:

$$u_1(\alpha) = \frac{\alpha P l^3}{81 EJ}. \qquad (6.2)$$

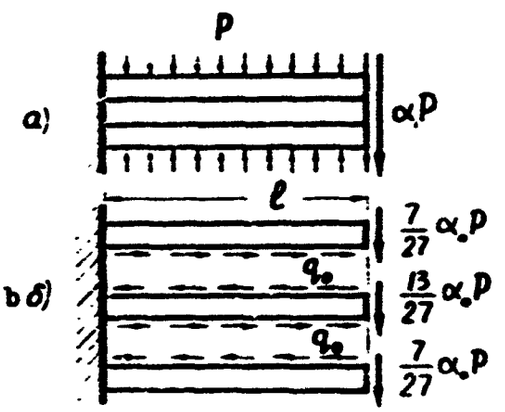

Fig. 42

Symbols b, h and $J = bh^3/12$ in Formulas (6.1) and (6.2) denote, respectively, the dimensions of the cross section and the moment of inertia of a single beam layer.

The first stage will be terminated at the instant when the tangential forces determined by Formula (6.1) will reach the value q_0. The force here has the value

$$\alpha_0 P = \frac{9}{4} q_0 h, \qquad (6.3)$$

and the deflection of the end amounts to

$$u_1(\alpha_0) = \frac{\alpha_0 Pl^3}{81EJ}. \qquad (6.4)$$

Force $\alpha_0 P$ is not distributed uniformly between the layers: 7/27 $\alpha_0 P$ is devolved upon each of the extreme layers and 13/27 $\alpha_0 P$ upon the median layer. This distribution can be found from the tangential forces diagram or from the equality of deflections of the ends of the median and extreme layers due to the load shown in Fig. 42b.

During the second stage ($\alpha_0 \leq \alpha \leq 1$), as soon as the force exceeds the value $\alpha_0 P$, simultaneous slip along both contact surfaces takes place over the entire length of the cantilever. The beam loses its monolithicity and subsequently bends as three separate beam-layers; since the deflections of these layers are identical, the load increase $(\alpha - \alpha_0)P$ will be equally distributed between the layers. The deflection of the cantilever end is here determined by the formula

$$u_2(\alpha) = u_1(\alpha_0) + \frac{Pl^3}{9EJ}(\alpha - \alpha_0) = \frac{Pl^3}{81EJ}(9\alpha - 8\alpha_0). \qquad (6.5)$$

At the end of the second stage, when the force reaches its greatest value ($\alpha = 1$), the deflection will be

$$u_2(1) = \frac{Pl^3}{81EJ}(9 - 8\alpha_0).$$

The unloading process also consists of two stages. During the first stage, when the load decreases, ($\alpha^*_0 \leq \alpha \leq 1$), the cantilever again bends as a beam with a monolithic cross section. The tangential forces on the contact surfaces

$$q = q_0 - \frac{4(1-\alpha)P}{9h} \qquad (6.6)$$

and the deflection of the beam's end

$$u_3(\alpha) = u_1(1) - \frac{(1-\alpha)Pl^3}{81EJ} = \frac{Pl^3}{81EJ}(8 - 8\alpha_0 + \alpha). \qquad (6.7)$$

If the load is completely removed ($\alpha = 0$), then the beam, obvious-

ly, will not return to its initial position. The residual deflection

$$u_3(0) = \frac{8Pl^3}{81EJ}(1 - \alpha_0).$$

The first stage of the unloading process will terminate at the instant when the tangential forces determined by Formula (6.6) will reach the value q_0 with a minus sign. The coefficient α_0^*, corresponding to the force at the end of the third stage

$$\alpha_0^* = 1 - \frac{9q_0h}{2P} = 1 - 2\alpha_0 \qquad (6.8)$$

is determined from this condition.

During the second unloading stage ($-1 \leq \alpha \leq \alpha_0^*$), as soon as the force becomes smaller than $\alpha_0^* P$, slip again occurs between the layers. But now the layers will be displaced in a direction opposite to the direction of slip during the second loading stage.

The deflection of the beam's end during the second unloading stage is determined from the formula

$$u_4(\alpha) = u_3(\alpha_0^*) - \frac{Pl^3}{9EJ}(\alpha_1 - \alpha) = \frac{Pl^3}{81EJ}(8\alpha_0 + 9\alpha). \qquad (6.9)$$

At the end of this stage, when $\alpha = -1$, the deflection will be

$$u_4(-1) = -\frac{Pl^3}{81EJ}(9 - 8\alpha_0).$$

As can be seen, the magnitude of the deflection for the smallest value of the force is equal to the deflection due to the greatest load magnitude, but is of opposite sign.

If we now again increase the force, varying the load coefficient between the limits from -1 to $+1$, then it becomes necessary to consider a secondary loading process which is fully analogous to the unloading process. The hysteresis loop can be constructed by Dependencies (6.2), (6.5), (6.7) and (6.9). A sample of its shape is given in Fig. 43. Curve 0 – 1 – 2 corresponds to the first loading period, curve 2 – 1* – 2* – t

the unloading period and the dashed curve – to the secondary loading period. The area of the hysteresis loop will be:

$$\Psi = 4u_3(0)\alpha_0 P = \frac{32\alpha_0(1-\alpha_0)P^2l^3}{81EJ}. \qquad (6.10)$$

Let us pass on to the consideration of a beam consisting of many identical layers (Fig. 41). Let us assume that n, the number of layers, is odd. The median layer will be called the first, and the numbering of layers will be subsequently extended for one, upper half of the beam, starting from the median layer to the extreme layer. The same numbering [system] is also retained for layers situated below the median layer.

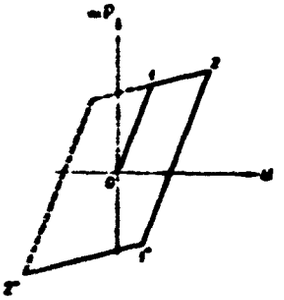

Fig. 43

Let us consider the first loading period, when the force increases from 0 to P. The first stage of this period is characterized by the fact that the tangential forces on all contact planes are smaller than their limiting value $q \leq q_0$. The cantilever bends as a beam of monolithic cross section; the tangential forces at an area situated at a distance y from the neutral layer are determined by the formula

$$q = \frac{\alpha P(\pi^2k^2 - 4y^2)}{8\pi^3 J}, \qquad (6.11)$$

and the deflections at the end will be

$$u(\alpha) = \frac{\alpha P l^3}{3\pi^3 EJ}. \qquad (6.12)$$

In particular, the tangential forces at the contact planes of the first layer (y = 1/2h) will be:

$$q_1 = \frac{3\alpha P(\pi^2 - 1)}{2\pi^3 k}. \qquad (6.13)$$

The first loading stage will terminate at the instant when these tangential forces will reach the value q_0. The value of the force

$\alpha_{01}P$, corresponding to the end of the first stage, is determined from Formula (6.13), if we set in it $q_1 = q_0$:

$$\alpha_{01}P = \frac{2n^3}{3(n^2-1)} q_0 h; \tag{6.14}$$

the value of the end deflection will here be:

$$u(\alpha_{01}) = \frac{\alpha_{01} l^3 P}{3n^3 EJ} = \frac{2q_0 l^3}{9(n^2-1)EJ}. \tag{6.15}$$

As soon as the load becomes greater than $\alpha_{01}P$, slip will occur along the contact planes of the first layer. The cantilever cross section is no longer monolithic and we now have three beams which bend together: the first layer and two banks, composed of layers situated above and below the first layer. The simultaneousness of bending of these three beams is expressed in identity of the deflections, and therefore the load increase $(\alpha - \alpha_{01})P$ is distributed between the beams proportional to their rigidities in bending.

It can be shown that secondary slip will occur along surfaces of contact between the second and third layers. The slip between layers will subsequently be propagated, with increasing load, from the middle to the extreme layers. For the sake of brevity, those beam layers which are subject to slip conditions will be called displaced. It is convenient to follow the process of slip transition from one contact plane to another on a tangential force diagram in any cross section of the cantilever (Fig. 44).

Let us consider the upper half of the section. Parabola q_1, analytically expressed by Formula (6.11), corresponds to the beginning of first slip. This parabola passes through the points $q_1 = 0$, $y = nh/2$ and $q_1 = q_0$, $y = h/2$. Secondary slip will occur at the instant when the tangential force diagram will be described by parabola q_2, which should pass through the points $q_2 = 0$, $y = nh/2$; $q_2 = q_0$, $y = 3/2h$ and

$q_2 = q_0$, $y = h/2$. Let us denote the corresponding value of the force by $\alpha_{02}P$. Since the bending of the already displaced layer also increases as the force is increased from $\alpha_{01}P$ to $\alpha_{02}P$, this layer will also accept a part of the load increment. Subsequent load increase to the value $\alpha_{03}P$ results in a third slip, with parabola q_3 corresponding to it, etc.

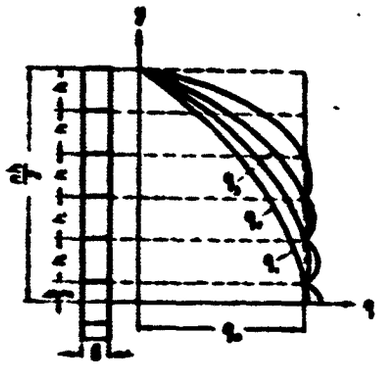

Fig. 44

Let the slip reach the kth contact plane when the magnitude of the force is $\alpha_{0k}P$ (Fig. 45). It is obvious that this plane is situated between layers k and k + 2. At the same time, the diagram of tangential forces on that part of the section which is situated between the kth and the extreme layer is described by parabola q_k, whose equation is

$$q_k = \frac{q_0}{k^2(n-k+2)(n-k)}\left[-4y^2 + 4(k-1)hy + k^2n(n-2k+2)\right]. \qquad (6.16)$$

In this formula k is the number of displaced layers. Since the slip process occurs simultaneously below as well as above the median layer, therefore k = 1, 3, 5, ... (n − 2). In particular, Dependence (6.11) corresponding to the first slip is obtained from Formula (6.16) for k = 1, the second slip will take place for k = 3, etc.

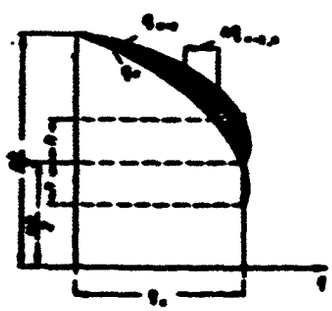

Fig. 45

Slip between layers (k + 2) and (k + 4) will occur when the force will have the value $\alpha_{0,\ k+2}P$, when the diagram of tangential forces in the extreme layers (6.5) will be represented by the parabola

$$q_{k+2} = \frac{q_0}{k^2(n-k)(n-k-2)}\left[-4y^2 + 4(k+1)hy + k^2n(n-2k-2)\right]. \qquad (6.17)$$

This expression is obtained from (6.16) by replacing $\underline{k}$ by (k + 2).

Thus, a load increase by the value

$$\Delta P_{(k+2),\,k} = (a_{0,\,k+2} - a_{0,\,k})P \tag{6.18}$$

displaces slip past one layer, if we consider only one half of the beam section. The load increment increases the tangential forces not only in the bank of extreme layers, but also in each of the displaced layers.

The tangential forces in the bank of extreme layers will increase by the value

$$\Delta q_{(k+2),\,k} = q_{k+2} - q_k = \frac{4q_0}{k(n-k)[(n-k)^2-4]} \cdot \\ \cdot [-4y^2 + 2(n+k)ky - k^2 nk]. \tag{6.19}$$

Force $\Delta Q_{k+2,k}$, corresponding to such an increment of the tangential stresses at one half of the cross section, is numerically equal to the area crosshatched in Fig. 45.

$$\Delta Q_{k+2,k} = \int_{\frac{kh}{2}}^{\frac{nh}{2}} \Delta q_{k+2,k}\,dy = \frac{(n-k)^2}{(n-k)^2-4} qh. \tag{6.20}$$

Let us denote the increment of the transverse force in one displaced layer, when the load increases by ΔP_k, by ΔQ_1. Each of the $\underline{k}$ displaced layers will have this increment of the shear force. Consequently, the load increment can be written in the form of an equality

$$\Delta P_{k+2,k} = 2\Delta Q_{k+2,k} + k\Delta Q_1. \tag{6.21}$$

In addition, quantities $\Delta Q_{k+2,k}$ and ΔQ_1 are related to one another by the condition of equality of the deflections of the extreme layer bank and one displaced layer, i.e.,

$$\Delta u_k = \frac{8\Delta Q_{k+2,k} l^3}{3(n-3)^3 EJ} = \frac{\Delta Q_1 l^3}{3EJ}. \tag{6.22}$$

From this

$$\Delta Q_k = \frac{8\Delta Q_k}{(n-k)^3}. \tag{6.23}$$

Consequently, we can write Equality (6.21) in the form

$$\Delta P_{k+2,k} = \frac{2(n-k)^3+8k}{(n-k)^3}\Delta Q_{k+2,k}. \tag{6.24}$$

Substituting here $\Delta Q_{k+2,k}$ from (6.20), we get

$$\Delta P_{k+2,k} = \frac{2(n-k)^3+8k}{(n-k)[(n-k)^3-4]}q_0 h. \tag{6.25}$$

The increment of force $\alpha_{0k}P$, necessary for the slip to be displaced through one layer, is determined by this formula.

The following dependence between the values of the load at the ends of two adjacent loading stages is now obtained from Formula (6.18):

$$\alpha_{0,k+2}P = \alpha_{0,k}P + \Delta P_{k+2,k} = \alpha_{0,k}P + \frac{2(n-k)^3+8k}{(n-k)[(n-k)^3-4]}q_0 h. \tag{6.26}$$

Dividing through all the terms of this equality by the maximal value of the load P, we will obtain the relationship between the loading coefficients of two adjacent loading stages

$$\alpha_{0,k+2} = \alpha_{0,k} + \frac{2(n-k)^3+8k}{(n-k)[(n-k)^3-4]}\cdot\frac{q_0 h}{P}. \tag{6.27}$$

If we utilize Equality (6.14) then we can represent this relationship by the coefficient $\alpha_{0,1}$, corresponding to the first slip, i.e.,

$$\alpha_{0,k+2} = \alpha_{0,k} + \frac{3(n^2-1)[2(n-k)^3+8k]}{2n^3(n-k)[(n-k)^3-4]}\alpha_{01}. \tag{6.28}$$

Formulas (6.26) and (6.27) represent recurrent dependencies, making it possible, starting with the first stage, to obtain the values of loads successively at the end of the second, third, fourth, etc., loading stages. The stage corresponding to $k = n - 4$, when slip will reach the extreme beam layers, will be the one before last. Thereafter the beam will act as n separate layers which have identical deflections.

Let us now turn to the determination of deflections of the beam's

end during different loading stages. The deflection at the end of the first stage is determined by Formula (6.12). Let the deflection have the value $u(\alpha_{0,k})$ at the instant layer $\underline{k}$ is slipping. Then the force increment $\Delta P_{k+2,k}$ increases the slip region again by one layer from each side and results in a deflection increment by the value Δu_k. Consequently, the deflection due to force $\alpha_{0,k+2}P$ can be written in the form

$$u(\alpha_{0,k+2}) = u(\alpha_{0,k}) + \Delta u_k. \tag{6.29}$$

The value of the deflection increment Δu_k is determined from Formula (6.22), where $\Delta Q_{k+2,k}$ from (6.24) should be substituted. Finally, we will get

$$u(\alpha_{0,k+2}) = u(\alpha_{0,k}) + \frac{8q_0 h^3}{3(n-k)[(n-k)^2-4]EJ}. \tag{6.30}$$

If we substitute here $q_0 h$ from (6.14), then

$$u(\alpha_{0,k+2}) = u(\alpha_{0,k}) + \frac{4(n^2-1)}{n^3(n-k)[(n-k)^2-4]} \cdot \frac{\alpha_{nn}PP^3}{EJ}. \tag{6.31}$$

We have obtained a recurrent formula, relating the deflections of the beam's end during two adjacent loading stages. Deflections of stages starting with the second and ending with the one before the last are determined by this formula. During the last loading stage, when slip has embraced all contact surfaces and the cantilever bends as a system of separate beam-layers, the deflections are determined from the following equality:

$$u(\alpha) = u(\alpha_{0,n-2}) + \frac{(\alpha + \alpha_{0,n-2})P^3}{3nEJ}. \tag{6.32}$$

Here $1 \geq \alpha \geq \alpha_{0,n-2}$.

When the force reaches its greatest value, the deflection will be:

$$u(1) = u(\alpha_{0,n-2}) + \frac{(1-\alpha_{0,n-2})P^3}{3nEJ}. \tag{6.33}$$

We shall now consider the unloading period, during which the force is decreased from P to − P. The values of load coefficients will be denoted by α^*. Stages analogous to those already considered in the first loading period can be observed during the unloading period. During the first unloading stage the cantilever bends as a beam with a monolithic cross section. The tangential forces in all layers of the cross section decrease during this time. In particular, the tangential forces on contact surfaces, displaced when the layers were loaded, i.e., for y = kh/2, will be

$$q = q_0 - \frac{(1-\alpha^*)k^2(\pi^2-k^2)Pb}{8\pi^2 J}. \qquad (6.34)$$

The displacement of the beam's end during the first unloading stage will be found as the difference between the deflection for the greatest value of the force and the deflection due to a change in the load by $(1 - \alpha^*)P$:

$$u(\alpha^*) = u(1) - \frac{(1-\alpha^*)Pl^3}{3\pi^2 EJ}. \qquad (6.35)$$

The first stage will terminate when the tangential forces at the contact surfaces of the first layer will reach the value q_0, i.e., $q = -q_0$. The value of the load coefficient at the end of the first unloading stage is determined from this condition. Utilizing Equality (6.14), we will get

$$\alpha_{01}^* = 1 - \frac{4\pi^2 q_0 h}{3(\pi^2-1)P} = 1 - 2\alpha_{01}. \qquad (6.36)$$

The result obtained for a multilayered beam will naturally be the same as for a beam formed by two or three identical layers. As can be seen, the absolute value of the force during the first unloading stage becomes twice as large as on the first loading stage. This is due to the fact that a force equal in magnitude to $\alpha_{01}P$ is needed

at the beginning of unloading so that the tangential forces on the contact surfaces of the first slip should become zero. The same magnitude of force is subsequently also needed so that the tangential forces on the same planes, on changing their sign, should again become equal to q_0.

Substituting α^*_{01} from (6.36) into (6.35), we will get the deflection at the end of the first unloading stage:

$$u(x^0_{01}) = u(1) - \frac{2\alpha_{01} P l^3}{3\pi^3 EJ}. \qquad (6.37)$$

Slip along the contact surface of the first layer will occur as soon as the force will become greater than $\alpha^*_{01}P$. On subsequent decrease of the force slip will be propagated from the middle to the extreme edges of the beam. But now the direction of relative displacements of the layers will be opposite to that existing during the loading stage.

The process of layer slippage with a decreasing force is analogous to the just considered process during the loading period. It should, however, be taken into account that the change in the force necessary for displacement of slip through one layer will, during each unloading stage, be twice as great as during the first loading period. Therefore the recurrent formula (6.27) takes on, in this case, the form

$$x^0_{0,k+2} = x^0_{0,k} + \frac{2(n-k)^2 + 8k}{(n-k)\left[(n-k)^2 - 4\right]} \cdot \frac{2q_0 k}{P} \qquad (6.38)$$

or

$$x^0_{0,k+2} = x^0_{0,k} + \frac{3(n^2-1)\left[2(n-k)^2 + 8k\right]}{n^3(n-k)\left[(n-k)^2 - 4\right]} \alpha_{01}. \qquad (6.39)$$

Formula (6.31) is also similarly modified. Now the deflections at the ends of two adjacent unloading stages are related by the rela-

tionship

$$u(\alpha^*_{k,\,k+2}) = u(\alpha^*_{k,\,k}) + \frac{8(n^2-1)}{n^2(n-k)\left[(n-k)^2-1\right]} \cdot \frac{\alpha_{01} P l^3}{EJ}. \qquad (6.40)$$

During the last unloading state, when slip has occurred on all contact surfaces and the cantilever bends as a system of separate layers under the action of a force varying between $\alpha^*_{0,n-2}P$ and P, the deflection is determined from Formula (6.33). The deflection for the smallest value of the load will be:

$$u(-1) = u(\alpha^*_{k,\,n-2}) - \frac{(1+\alpha^*_{k,\,n-2})Pl^3}{3nEJ}. \qquad (6.41)$$

The period of the renewed load increase, now from the smallest to the largest value, fully repeats the unloading period. Formulas (6.35), (6.39) and (6.40) remain valid for this period.

The character of the hysteresis loop on transverse bending of a multilayered cantilever is shown in Fig. 46. The area of this loop can be calculated by the formula

$$\Psi = 2\int_{u(-1)}^{u(1)} \left[P\frac{u(\alpha)}{u(1)} - P(\alpha^*)\right] du(\alpha). \qquad (6.42)$$

The first term in the square braces represents the equation of a straight line connecting points 5 and 5*, the second term – the unloading curve between the same points.

As an example, let us consider a beam consisting of nine layers (n = 9). The first loading period ($0 \leq \alpha \leq 1$). The load coefficient and the deflection at the end of the first stage are calculated by Formulas (6.14) and (6.15):

$$\alpha_{01} = \frac{2 \cdot 9^2}{3(9^2-1)} \frac{q^k}{P} =$$

$$= 6{,}06 \frac{q^k}{P},$$

$$u(\alpha_{01}) = \frac{\alpha_{01} Pl^3}{3 \cdot 9^2 EJ}.$$

The load coefficient and the value of the deflection at the ends of the second, third and fourth stages are subsequently found by Formulas (6.28) and (6.31).

The second stage, k = 1.

$$\alpha_{0,3} = \alpha_{01} + \frac{(9^2-1)\cdot 3\,[2(9-1)^2+8\cdot 1]}{2\cdot 9^3\,[(9-1)^2-4]}\,\alpha_{01} = 1{,}355\alpha_{01},$$

$$u(\alpha_{0,3}) = \frac{\alpha_{01}Pl^3}{3\cdot 9^3EJ} + \frac{4\cdot(9^2-1)}{9^3(9-1)\,[(9-1)^2-4]}\cdot\frac{\alpha_0 Pl^3}{EJ} = \frac{\alpha_{01}Pl^3}{9^3EJ}.$$

The third stage, k = 3.

$$\alpha_{2,5} = 1{,}355\alpha_{01} + \frac{3(9^2-1)\,[2(9-3)^2+8\cdot 3]}{2\cdot 9^3\,[(9-3)^2-4]}\,\alpha_{01} = 1{,}747\alpha_{01},$$

$$u(\alpha_{0,5}) = \frac{\alpha_{01}Pl^3}{9^3EJ} + \frac{4(9^2-1)}{9^3(9-3)\,[(9-3)^2-4]}\cdot\frac{\alpha_{01}Pl^3}{EJ} =$$

$$= 2{,}667\,\frac{\alpha_{01}Pl^3}{9^3EJ}.$$

The fourth stage, k = 5.

$$\alpha_{4,7} = 1{,}747\alpha_{01} + \frac{3(9^2-1)\,[2(9-5)^2+8\cdot 5]}{2\cdot 9^3\,[(9-5)^2-4]}\,\alpha_{01} = 2{,}324\alpha_{01},$$

$$u(\alpha_{4,7}) = 2{,}667\,\frac{\alpha_{01}Pl^3}{9^3EJ} + \frac{4(9^2-1)}{9^3(9-5)\,[(9-5)^2-4]}\cdot\frac{\alpha_{01}Pl^3}{EJ} =$$

$$= 9{,}333\,\frac{\alpha_{01}Pl^3}{9^3EJ}.$$

During the fifth stage, when the cantilever bends as a system of separate layers, we find by Formula (6.33):

$$u(1) = 9{,}333\,\frac{\alpha_{01}Pl^3}{EJ} + \frac{(1-2.324\alpha_{01})Pl^3}{3\cdot 9\cdot EJ} = (27-53.42\alpha_{01})\,\frac{Pl^3}{9^3EJ}.$$

The polygonal line 0 – 1 – 2 – 3 – 4 – 5 in Fig. 46 represents the relationship between the end deflections and the load variation during the first loading period. Loads, which should be multiplied by P, are laid off on the ordinate axis, and the deflection coefficients, which should be multiplied by $Pl^3/9^3EJ$ – on the abscissa axis. For the sake of definiteness of construction, coefficient α_{01} was taken to be equal to 0.4.

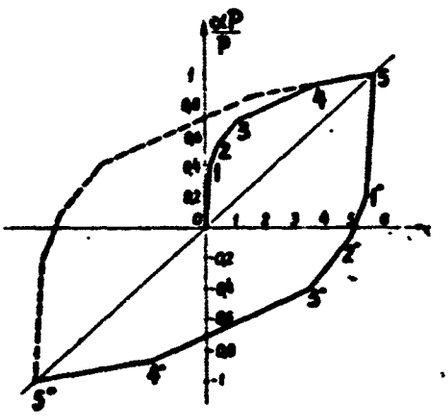

Fig. 46

The number at the point where the line is broken corresponds to the end of the corresponding loading stage.

The unloading period. The value of the load coefficient and the deflection at the end of the first stage are found by Formulas (6.36) and (6.37):

$$\alpha_{01}^{\circ} = 1 - 2\alpha_{01};$$

$$u^{\circ}(\alpha_{01}^{\circ}) = (27 - 53{,}42\alpha_{01})\frac{Pl^3}{9^3EJ} - \frac{2\alpha_{01}Pl^3}{3 \cdot 9EJ} = (27 - 54{,}1\alpha_{01})\frac{Pl^3}{9^3EJ}.$$

The value of the load coefficient and of the deflection at the end of the second, third and fourth stages will be found by Formulas (6.39) and (6.40). The constant quantity

$$\frac{3(n^2-1)}{n^3} = \frac{3(9^2-1)}{9^3} = 0{,}33.$$

enters these formulas.

The second stage, k = 1.

$$\alpha^{\bullet}_{0,3} = 1 - 2\alpha_{01} - \frac{0{,}33\,(2\cdot 8^3 + 8\cdot 1)}{8\cdot(8^2-4)}\alpha_{01} = 1 - 2{,}71\alpha_{01};$$

$$u(\alpha^{\bullet}_{0,3}) = \left(27 - 54{,}1\alpha_{01} - \frac{8\cdot(8^2-1)}{8\,(8^2-4)}\alpha_{01}\right)\frac{Pl^3}{9^3\,EJ} =$$

$$= (27 - 58{,}76\alpha_{01})\frac{Pl^3}{9^3\,EJ}.$$

The third stage, k = 3.

$$\alpha^{\bullet}_{0,5} = 1 - 2{,}71\alpha_{01} - \frac{0{,}3\,(2\cdot 6^3 + 8\cdot 3)}{6\,(6^2-4)}\alpha_{01} = 1 - 3{,}51\alpha_{01};$$

$$u(\alpha^{\bullet}_{0,5}) = \left[27 - 55{,}43\alpha_{01} - \frac{8\cdot 80}{6\,(6^2-4)}\alpha_{01}\right]\frac{Pl^3}{9^3\,EJ} =$$

$$= (27 - 58{,}76\,\alpha_{01})\frac{Pl^3}{9^3\,EJ}.$$

The third stage, k = 5.

$$\alpha^{\bullet}_{0,7} = 1 - 3{,}51\alpha_{01} - \frac{0{,}33\,(2\cdot 4^3 + 8\cdot 5)}{4\,(4^2-4)}\alpha_{01} = 1 - 4{,}67\alpha_{01}.$$

$$u(\alpha^{\bullet}_{0,7}) = \left[27 - 58{,}76\alpha_{01} - \frac{8\cdot 80}{4\,(4^2-4)}\alpha_{01}\right]\frac{Pl^3}{9^3\,EJ} =$$

$$= (27 - 72{,}1\alpha_{01})\frac{Pl^3}{9^3\,EJ}.$$

The deflection at the end of the fifth unloading stage is calculated by Formula (6.41):

$$u(-1) = (27 - 72{,}1\alpha_{01})\frac{Pl^3}{9^3\,EJ} - \frac{(1 + 1 - 4{,}67\alpha_{01})Pl^3}{3\cdot 9\,EJ} =$$

$$= (-27 + 53{,}9\alpha_{01})\frac{Pl^3}{9^3\,EJ}.$$

As can be seen when the results of calculations are plotted on a logarithmic scale, the magnitude of displacement u(– 1) almost coincides with that of u(1).

The unloading stage is in Fig. 46 represented by the dashed line 5 – 1* – 2* – 3* – 4* – 5*. If the force now increases from the smallest to the greatest value, then the line shown by dashes in Fig. 46 can be obtained similarly.

The area of the hysteresis loop can now be calculated by Formula (6.42).

§7. TRANSVERSE BENDING OF A THIN-WALLED BEAM

Let us determine the energy dissipation in a thin-webbed riveted beam. We will assume a simplified computational scheme, assuming that the beam web works in shear and the flanges and standards in compression-tension. In this case the bending moment in each beam cross section is taken up by the flanges and the transverse force by the web. We shall consider the above problem for relationships between the acting load and the wall dimensions such that the shear has not as yet caused the wall to lose stability.

Since structural damping is due to the friction of components joined with one another, it is necessary to investigate relative displacements between the rods (flanges and standard) and the wall in the case of thin-webbed beams. Energy dissipation occurs in the seams at which the web is connected to the rods. The problem consists in finding the energy absorbed by the seams during one loading cycle.

Let us consider a purely frictional scheme of the problem, when tangential forces between the rods and the web are created only in the form of friction. We do not go into the factors that compressed the web to the rods. This, for example, might be tightening by clamps or rivets if the rivet shanks do not fill the holes. The important thing is that such compression exists and the factor causing it does not by itself prevent the possible displacements of the web relative to the rods. Only frictional forces between the web and the rods prevent these displacements within certain limits. It is assumed that the frictional forces obey the law of dry friction and the deformation of the elements from which the beam is built up lie within the limits of proportionality.

It is convenient to clarify the peculiarities of the problem under consideration on a simple example of a single-panel beam (See Fig. 9)

formed by a wall flanged by two parallel flanges and two standards. The beam is fastened at nodes A and B and is loaded by a variable force αP at node C.

When force αP acts in any vertical section of the beam, according to the assumed scheme, two normal forces causing tension in one flange and compression in the other and also tangential forces in the web, the intensity of which is found from the formula

$$q = \alpha \frac{P}{H}, \tag{7.1}$$

where H is the computational height of the beam, will arise. We wish to attract the reader's attention to the fact that in this paragraph q denotes the magnitude of tangential forces in the web of the beam.

As a result of longitudinal deformations of the flanges and standards, and also of the shear deformation in the wall, the panel will warp and the point C, where the force is applied, will be displaced. Determining this displacement, by the Mohr's method, for example, possible slip of the web in the region of the seams relative to the standards and flanges is usually not taken into account. It is precisely during this slip that the frictional forces do their work. Finding the relative displacements of the web and the rods in the region of the seams we will further simplify the problem and we will assume that the rods are absolutely rigid and the sought displacemements are due to the shear deformation of the wall.

Since the seam is under the same loading conditions along the entire perimeter of the joint, it is sufficient to consider a seam element the length of which is unity. Let us isolate a unit seam element for example, from the lower flange (Fig. 47) and let us orient it to an orthogonal xy coordinate system, directing the x-axis parallel to the axis of the flange and the y-axis in the plane of the wall. The

width within the limits of which the wall is clamped between the flanges is shown in this figure by the letter a.

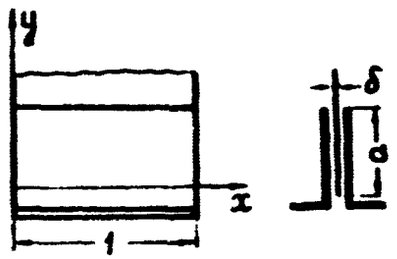

Fig. 47

Let us clarify what takes place, as the force αP is varied, on that segment of the web which is pressed to the rod. Let us consider the first loading stage, when α varies from zero to a certain moderate value α_1. As soon as the force is applied tangential forces and shear deformations corresponding to it will arise in the web. These deformations extend only to a certain depth a_1 (Fig. 48) measured from the top edge of the rod; it is only over this width that slip of the web relative to the rod will take place. Frictional forces at the contact surface will arise as a result. If we denote the force of normal compression of the wall to the flanges per unit contact surface by p, then the specific frictional force $\tau_0 = fp$ (here f, as before, is the friction coefficient). No relative displacements of the rod and the wall exist in region $a - a_1$.

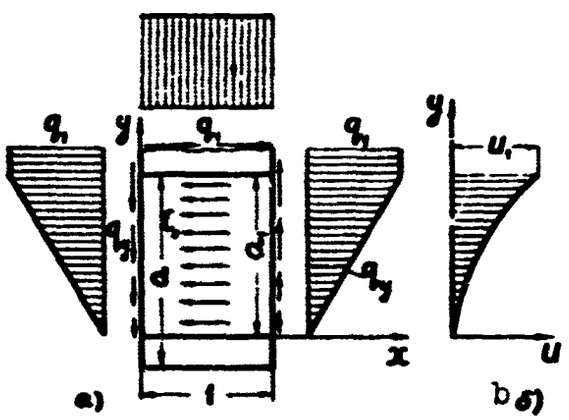

Fig. 48

In Fig. 48, as well as in the following figures, the specific frictional forces τ_0 are shown only for one side of the clamped web segment.

Quantity a_1 will be found from the condition of equilibrium of the clamped wall:

$$a_1 = \frac{q_1}{2\tau_0} = \frac{a_1 P}{2\tau_0 H}. \tag{7.2}$$

The multiplier 2 is here employed due to the fact that the wall is clamped by the rod from both sides.

The x-axis of the adopted coordinate system will be directed along the lower boundary of the slip zone.

The limiting value of the tangential force q_{pr}, for which slip is propagated over the entire width $\underline{a}$ of contact between the wall and the rod will be

$$q_{пр} = 2\tau_0 a. \tag{7.3}$$

The corresponding value of the force

$$P_{пр} = q_{пр} H = 2\tau_0 a H. \tag{7.4}$$

From the condition of equilibrium of forces acting on the plate element isolated in the slip zone (Fig. 49), we will get

$$\frac{dq_y}{dy} = 2\tau_0. \tag{7.5}$$

Here q_y is the tangential force in the section y = constant. Considering the deformation of the same element (Fig. 50), we will find

$$\frac{du}{dy} = \gamma. \tag{7.6}$$

Here $\underline{u}$ is the displacement in the direction of the x-axis and γ is the angle of displacement. We assume that the shear deformations are within the proportionality limits and, therefore, according to Hooke's law,

$$\gamma = \frac{\tau}{G} = \frac{q_y}{G\delta}.$$

Consequently,

$$\frac{du}{dy} = \frac{q_y}{G\delta}. \qquad (7.7)$$

Here δ is the thickness of the wall and G is the shear modulus. Differentiating this equation in respect to y and equating to (7.5),

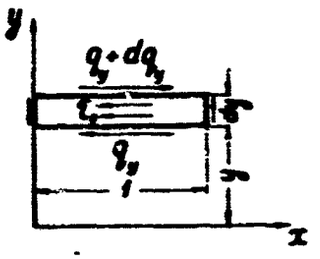

Fig. 49

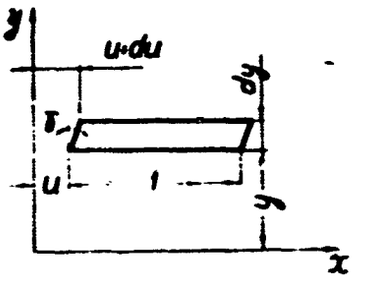

Fig. 50

we will obtain the following differential equation:

$$\frac{d^2u}{dy^2} = \frac{2\tau_0}{G\delta}. \qquad (7.8)$$

From this

$$u = \frac{\tau_0}{G\delta} y^2 + C_1 y + D_1. \qquad (7.9)$$

The displacement and stress at the lower edge of the slip zone (y = 0) are equal to zero $\left(u = 0; \frac{\partial u}{\partial y} = 0\right)$. Consequently, constants $C_1 = D_1 = 0$,

$$u = \frac{\tau_0}{G\delta} y^2. \qquad (7.10)$$

The displacement diagram during the first loading stage is shown in Fig. 49.

The tangential forces are determined from Eqs. (7.7) and (7.10):

$$q_y = G\delta \frac{du}{dy} = 2\tau_0 y. \qquad (7.11)$$

The displacement of the upper edge of the clamped wall segment where the force q_1 acts will, at a certain loading instant, be:

$$u_1 = \frac{q_1^2}{4\tau_0 G\delta} = \frac{a_1^2 p^2}{\tau_0 G\delta H^2}. \qquad (7.12)$$

Let us consider now the unloading stage, when the force, having

reached the value $\alpha_1 P$, begins to decrease. As soon as the value of force q will decrease, the shears will decrease also and as a result the wall will slip relative to the rod in the opposite direction. This slip will also begin at the upper mating edge and will be propagated downward.

Let us assume that the force, without changing direction, reached the value $\alpha_2 P$ at a certain instant of unloading. The reverse slip in this case will spread out by an amount a_2. Forces acting at this instant on the clamped panel element are shown in Fig. 51.

The width a_2 of the reverse slip zone is found from the condition of the element's equilibrium:

$$a_2 = \frac{2\tau_0 - q_2}{4\tau_0} = (\alpha_1 - \alpha_2)\frac{P}{4\tau_0 H}. \qquad (7.13)$$

All the previously obtained differential dependences remain valid for segment a_2, except that the sign of the frictional force τ_0 should be reversed.

In particular, the displacements are equal to:

$$u = -\frac{\tau_0}{G\delta} y^2 + C_2 y + D_2. \qquad (7.14)$$

Constants C_2 and D_2 are determined from the conditions of equality of displacements and of the equality of tangential forces at the edge $y = a_1 - a_2$, separating the remainder of the first zone from the second zone. This gives

$$C_2 = \frac{4\tau_0}{G\delta}(\alpha_1 - \alpha_2); \quad D_2 = -\frac{2\tau_0}{G\delta}(\alpha_1 - \alpha_2)^2.$$

Consequently,

$$u = \frac{\tau_0}{G\delta}[-y^2 + 4(\alpha_1 - \alpha_2)y - 2(\alpha_1 - \alpha_2)^2]. \qquad (7.15)$$

The diagram of displacements during the unloading stage is presented in Fig. 51.

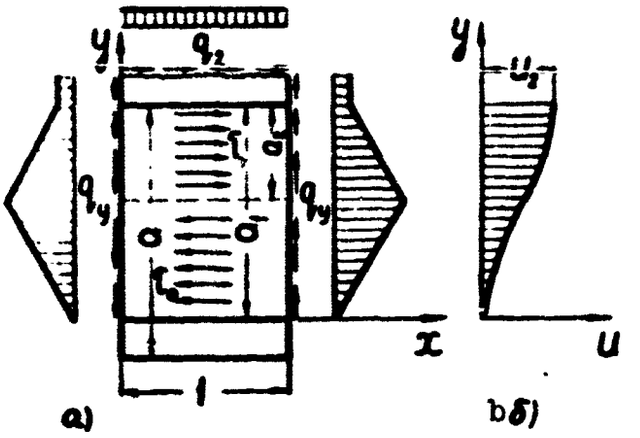

Fig. 51

In particular, for a certain intermediate value of α ($\alpha_2 \leq \alpha \leq \alpha_1$) the displacements at the upper edge of the clamped wall segment, where the tangential forces q_2 are applied, are equal to:

$$u_2 = \frac{p^2}{8\tau_0 G\delta H^2}(\alpha_1^2 + 2\alpha_1\alpha - \alpha^2). \tag{7.16}$$

The tangential forces in the wall cross section on the reverse slip region are determined by the formula

$$q_y = G\delta\frac{du}{dy} = 2\tau_0(2\alpha_1 - 2\alpha_2 - y). \tag{7.17}$$

The diagram of tangential forces is seen in Fig. 51.

All the quantities characterizing the stressed state of the wall segment on unloading when the load coefficient has a certain value $\alpha_2 \leq \alpha_1$, can be determined by the relations (7.13), (7.15) and (7.17). For example, in the case $\alpha = 0$ the external load is completely taken off, but a force system shown in Fig. 52 continues to act on the element. It is obvious that the upper edge does not return to its initial position at this instant. Residual displacements, determined by Formula (7.16) for $\alpha = 0$, are:

$$u(0) = \frac{\alpha_1^2 p^2}{8\tau_0 G\delta H^2}.$$

Let us assume that the load is decreased to the minimal value

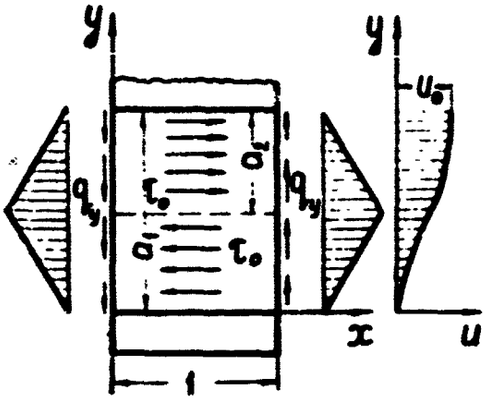

a) b б)

Fig. 52

of the force corresponding to the coefficient $\alpha_2 = r\alpha_1$ and then the loading begins again. Let us now consider this renewed loading. As the force is increased, slip of the web relative to the flange will occur, starting with the upper edge, in the same direction as during the first loading stage. As the force is increased, the slip region is propagated downward, shortening the reverse slip region.

Forces acting on the clamped wall element at a certain instant of the renewed loading are shown in Fig. 53. Width a_3 of the slip zone is found from the equation of the element's equilibrium:

$$a_3 = \frac{q_3 + 2\tau_0(2a_1 - a_3)}{4\tau_0} = \frac{(\alpha - a_3)P}{4\tau_0 H}. \qquad (7.18)$$

Here $\alpha_1 \geq \alpha \geq \alpha_2$.

Constants C_3 and D_3 of the expression for the displacements in the third zone

$$u = \frac{\tau_0}{G\delta} y^2 + C_3 y + D_3$$

are determined from the conditions of equality of displacements and of equality of the tangential forces on the straight line $y = a_1 - a_3$ separating the remainder of the second from the third zone. Performing the necessary calculations, we will get:

$$u = \frac{\tau_0}{G\delta}\left[y^2 + 4(a_2 - a_3)y + 2(a_1 - a_3)^2 - 2(a_1 - a_2)^2\right]. \qquad (7.19)$$

The displacement diagram is shown in Fig. 54. The tangential forces

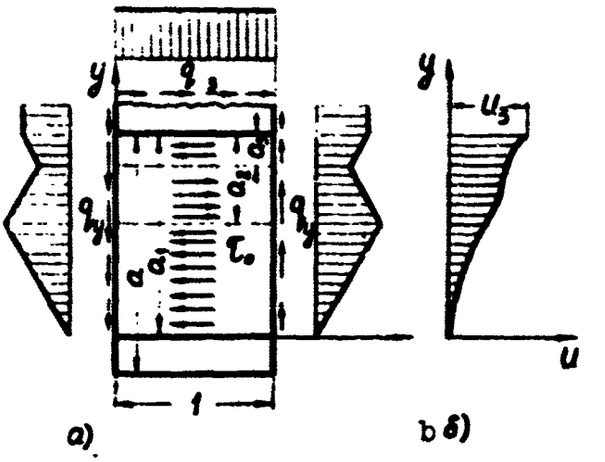

Fig. 53

in the third zone are equal to:

$$q_y = 2\tau_0[y + 2(a_2 - a_3)]. \qquad (7.20)$$

The force diagram is shown in Fig. 54. In Expressions (7.19) and (7.20) $y \geq a_1 - a_3$. In particular, the displacements at the upper edge of the clamped wall segment ($y = a_1$) will be

$$u_0 = \frac{\tau_0}{G\delta}(a_1^2 + 2a_2^2 - a_3^2) = \frac{P^2}{8\delta_0 GBH^2}(a^2 - 2aa_3 + a_1^2 + 2a_1a_2). \qquad (7.21)$$

The hysteresis loop for the joint under consideration is shown in Fig. 54. The values of displacements u for the upper edge of the clamped wall segment are laid off on the abscissa axis and the values of the tangential forces, determined by Formula (7.1), – on the ordinate axis. Curve 1 is constructed by Dependence (7.12) and corresponds to the first loading stage, curve 2 represents the unloading stage and Dependence (7.16), curve 3 pertains to the

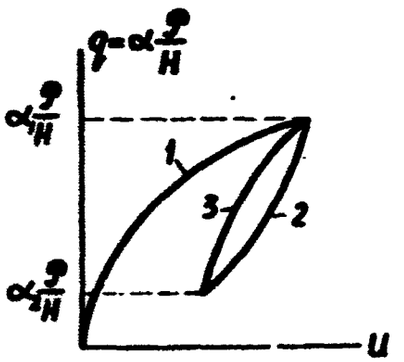

Fig. 54

secondary loading stage and corresponds to Dependence (7.21). The area of the hysteresis loop Ψ_1 is numerically equal to the energy irreversibly absorbed by a unit seam element during one loading cycle. The point is that force $\underline{q}$ is an external force relative to the seam element under consideration, the energy of which is used up in elastic deformations of the clamped wall segment and in the overcoming of the frictional forces.

This area, calculated by formula

$$\Psi_1 = \frac{P}{H}\int_{\alpha_1}^{\alpha_2} (u_2 - u_3)\, d\alpha, \tag{7.22}$$

for $\alpha_1 = 1$ and $\alpha_2 = r$ becomes equal to

$$\Psi_1 = \frac{(1-r)^2 P^2}{24\tau_0 G\delta H^2} = \frac{P_v^2}{3\tau_0 G\delta H^2}; \tag{7.23}$$

P_v is the amplitude of the cycle.

The total energy, dissipated per cycle by a seam of length $\underline{l}_{sh}$ is determined in the form:

$$\Psi = \Psi_1 \cdot l_{sh}. \tag{7.24}$$

The total energy absorption in several seams will be found as a sum of energies absorbed by each seam separately.

[Footnote]

Manuscript Page No.

51 It is more convenient for this purpose to utilize the graphicoanalytic method, considering the ensemble of frictional forces as a uniformly distributed moment load.

Manuscript Page No.	[List of Transliterated Symbols]
59	опт = opt = optimal'nyy = optimum
59	прел = pred = predel'nyy = limiting
91	пр = pr = predel'nyy = limiting
97	ш = sh = shov = seam

Chapter 3

FRICTION CLUTCHES

§8. TWIN-DISK CLUTCH

The system represented above in Fig. 8 consists of two clutch halves, each of which has a finite torsional rigidity when loaded by torques αM. To clarify the methodology of construction of the hysteresis loop, we will consider here the axially symmetrical scheme illustrated in Fig. 55. It is assumed in this scheme that one of the disks is undeformable and constitutes a rigid foundation to which the second, deformable disk is pressed by the given constant pressure. The disk is bounded by two parallel planes and two circular cylindrical surfaces; the internal and external disk diameters are, respectively, $2\underline{a}$ and $2\underline{b}$, the disk thickness is $\underline{h}$. The given torque is achieved in the form of a system of tangential stresses, uniformly distributed along the internal periphery and equal to

$$\tau(a) = \frac{\alpha M}{2\pi a^2 h}. \qquad (8.1)$$

It is assumed that, even for $\alpha = 1$, when the torque reaches its greatest value, no complete slip of the disk along the foundation takes place. In view of the fact that the thickness of the disk is small, we will consider the problem as being two-dimensional.

The stress system $\tau(a)$ is balanced by a system of tangential frictional forces, which develop between the disk and the rigid foundation. As in Section 1, frictional forces arise only in the zones of the disk's deformation and are equal to the limiting value $\tau_0 = \underline{fp}$. An assumption

stating that any whatever frictional forces exist in the undeformable zone would have contradicted Hooke's law, and an assumption stating that the intensity of frictional forces in the deformed zone where slip takes place is different than τ_0 does not agree with Coulomb's law.

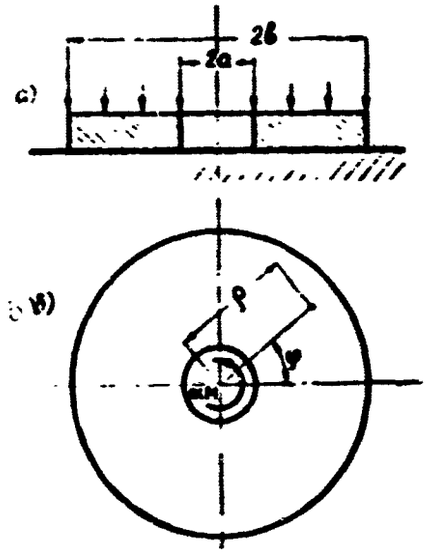

Fig. 55

Let us consider in detail the first stage of loading the disk, when the dimensionless load parameter increases gradually from zero to unity. An annular zone along which the disk slips on the foundation will appear near the internal disk periphery for any as small as desired load αM. The disk is in equilibrium under the action of loads described in Fig. 56a. The external boundary of the slip region is determined from the equilibrium condition

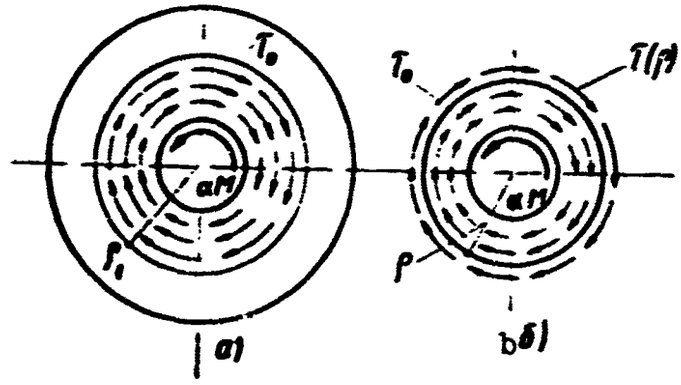

Fig. 56

$$2\pi\tau_0\int_a^{\rho_1}\rho^2 d\rho = \alpha M, \qquad (8.2)$$

where ρ_1 is the external radius of the slip zone. We find from (8.2)

$$\rho_1 = \sqrt[3]{\frac{3\alpha M}{2\pi\tau_0} + a^3}. \qquad (8.3)$$

Further, from the condition of equilibrium of the part of the disk described in Fig. 56b, we will find the tangential stresses, corresponding to the current coordinate ρ:

$$\tau(\rho) = \frac{\rho_1^2 - \rho^2}{3\rho^2\tau_0}. \tag{8.4}$$

Determining the tangential stresses, we can write the expression for shear in any point of the disk, according to Hooke's law:

$$\gamma(\rho) = -\frac{\tau(\rho)}{G}. \tag{8.5}$$

Since radial displacements are absent, the shear is expressed only by the tangential displacement $\underline{v}$

$$\gamma = -\frac{v}{\rho} + \frac{dv}{d\rho}. \tag{8.6}$$

As a result of axial symmetry of our problem, the tangential displacement is independent of the φ-coordinate and is only a function of the ρ-coordinate. The differential equation for determination of the displacement $\underline{v}$

$$\frac{dv}{d\rho} - \frac{v}{\rho} = -\frac{\tau(\rho)}{G}. \tag{8.7}$$

is thus obtained from (8.5) and (8.6). Substituting here (8.4) and integrating, we will obtain the following solution, satisfying the boundary condition $v(\rho_1) = 0$:

$$v(\rho) = \frac{\tau_0}{6Ck\rho}(\rho_1 - \rho)(\rho_1^2 + \rho_1\rho - 2\rho^2). \tag{8.8}$$

Let us introduce the structural parameters: $\zeta = \frac{\tau_0 a}{6}$, $\nu = \frac{3}{2\pi\tau_0 a^3}$, $k = Ch$.
Then, substituting for ρ_1 by Formula (8.3), we will obtain for the points on the internal periphery ($\rho = a$)

$$v_1(a) = a\frac{\zeta}{k}\left[(\pi\nu M + 3) - 3(\pi\nu M + 1)^{\frac{1}{3}}\right]. \tag{8.9}$$

This expression describes the first stage of the process.

The investigation of the succeeding unloading and secondary loading stages is substantially similar to the corresponding investigation for the elementary system (§ 1). Leaving out detailed calculations, we will present the final results (for conclusions see [13]); the relationships between the displacement $v_2(a)$ and the torque during the unloading stage

$$r_2(a) = a\frac{\beta}{k}\left\{(\nu M - 3) - 3(\nu M + 1)^{\frac{1}{3}} + \right.$$
$$\left. + 6\left[\frac{r}{2}(1-x)M + 1\right]^{\frac{1}{3}}\right\}; \tag{8.10}$$

[We have] the same relationship during the renewed loading stage

$$r_3(a) = a\frac{\beta}{k}\left\{(\alpha\nu M + 3) - 3(\nu M + 1)^{\frac{1}{3}} + \right.$$
$$\left. + 6\left[\frac{\nu}{2}(1-r)M + 1\right]^{\frac{1}{3}} - 6\left[\frac{\nu}{2}(\alpha - r)M + 1\right]^{\frac{1}{3}}\right\}. \tag{8.11}$$

The hysteresis loop, calculated by Expressions (8.9), (8.10) and (8.11), coincides with the hysteresis loop for the elementary system (Fig. 14). The energy dissipated during one cycle amounts to

$$\Psi = \frac{M}{a}\int_{a=r}^{1}(v_2 - v_3)\,d\alpha. \tag{8.12}$$

Performing quadratures and introducing the value of the load amplitude $M_a = \frac{1-r}{2}M_0$ we will find

$$\Psi = \frac{6\beta}{\nu\alpha}\left\{(\nu M_a + 3)\left[(\nu M_a + 1)^{\frac{1}{3}} - 1\right] - \nu M_a\right\}. \tag{8.13}$$

It can be seen from Expression (8.13) that energy dissipation, as in cases presented above, is independent of the mean value of the load; the dependence of the quantity Ψ on the amplitude of the cycle is slightly more complex than in the case of previously considered problem (this dependence is represented graphically in Fig. 57).

If both disks are deformable and have characteristics k_1 and k_2,

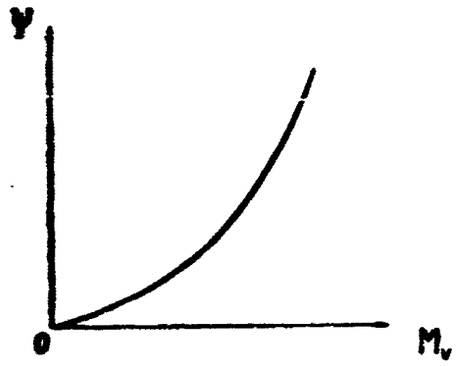

Fig. 57

then the energy dissipated per one cycle is equal to:

$$\Psi = \frac{6\beta}{\nu}\left(\frac{1}{k_1}+\frac{1}{k_2}\right)\left\{(\nu M_0+3)\left[(\nu M_0+1)^{\frac{1}{2}}-1\right]-\nu M_0\right\}. \qquad (8.14)$$

§9. A MULTIPLE-DISK CLUTCH

Figure 58a illustrates the schematic of a multiple-disk friction clutch, representing a system of flat disks with finite rigidity. Let us assume that the external torque is uniformly distributed among the disks, so that a fraction of the load αM is devolved upon each disk pair. Let us analyze the operation of this pair. The disks are pressed to one another by a constant pressure p (Fig. 58b) and are loaded by variable, equal and oppositely directed torques denoted by αM (the first – along the internal periphery, and the second – along the external).

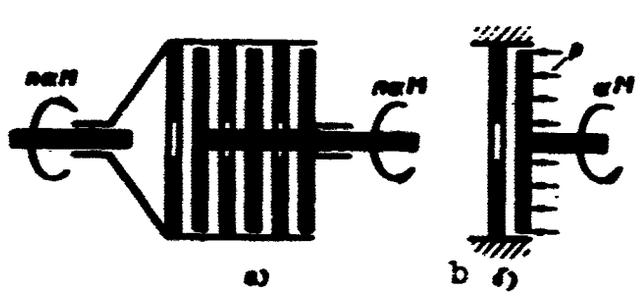

Fig. 58

Annular slip zones (Fig. 59a), where the frictional forces τ_0 balancing the external torque are developed, arise on loading, in the

vicinity of the internal and external peripheries. The middle part of the disks deforms as a separate entity and each disk takes up a part

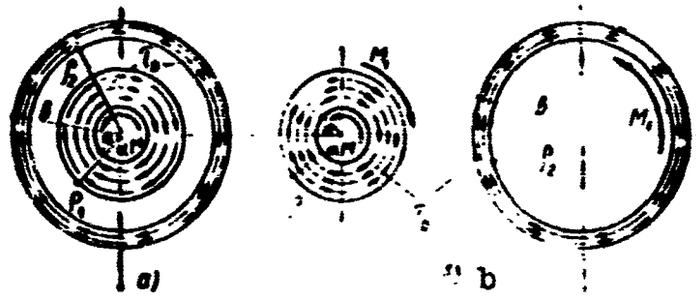

Fig. 59

of the load proportional to its rigidity

$$M_1 = \frac{\alpha M k_1}{k_1 + k_2}, \quad M_2 = \frac{\alpha M k_2}{k_1 + k_2}. \tag{9.1}$$

It is possible to disregard the deformation of the middle part in the calculation of the dissipated energy, setting shear at its boundaries equal to zero. The energy dissipation is determined as the work of the external torque αM on the angular displacements $\varphi(a) = \frac{v_1(a)}{a}$ and $\varphi(b) = \frac{v_2(b)}{b}$, where $v_1(a)$ is the tangential displacement of points of the internal periphery of the first disk and $v_2(b)$ – the tangential displacement of the points on the external periphery of the second disk, relative to the "nondeforming" middle part. The boundaries of the slip zones (ρ_1 and ρ_2) are found considering separately the equilibrium of the internal and external regions (Fig. 59b). The equilibrium equations are written in the form

$$\begin{aligned} \alpha M - 2\pi\tau_0 \int_a^{\rho_1} \rho^2 d\rho &= M_1, \\ M_1 - 2\pi\tau_0 \int_{\rho_2}^{b} \rho^2 d\rho &= 0. \end{aligned} \tag{9.2}$$

From the conditions of equilibrium of the annular segments, isolat in the vicinity of the internal periphery of the first disk and in the

vicinity of the external periphery of the second disk, we determine

$$\tau_1 = \frac{1}{3\rho^3 h}(\rho_1^3 - \rho^3)\tau_\varphi \qquad (9.3)$$

$$\tau_2 = \frac{1}{3\rho^3 h}(\rho^3 - \rho_2^3)\tau_\varphi \qquad (9.4)$$

The tangential displacement $v(\rho)$ is independent of φ and is determined from Eq. (8.7) after $\tau(\rho)$ is replaced by its value from Formula (9.3) for the internal region of the first disk and by Formula (9.4) for the external region of the second disk. Thence the problem is solved in the same manner as the preceding one. Introducing the parameters β, ν and k and the notation $t = a/b$, we obtain the following expressions for energy dissipation in one disk pair per cycle:

$$\Psi_1 = \frac{18\beta}{\nu}\cdot\frac{(k_1^2 - k_2^2)}{k_1 k_2^2} - \frac{12\beta}{k_1}M_\tau + \frac{2\beta}{k_1}\left(1 - \nu\frac{k_2}{k_1 + k_2}M_\sigma\right)^{-\frac{2}{3}}\cdot$$
$$\cdot\left[\frac{9}{\nu}\cdot\frac{(k_2^2 - k_1^2)}{k_2^2} + \frac{6(2k_2 - k_1)}{k_2}M_\sigma + \frac{3k_2 + k_1}{k_1 + k_2}\nu M_\sigma^2\right]. \qquad (9.5)$$

$$\Psi_2 = \frac{18\beta}{\nu t^4}\cdot\frac{(k_1^2 - k_2^2)}{k_1^2 k_2} - \frac{12\beta}{k_2 t}M_\tau - \frac{2\beta}{k_2 t}\left(1 - \nu t^3\frac{k_1}{k_1 + k_2}M_\sigma\right)^{-\frac{2}{3}}\cdot$$
$$\cdot\left[\frac{9}{\nu t^3}\cdot\frac{(k_1^2 - k_2^2)}{k_1^2} - \frac{6(2k_1 - k_2)}{k_1}M_\sigma + \frac{3k_1 + k_2}{k_1 + k_2}\nu t^3 M_\sigma^2\right]. \qquad (9.6)$$

$$\Psi = \Psi_1 + \Psi_2.$$

Here Ψ_1 is that part of energy which is dissipated in the internal region, Ψ_2 – in the external region. In the case when $k_1 = k_2 = k$ Expressions (9.5) and (9.6) are substantially simplified and take on the form

$$\Psi_1 = \frac{12\beta}{k}M_\sigma\left[\left(1 - \frac{\nu}{2}M_\sigma\right)^{-\frac{2}{3}}\cdot\left(1 + \frac{\nu}{3}M_\sigma\right) - 1\right]. \qquad (9.7)$$

$$\Psi_2 = \frac{12\beta}{kt}M_\sigma\left\{\left(1 - \frac{\nu}{2}t^3 M_\sigma\right)^{-\frac{2}{3}}\cdot\left(1 - \frac{\nu}{3}t^3 M_\sigma\right) - 1\right\}. \qquad (9.8)$$

These dependencies are represented graphically in Fig. 60. It can be seen from the graph that $\Psi_2 \ll \Psi_1$ for any given values of the cycle's amplitude. The energy dissipation is independent of the mean value of

the load. The dependence of the energy dissipation on the intensity of the compression force for one disk pair is shown in Fig. 61. The energy dissipation curve in a two-disk clutch is also given here for comparison (by the dashed line).

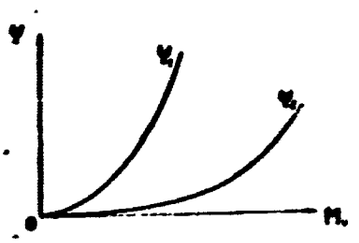

Fig. 60.

Fig. 61.

Chapter 4

DRY FRICTION ABSORBERS

§10. SEPARATOR STRIP

Let us consider the process of cyclical compression of a short elastic parallelepiped by two completely rigid plates (Fig. 62). We shall assume that the dimensions of the parallelepiped are of different order of smallness: the dimension in the direction of the x-axis considerably exceeds the dimension $2l$ in the direction of the y-axis, and the latter exceeds manyfold the height of the parallelepiped h, measured in the direction of the z-axis (Fig. 62b). Such a

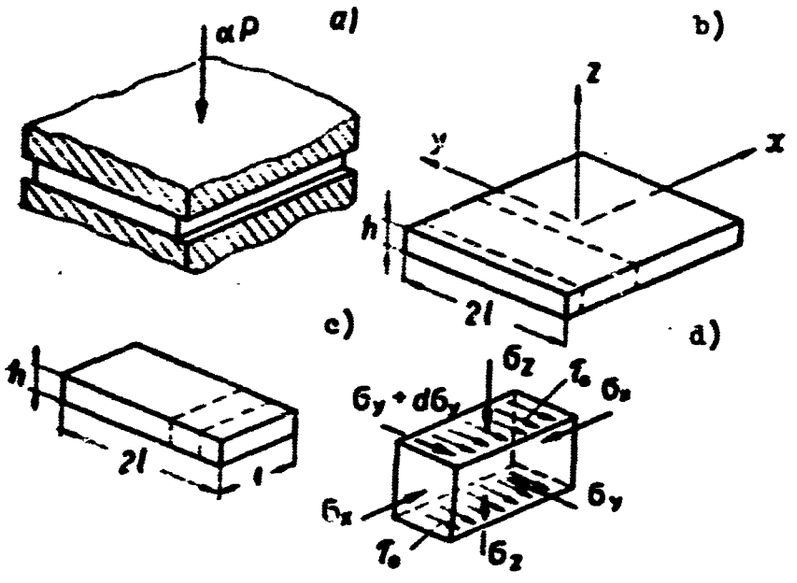

Fig. 62

scheme can be arrived at in the investigation of the operation of elastic separators of the strip type, used for cushioning of various types of machinery.

When the strip is compressed its dimension in the direction of the

z-axis will decrease and the dimensions in the directions of the x- and y-axes will increase. Frictional forces which are here developed along the strip's horizontal surfaces will tend to restrict the widening of the strip in the direction of the x- and y-axes, in which case displacements in the direction of the x-axis can be considered to be completely nonexistent due to the great length of the strip. In this case it is sufficient to investigate the compression of any unit strip, isolated at a certain distance away from the short edges, represented in Fig. 62c; all the remaining strips of this type will be subject to the same conditions as the strip under consideration.

We shall imagine that an element shown in Fig. 62d is isolated from the strip by two plane sections perpendicular to the y-axis. All the facets of the element experience the action of normal stresses; in addition the horizontal facets are loaded by tangential forces τ_0; the latter are frictional stresses on the surfaces of contact between the strip and the plates. We will consider all the above stresses to be uniformly distributed over the entire area of each face of the element.

Slightly contradicting the evolved traditions, we have taken as positive compressive stresses, which is more natural in our problem. The direction of the tangential stresses shown in the figure corresponds to the assumption that the element is displaced in the positive y-direction.*

The equation of the element's equilibrium in projection on the y-axis is

$$h\frac{d\sigma_y}{dy}+2f\sigma_z=0. \tag{10.1}$$

Utilizing Hooke's law

$$\varepsilon_z=\frac{1}{E}[\sigma_z-\mu(\sigma_y+\sigma_x)], \tag{10.2}$$

$$\varepsilon_y = \frac{1}{E}[\sigma_y - \mu(\sigma_x + \sigma_z)],$$

$$\varepsilon_z = \frac{1}{E}[\sigma_z - \mu(\sigma_x + \sigma_y)] \qquad (10.2)$$

(the compression deformation should now be considered as positive) and keeping in mind that $\varepsilon_x \equiv 0$, we find from the first and third equalities

$$\sigma_z = \frac{E\varepsilon_z}{1-\mu^2} + \frac{\mu\sigma_y}{1-\mu}. \qquad (10.3)$$

We will consider quantity ε_z as constant at all points of the strip and equal to

$$\varepsilon_z = \frac{w}{h}, \qquad (10.4)$$

where w is the distance separating the loading plates, which is the given quantity. Substituting (10.3) and (10.4) into (10.1) we arrive at the equation for the stress σ_y

$$\frac{d\sigma_y}{dy} + \frac{2\mu f\sigma_y}{h(1-\mu)} + \frac{2fEw}{h(1-\mu^2)} = 0. \qquad (10.5)$$

Under the boundary condition $\sigma_y(l) = 0$, the solution of this equation has the form

$$\sigma_y = \frac{Ew}{\mu(1+\mu)h}\left[e^{\lambda\left(1-\frac{y}{l}\right)} - 1\right], \qquad (10.6)$$

where

$$\lambda = \frac{2\mu fl}{h(1-\mu)} \qquad (10.7)$$

is the strip constant.

According to (10.3) we now have for the normal stress σ_z:

$$\sigma_z = -\frac{Ew}{h(1-\mu^2)}e^{\lambda\left(1-\frac{y}{l}\right)}. \qquad (10.8)$$

Figure 53 shows the graphs of the distribution of the normal stresses σ_y and σ_z along the length of the strip.

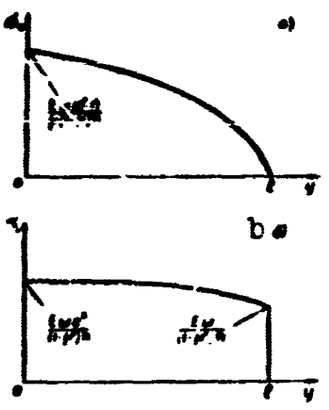

Fig. 63

It should be kept in mind that Expressions (10.6) and (10.8) are valid only in the strip's deformation zone, where slip is present. The median part of the strip length can turn out to be in a state of rigid coupling with the clamping plates; not only $\varepsilon_x = 0$ in this part but also $\varepsilon_y = 0$. Then, according to (10.2),

$$\sigma_x = \sigma_y = \frac{\mu E w}{(1+\mu)(1-2\mu)h}, \qquad (10.9)$$

$$\sigma_z = \frac{E w (1-\mu)}{(1+\mu)(1-2\mu)h} \qquad (10.10)$$

Let y* be a coordinate of the section, situated on the boundary of the rigid coupling region. Expression (10.9) should be equal to Expression (10.6) in this region:

$$\frac{\mu E w}{(1+\mu)(1-2\mu)h} = \frac{E w}{\mu(1+\mu)h}\left[e^{\lambda\left(1-\frac{y^*}{l}\right)} - 1\right].$$

Consequently,

$$y^* = l\left[1 - \frac{1}{\lambda}\ln\frac{(1-\mu)^2}{1-2\mu}\right]. \qquad (10.11)$$

It can be seen from this that if

$$\lambda \leq \ln\frac{(1-\mu)^2}{1-2\mu}. \qquad (10.12)$$

then no rigid coupling region exists at all. Thus, for $\mu = 0.47$ (rubber) it follows from (10.12) that no rigid coupling zone will exist for $\lambda \leq 1.55$. If, for example, $f = 0.2$, then ratio $l/h \leq 4.36$ follows from (10.12). We shall assume that Condition (10.12) is satisfied and we will limit ourselves to the case when no rigid coupling zone exists.

In this case it is possible to find the total load on the strip αP, by integrating the expressions for σ_z over the entire length of the strip

$$\alpha P = 2\int_0^l \sigma_z\, dy = \frac{2El\,(e^{\lambda}-1)}{\lambda h\,(1-\mu^2)}\,w \qquad (10\ 13)$$

During the load increase stage w is thus a linear function of αP, and the coefficient of rigidity is equal to

$$c_1 = \frac{2El\,(e^{\lambda}-1)}{\lambda h\,(1-\mu^2)}. \qquad (10.14)$$

For a very small value of parameter λ (for example, due to the fact that the friction coefficient f is small) we can take $e^{\lambda} \approx 1+\lambda$, and Formula (10.14) will take on the form

$$c_0 = \frac{2El}{h\,(1-\mu^2)} \qquad (10.15)$$

This expression determines the rigidity of the strip for vanishingly small frictional forces.

Let us now turn to the strip's unloading stage and first of all let us clarify the stress distribution when the frictional force q changes direction. There is no need to repeat all the calculations, since the expressions which are needed can be written immediately by the dependencies derived above simply by changing the sign of the friction coefficient f.

Thus, we will get from (10.6)

$$\sigma_y = \frac{Ew}{\mu\,(1+\mu)\,h}\left[e^{-\lambda\left(1-\frac{z}{l}\right)}-1\right], \qquad (10.16)$$

and, in accordance with Expression (10.8), the stress σ_z will be:

$$\sigma_z = \frac{Ew}{h\,(1-\mu^2)}\,e^{-\lambda\left(1-\frac{z}{l}\right)}. \qquad (10.17)$$

The distribution of stresses σ_y and σ_z during the unloading stage is given in Fig. 64. Dependence (10.13) will now be replaced by

$$\alpha P = \frac{2El\,(1-e^{-\lambda})}{\lambda h\,(1-\mu^2)}\,w, \qquad (10.18)$$

i.e., the rigidity coefficient of the stage under consideration is different from the value of (10.14):

$$c_3 = \frac{2EI(1-e^{-\gamma})}{\lambda h(1-\mu^2)}. \qquad (10.19)$$

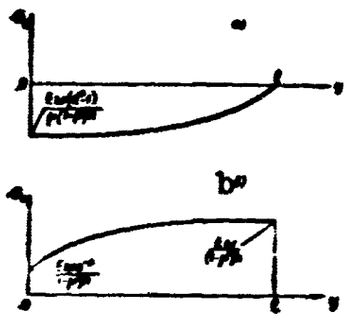

Fig. 64

Dependencies (10.13) and (10.18) (straight lines 1 and 3) are represented in Fig. 65. The figure shows clearly that a stage, during which neither direct nor reverse slip is taking place – a rigid coupling stage along the entire length – must inevitably lie between the processes described by rays 1 and 3.* This stage is illustrated in Fig. 65a by segment 2.

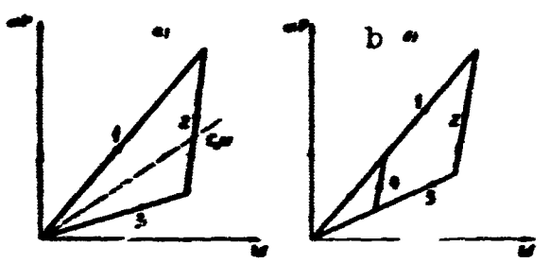

Fig. 65

According to Expression (10.9) the change in quantity $\underline{w}$ by Δw results in a change in stress σ_z by

$$\Delta\sigma_z = \frac{E(1-\mu)}{(1+\mu)(1-2\mu)h}\Delta w. \qquad (10.20)$$

Since $\Delta\sigma_z$ is independent of the y-coordinate, then the corresponding change in force αP amounts to:

$$\Delta(\alpha P) = 2l\Delta\sigma_z = \frac{2El(1-\mu)}{(1+\mu)(1-2\mu)}\Delta w. \qquad (10.21)$$

Consequently, the rigidity of the strip during this stage is equal to:

$$c_3 = \frac{2El(1-\mu)}{(1+\mu)(1-2\mu)}. \qquad (10.22)$$

The hysteresis loop for a pulsating cycle thus has the shape of a

triangle. The straight line

$$\alpha P = c_0 w = \frac{2Fl}{h(1-\mu^2)} w. \qquad (10.23)$$

corresponding to the value of c_0 for f = 0 given in (10.15) is given in the same Fig. 65a by a dashed line.

If unloading does not go to zero, then the hysteresis loop acquires the shape of a trapezoid (Fig. 65b); its side 4 is parallel to the side 2.

§11. A ROUND SPACER

This paragraph considers the problem of compression of a thin round disk between two absolutely rigid plates (Fig. 66); in its substance this problem is closely related to that considered in Section 10. Figure 67b shows a typical element of a disk-spacer, isolated by two infinitesimally close axial sections and by two infinitesimally close cylindrical sections. As in Section 10, the compression stresses are taken here to be positive. The equation of the element's equilibrium has the form

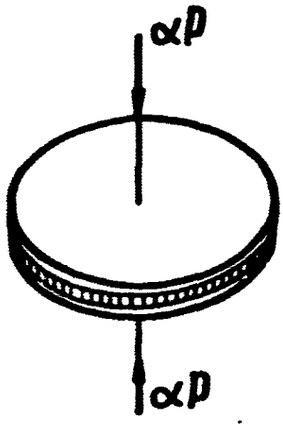

Fig. 66

$$\frac{d\sigma_\rho}{d\rho} + \frac{\sigma_\rho - \sigma_\varphi}{\rho} + \frac{2\sigma_z f}{h} = 0. \qquad (11.1)$$

We shall use the usual sign convention (positive displacement [starting] from the center) for the displacements u in the radial direction, while for deformation we shall utilize the sign convention assumed for the stresses (compression deformation is considered positive). In this case the relationship between the displacements and deformations will become such: $\varepsilon_\rho = -\frac{du}{d\rho}$; $\varepsilon_\varphi = -\frac{u}{\rho}$; $\varepsilon_z = \frac{w}{h}$.

According to the assumed sign convention, Hooke's law will be written in the following form [8]:

$$\sigma_\rho = \frac{2G(1-\mu)}{1-2\mu}\left(-\frac{du}{d\rho} - \frac{\mu}{1-\mu}\cdot\frac{u}{\rho} + \frac{\mu}{1-\mu}\varepsilon_z\right),$$

$$\sigma_\varphi = \frac{2G(1-\mu)}{1-2\mu}\left(-\frac{\mu}{1-\mu}\frac{du}{d\rho} - \frac{u}{\rho} + \frac{\mu}{1-\mu}\varepsilon_z\right). \qquad (11.2)$$

$$\sigma_z = \frac{2G(1-\mu)}{1-2\mu}\left(-\frac{\mu}{1-\mu}\frac{du}{d\rho} - \frac{\mu}{1-\mu}\frac{u}{\rho} + \varepsilon_z\right).$$

Substituting these expressions into the equilibrium equation

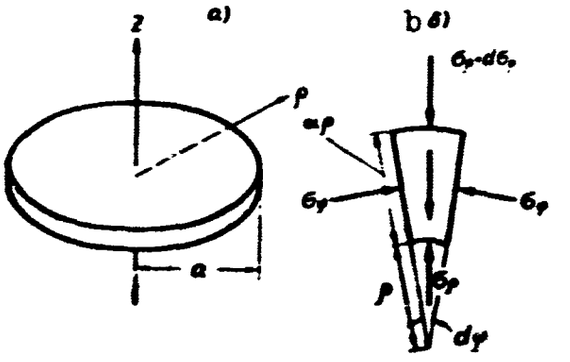

Fig. 67

(11.1), we will get

$$\frac{d^2u}{d\rho^2} + \frac{1}{\rho}\frac{du}{d\rho}\left(1 + \frac{\lambda\rho}{a}\right) - \frac{u}{\rho^2}\left(1 - \frac{\lambda\rho}{a}\right) = \frac{\lambda(1-\mu)}{a\mu}\cdot\frac{w}{h}, \qquad (11.3)$$

where $w/h = \varepsilon_z$ and

$$\lambda = \frac{2\mu fa}{h(1-\mu)} \qquad (11.4)$$

is the spacer constant.

If slip occurs in the reverse direction, i.e., toward the spacer center, which can happen on unloading, then the frictional forces change directions and tne equilibrium equation (11.1) takes on the form

$$\frac{d\sigma_\rho}{d\rho} + \frac{\sigma_\rho - \sigma_\varphi}{\rho} - \frac{2\sigma_z f}{h} = 0. \qquad (11.5)$$

Correspondingly,

$$\frac{d^2u}{d\rho^2} + \frac{1}{\rho}\frac{du}{d\rho}\left(1 - \frac{\lambda\rho}{a}\right) - \frac{u}{\rho^2}\left(1 + \frac{\lambda\rho}{a}\right) = -\frac{\lambda(1-\mu)}{a\mu}\cdot\frac{w}{h}. \qquad (11.6)$$

will be obtained instead of (11.3).

As in the preceding paragraph, the case when slip is propagated only over a part of the spacer is not considered. Three spacer deformation stages are thus possible:

1) the loading stage, when Eq. (11.3), assuming existence of slip from the spacer center, is valid;

2) the unloading commencement stage, when slip is completely absent;

3) the renewed loading stage, when slip takes place toward the center of the spacer; Eq. (11.6) corresponds to this stage.

The solutions of Eqs. (11.3) and (11.6) should be subjected to the boundary conditons

$$u(0)=0; \quad \sigma_\rho(a)=0. \tag{11.7}$$

The solution of Eq. (11.3) for the loading stage has the form

$$u_1=\frac{\omega a}{2\mu\lambda}\left\{\frac{(1-\mu-2\mu^2)e^{\lambda}\left[\left(\frac{a}{\rho}+\lambda\right)e^{-\frac{\lambda\rho}{a}}-\frac{a}{\rho}\right]}{(1-\mu)\lambda^2+(1-2\mu)(1-\lambda-e^{-\lambda})}+(1-\mu)\frac{\rho}{a}\right\}. \tag{11.8}$$

The solution of the equation for the stage of unloading with slip is obtained as follows:

$$u_2=\frac{\omega a}{2\mu\lambda}\left\{\frac{(1-\mu-2\mu^2)e^{-\lambda}\left[\left(\frac{a}{\rho}-\lambda\right)e^{\frac{\lambda\rho}{a}}-\frac{a}{\rho}\right]}{(1-\mu)\lambda^2+(1-2\mu)(1-\lambda-e^{-\lambda})}+(1-\mu)\frac{\rho}{a}\right\}. \tag{11.9}$$

Substituting now the just found solutions into the third of equations (11.2) we will find the distribution of stresses σ_z along the spacer radius. For the loading stage

$$\sigma_z=\frac{G\omega r}{h}\frac{(1+\mu)\lambda^2 e^{\lambda\left(1-\frac{\rho}{a}\right)}}{(1-\mu)\lambda^2+(1-2\mu)(1+\lambda-e^{\lambda})} \tag{11.10}$$

and for the stage of unloading with slip

$$\sigma_z=\frac{G\omega r}{h}\frac{(1+\mu)\lambda^2 e^{-\lambda\left(1-\frac{\rho}{a}\right)}}{(1-\mu)\lambda^2+(1-2\mu)(1-\lambda-e^{-\lambda})}. \tag{11.11}$$

Integrating Expressions (11.10) and (11.11) along the spacer's contact surface, we will obtain a relationship between the compressing force and the convergence of the compressing plates. In the first case we find:

$$\alpha P = \frac{2\pi a^2 G w}{h} \cdot \frac{(1+\mu)(e^{\lambda} - 1 - \lambda)}{(1-\mu)\lambda^2 + (1-2\mu)(1+\lambda-e^{\lambda})} \tag{11.12}$$

The analogous expression for the second case has the form

$$\alpha P = \frac{2\pi a^2 G w}{h} \frac{(1+\mu)(e^{-\lambda} - 1 + \lambda)}{(1-\mu)\lambda^2 + (1-2\mu)(1-\lambda-e^{-\lambda})}. \tag{11.13}$$

The dependencies thus found are illustrated by rays 1 and 3 in Fig. 65. Accordingly, the rigidity of the spacer during these loading stages comes to

$$c_1 = \frac{2\pi a^2 G}{h} \frac{(1+\mu)(e^{\lambda} - 1 - \lambda)}{(1-\mu)\lambda^2 + (1-2\mu)(1+\lambda-e^{\lambda})}. \tag{11.14}$$

$$c_3 = \frac{2\pi a^2 G}{h} \frac{(1+\mu)(e^{-\lambda} - 1 + \lambda)}{(1-\mu)\lambda^2 + (1-2\mu)(1-\lambda-e^{-\lambda})}. \tag{11.15}$$

For the intermediate second stage, to which rigid coupling between the spacer and the plates corresponds, we have from the third equation

$$\sigma_z = \frac{2G(1-\mu)\varepsilon_z}{1-2\mu}. \tag{11.16}$$

Integrating this expression along the contact surface of the spacer, we will find the relationship between the load increment and the increment of the quantity Δw:

$$\Delta(\alpha P) = \frac{2\pi a^2 G(1-\mu)}{(1-2\mu)h} \Delta w. \tag{11.17}$$

Consequently, the coefficient of rigidity during the second stage is equal to

$$c_2 = \frac{2\pi a^2 G(1-\mu)}{(1-2\mu)h}. \tag{11.18}$$

If $\lambda = 0$ is substituted into Expressions (11.14) and (11.15) then,

after evaluating the indeterminate function we will find the rigidity of the spacer in the absence of friction:

$$c_0 = \frac{2\pi a^2 G(1+\mu)}{\mu h}. \qquad (11.19)$$

The relationship governing the deformation of this spacer is shown in Fig. 65a by a dashed line.

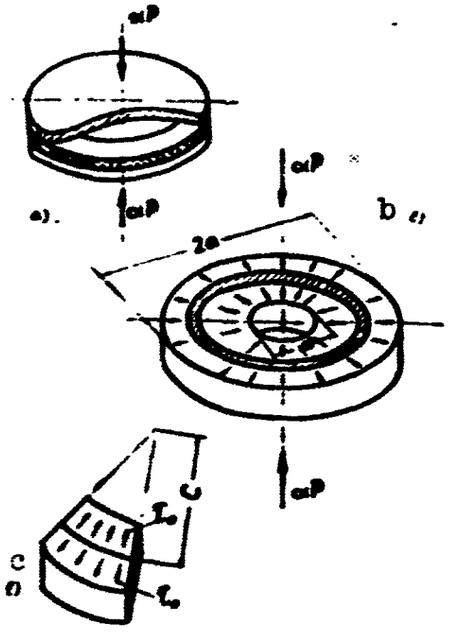

Fig. 68

If the spacer is deformed with friction not according to the pulsating cycle, then the hysteresis loop takes on the shape of a trapezoid, as shown in Fig. 65b.

The problem of cyclical compression of an elastic washer between rigid disks (Fig. 68a) is of interest. The main peculiarity of this problem consists in the fact that slip along the surfaces of contact between the washer and the disks takes opposite directions in two different annular regions. The slip arising on loading is directed to the center along the internal annular region and away from the center along the external annular region. These two regions are separated from one another by a rigid coupling zone (Fig. 68b). Depending on the value of the characteristic λ, this annular zone can degenerate into a circle (Fig. 68c). It is namely this case, as being of practical significance, that is subsequently considered.

The equation of equilibrium of a typical element, situated in the internal slip region is written in the form of (11.5) on loading; during the unloading stage, when slip changes direction, the equation of equilibrium of the same element is written in the form of (11.1). The

equilibrium equations during the loading stage (11.1), and the unloading [stage] (11.5) for an element of the external slip region are written similarly.

Without going into a detailed investigation of the loading stages, let us point out that the relationship between the separation $\underline{w}$ and the load during the loading stage is written in the form

$$\alpha P = \frac{2G\pi a^2 w}{\lambda^2 h(1-2\mu)}\left\{\frac{[(1+\mu)b^2+(1-\mu)c^2]\cdot\left[\left(1-\frac{\lambda b}{a}\right)e^{\frac{\lambda b}{a}}-\left(1-\frac{\lambda c}{a}\right)e^{\frac{\lambda c}{a}}\right]}{\left(\frac{1-\mu}{1-2\mu}b^2-\frac{ab}{\lambda}+\frac{a^2}{\lambda^2}\right)e^{\frac{\lambda b}{a}}-\left(1-\frac{\lambda c}{a}\right)e^{\frac{\lambda c}{a}}}+\right.$$
$$\left.+\frac{[(1-\mu)a^2+(1-\mu)c^2]\cdot\left[\left(1+\frac{\lambda c}{a}\right)e^{-\frac{\lambda c}{a}}-(1+\lambda)e^{-\lambda}\right]}{\left(\frac{1-\mu}{1-2\mu}+\frac{1}{\lambda}+\frac{1}{\lambda^2}\right)a^2e^{-\lambda}-\left(1-\lambda\frac{c}{a}\right)e^{-\frac{\lambda c}{a}}}\right\}. \qquad (11.20)$$

Here $\underline{c}$ is the radius of a circle separating the two slip regions.

For loading, this dependence takes on the form

$$\alpha P = \frac{\pi a^2 G w}{\lambda^2 h(1-2\mu)}\left\{\frac{[(1+\mu)b^2+(1-\mu)c^2]\cdot\left[\left(\frac{\lambda b}{a}+1\right)e^{-\frac{\lambda b}{a}}-\left(\frac{\lambda c}{a}+1\right)e^{-\frac{\lambda c}{a}}\right]}{\left(\frac{1-\mu}{1-2\mu}\cdot b^2-\frac{ab}{\lambda}+\frac{a^2}{\lambda^2}\right)e^{-\frac{\lambda b}{a}}-\left(\frac{\lambda c}{a}+1\right)e^{-\frac{\lambda c}{a}}}+\right.$$
$$\left.+\frac{[(1+\mu)a^2+(1-\mu)c^2]\cdot\left[\left(1-\frac{\lambda c}{a}\right)e^{\frac{\lambda c}{a}}-(1-\lambda)e^{\lambda}\right]}{\left(\frac{1-\mu}{1-2\mu}-\frac{1}{\lambda}+\frac{1}{\lambda^2}\right)a^2e^{\lambda}+\left(\frac{\lambda c}{a}-1\right)e^{\frac{\lambda c}{a}}}\right\}. \qquad (11.21)$$

The relationship between the load increment and the separation $\underline{w}$ during the intermediate rigid coupling stage has the form

$$\Delta(\alpha P) = P - \frac{2\pi G(1-\mu)(a^2-l^2)}{h(1-2\mu)}w. \qquad (11.22)$$

The hysteresis loop for a washer deformed between rigid plates is shown in Fig. 65.

§12. ABSORBERS WITH TAPERED RINGS

We are considering here systems of ring-shaped springs, which can be assembled from two different types of rings - split and continuous. A spring with continuous rings is shown in Fig. 69a, and with split rings in Fig. 69b. The continuous rings experience primarily expansion or

compression when the spring shrinks, while the split [rings] experience bending; therefore the computational dependencies for determination of damping characteristics will be different.

Let us first consider continuous rings. As each ring comes under pressure, it is loaded by a system of uniformly distributed loads p and fp (Fig. 70).

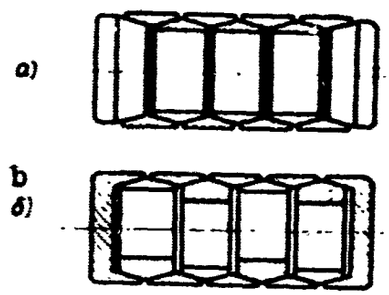

Fig. 69

The problem of the rings' deformation can be solved approximately [and] with sufficient accuracy, regarding each of them as a thin ring with radius R, loaded by a uniformly distributed radial load of intensity q_r, which is equal to the sum of the projections of loads p and fp on the radial direction.

The first stage. The direction in which the frictional force acts during the first stage corresponds to Fig. 70. From the sum of load projections on the spring axis

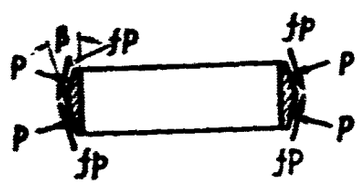

Fig. 70

$$2\pi R\,(p\sin\beta + fp\cos\beta) = \pi P \qquad (12.1)$$

and on the radial direction

$$2\,(p\cos\beta - fp\sin\beta) = q_r \qquad (12.2)$$

we will find the value of the radial load.

$$q_r = \pi P\,\frac{1 - f\operatorname{tg}\beta}{\pi R\,(\operatorname{tg}\beta + f)}. \qquad (12.3)$$

The circumferential deformation of the ring is determined by Hooke's law for a uniaxial stressed state

$$\varepsilon = \frac{q_r R}{EF}, \qquad (12.4)$$

where E is the modulus of elasticity of the ring material and F – the

cross-sectional area of the ring.

The axial approximation of two rings in the vicinity of the ring under consideration and caused only by the deformation of the latter is equal to

$$w = 2\varepsilon R \operatorname{ctg} \beta. \tag{12.5}$$

The total upsetting of the spring can be calculated as a result of multiplying w by the number of rings. The relationship between the convergence of rings and the load during the first loading stage can be found after the expressions found earlier for quantities

$$w = \frac{2R(\operatorname{ctg}\beta - f)}{\pi EF(\operatorname{tg}\beta + f)} \alpha P \tag{12.6}$$

are substituted in the latter. This dependence is represented in the graph (Fig. 71) by a straight line passing through points 0 and 2. At the end of the stage under consideration $\alpha = 1$, so that

$$w_{max} = \frac{2R(\operatorname{ctg}\beta - f)}{\pi EF(\operatorname{tg}\beta + f)} P. \tag{12.7}$$

The second stage. When the load is decreased, parameter α assumes successively diminishing values, smaller than unity. Relative slip of the mating surfaces is absent for a certain value $\alpha = \alpha_3$ and the axial convergence of the rings becomes constant and equal to w_{max}. On the graph (Fig. 71), this process is represented by a straight line parallel to the ordinate axis and passing through points 2 and 3. The value of α_3 will be determined below.

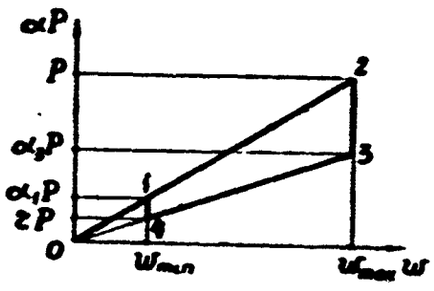

Fig. 71

The third stage. After parameter α reaches values smaller than α_3, the rings will begin to move apart. During this stage the load continues to decrease, therefore the frictional forces have directions

opposite to those which they had during the first stage; the radial load is determined by the dependence

$$q_r = \alpha P \frac{1 + f \operatorname{tg} \beta}{\pi R (\operatorname{tg} \beta - f)}. \qquad (12.8)$$

After repeating the calculations performed for the first stage, but for a new value of q_r, we will obtain a relationship between the axial convergence of the rings and the load in the form

$$w = \frac{2R (\operatorname{ctg} \beta + f)}{\pi EF (\operatorname{tg} \beta - f)} \alpha P. \qquad (12.9)$$

The value of α_3 can now be determined from the condition of equality of displacements calculated by Formulas (12.7) and (12.9) for point 3 on the graph (Fig. 71):

$$\alpha_3 = \frac{(\operatorname{ctg} \varphi - f)(\operatorname{tg} \varphi - f)}{(\operatorname{ctg} \varphi + f)(\operatorname{tg} \beta + f)}. \qquad (12.10)$$

The straight line corresponding to the dependence (12.9) passes, in Fig. 71, through points 0 and 3.

The fourth stage. After the load has reached the minimal value (for $\alpha = r$) it again begins to increase. No slip exists along the contact surfaces up to a certain value $\alpha = \alpha_1$ and the axial convergence remains constant and equal to w_{min}:

$$w_{min} = \frac{2R (\operatorname{ctg} \varphi + f)}{\pi EF (\operatorname{tg} \beta - f)} \alpha P. \qquad (12.11)$$

A straight line parallel to the ordinate axis and passing through points 4 and 1 corresponds to this dependence on the graph (Fig. 71).

After the load reaches the value $\alpha_1 P$, the convergence of the rings is again determined by Dependence (12.6) and the cycle is repeated.

The value of α_1 is determined from the condition of equality of displacements, calculated by Formulas (12.6) and (12.11) for the point 1:

$$\alpha_1 = -\frac{(\operatorname{ctg}\beta - f)(\operatorname{tg}\beta + f)}{(\operatorname{ctg}\beta + f)(\operatorname{tg}\beta - f)} r. \qquad (12.12)$$

The area of the hysteresis loop described in Fig. 71 is equal to:

$$\psi = \frac{2Rf(\operatorname{ctg}\beta + \operatorname{tg}\beta)}{\pi EF(\operatorname{ctg}^2\beta - f)}\left[\left(\frac{\operatorname{ctg}\beta - f}{\operatorname{tg}\beta + f}P\right)^2 - \left(\frac{\operatorname{ctg}\beta + f}{\operatorname{tg}\beta - f}rP\right)^2\right]. \qquad (12.13)$$

Taking into account Relationships (12.10) and (12.12), we can rewrite Expression (12.13) in the form

$$\psi = \frac{2Rf(\operatorname{ctg}\beta + \operatorname{tg}\beta)(\operatorname{ctg}\beta + f)}{\pi EF(\operatorname{ctg}\beta - f)(\operatorname{tg}\beta - f)^2}[(\alpha_1 P)^2 - (rP)^2] \qquad (12.14)$$

or

$$\psi = \frac{2Rf(\operatorname{ctg}\beta + \operatorname{tg}\beta)(\operatorname{ctg}\beta - f)}{\pi EF(\operatorname{ctg}\beta + f)(\operatorname{tg}\beta + f)^2}[P^2 - (\alpha_1 P)^2]. \qquad (12.15)$$

It can be seen from Expressions (12.14) and (12.15) that the energy dissipated during a cycle is proportional to the difference between the squares of the loads corresponding to the beginning and end of relative slip of the mating planes on loading or unloading.

Analyzing Dependence (12.13), we can see that the value of the energy dissipated during a cycle increases with a decrease of angle β and for the value $\beta = \beta_1$, determined from the condition

$$\operatorname{tg}\beta_1 = f. \qquad (12.16)$$

the entire supplied energy is dissipated during one loading cycle. The same value of β is also the minimal allowable, since jamming ensues for smaller angles..

Let us now turn to split rings. Let us consider a split ring with variable cross section, with geometrical dimensions shown in Fig. 72. It is loaded in the same manner as the continuous one, by forces distributed over the contact surfaces, the resultant of which is equal to the external axial load αP.

The ring bends under the action of the radial pressure component

and of the frictional forces acting along the mating surfaces. It is obvious that the axial convergence of rings neighboring on the one under consideration will be basically determined by the bending deformation due to the action of radial forces; the remaining effects can be disregarded. For the sake of simplification of computations, let us replace the pentagonal ring sections by rectangular. This will not introduce substantial errors if the triangular parts of the sections are replaced by rectangular ones with sides b and $\frac{b}{2\sqrt{3}}\operatorname{tg}\beta$. The width of the ring bounded by eccentric annular cylindrical surfaces, measured along the normal to the center line, passing through the section's centers of gravity, is determined by the dependence

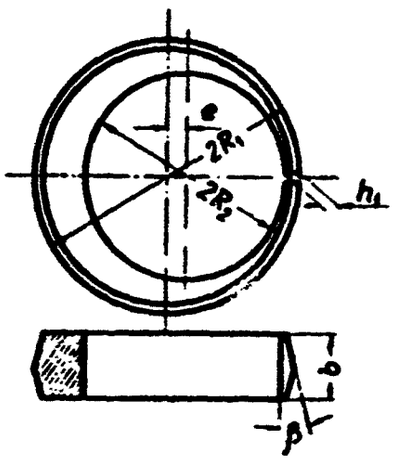

Fig. 72

$$h = h_0 + e\cos\varphi + \sqrt{\left(\frac{e\cos\varphi}{2}\right)^2 + \left(R + \frac{e}{2}\right)^2} - \sqrt{\left(\frac{e\cos\varphi}{2}\right)^2 + \left(R - \frac{e}{2}\right)^2}. \qquad (12.17)$$

Here R is the radius of the central axial line; e – the eccentricity of the internal and external circles; h_0 the width of the ring at the joint lock and φ is an angle reckoned from the radius passing through the joint lock. Dropping terms $\left(\frac{e\cos\varphi}{2}\right)^2$, we will write the approximate expression for the width of the ring

$$h = e(1 - \cos\varphi) + h_0. \qquad (12.18)$$

which will be further utilized in the calculations of the section moments of inertia.

The scheme of force distribution along the ring based on the known

concepts of the interaction of a split ring with the rigid cylindrical surface in contact with it is shown in Fig. 73.

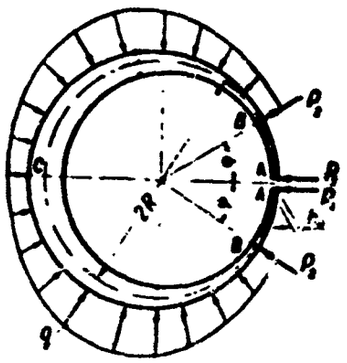

Fig. 73

It follows from the differential equation of the elastic curve of a curved rod

$$M = EJ\left(\frac{d^2u}{ds^2} + \frac{u}{R^2}\right) \qquad (12.19)$$

that on segment BCB, where the radial displacement is constant, the bending moment is equal to

$$M_{BB} = EJ\frac{u}{R^2}. \qquad (12.20)$$

Substituting for J its value found according to Expression (12.18) we will get:

$$M_{BB} = \frac{uEbc^3(1+k-\cos\varphi)^3}{12R^2}. \qquad (12.21)$$

where

$$k = \frac{h_0}{c}.$$

The bending moment at the segment AB

$$M_{AB} = P_1 \sin\varphi. \qquad (12.22)$$

From the equality of M_{BB} and M_{AB} at section B for $\varphi = \psi$, we can find

$$P_1 = \frac{uEbc^3(1+k-\cos\psi)^3}{12R^2\sin\psi}. \qquad (12.23)$$

Starting with differential dependences for a curved beam with a circular axis (Fig. 74) loaded by distributed radial forces of intensity q_r

$$\left.\begin{aligned}\frac{dQ}{d\varphi} &= q_r R + N\\ \frac{dM}{d\varphi} &= QR\\ \frac{dN}{d\varphi} &= -Q\end{aligned}\right\}, \qquad (12.24)$$

we can get

$$\frac{d^2M}{d\varphi^2} + \frac{dM}{d\varphi} = R^3 \frac{dq_r}{d\varphi} \qquad (12.25)$$

or, after integrating once,

$$\frac{d^2M}{d\varphi^2} + M = R^2 q_r + C. \qquad (12.26)$$

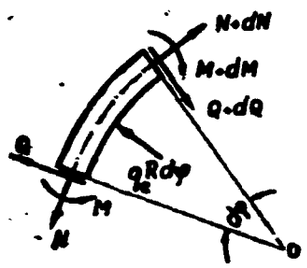

Fig. 74

The constant of integration C will be determined after the value

$$\frac{d^2M}{d\varphi^2} = R^2 Q + RN$$

found from Expressions (12.24) and the boundary conditions for $\varphi = \psi$

$$M = P_1 R \sin\psi \text{ and } N = -P_1 \sin\psi. \qquad (12.27)$$

are substituted into (12.26). It follows from this that C = 0.

Let us substitute into the thus found dependence

$$q_r = \frac{1}{R^2}\left(\frac{d^2M}{d\varphi^2} + M\right) \qquad (12.28)$$

the expression for the bending moment M; then the relationship governing the pressure distribution along segment BCB will be written in the form

$$q_r = \frac{uEbc^3}{12R^3}[(k+1)^3 - 3(k+1)\cos\varphi + 6(k+1)\sin^2\varphi - 6\cos\varphi\sin^2\varphi + 2\cos^3\varphi]. \qquad (12.29)$$

The moment equation relative to point C makes it possible to find the force P_2:

$$P_2 = \frac{uEb^3}{12R^3 \sin\psi}\left[(k+1)^2 - (k+2)^2 - 3(k+1) - \frac{1}{4}\right]. \qquad (12.30)$$

The condition relating the radial displacement of point A to the previously found values of the bending moments

$$2u = \int_0^{\psi} \frac{M_{AB}}{EJ} \frac{\partial M_{AB}}{\partial P_1} Rd\varphi + \int_{\psi}^{\pi} \frac{M_{BB}}{EJ} \frac{\partial M_{BB}}{\partial P_1} Rd\varphi. \qquad (12.31)$$

after the quantities entering it are substituted and after integration, gives an equation for the determination of the angle ψ, bounding the rings' contact zone:

$$s \cdot \operatorname{tg}\frac{\psi}{2}\left(\operatorname{tg}^4\frac{\psi}{2} - s^2\right) + \left(\operatorname{tg}^2\frac{\psi}{2} + s^2\right) \operatorname{arc\,ctg}\left(\frac{\operatorname{tg}\frac{\psi}{2}}{s}\right) = 2s^2 \operatorname{tg}^2\frac{\psi}{2}\left(1 + \operatorname{tg}^2\frac{\psi}{2}\right). \qquad (12.32)$$

where $s = \sqrt{\frac{k}{k+2}}$.

For k = ∞, the equation (12.32) for a ring with constant thickness will be written in the form

$$2 = \frac{\psi}{\sin\psi} + \cos\psi. \qquad (12.33)$$

which gives $\psi \simeq 122°$; for k = 0 we will find that $\psi = 0$.

The condition of equivalence between the radial forces and the external load is determined by the dependence

$$qP(\operatorname{ctg}\beta \mp f) = 2P_1 + 2P_2 + 2\int_{\psi}^{\pi} qRd\varphi. \qquad (12.34)$$

After the values of the appropriate quantities are substituted into the last expression we will find

$$qP(\operatorname{ctg}\beta \mp f) = \frac{uEbe^3}{R^3}\gamma, \qquad (12.35)$$

where

$$\gamma = \frac{1}{\sin^4\frac{\psi}{2}}\{[1 + 2(2 + k)^3 - 6(1 + k)] - [2(k+1)^3 + 6(k+1)^2 + 12(k+1)]\cos\psi + 6(k+1)\cos^2\psi + (6k+4)\cos^3\psi - \cos^4\psi\} + \frac{1}{6}(k+1)^3(\pi - \psi) + \frac{1}{4}(k+1)(\pi-\psi) + \frac{3}{8}(k+1)\sin 2\psi + \frac{7}{36}\sin^3\psi - \frac{1}{3}\sin\psi. \quad (12.36)$$

Repeating the same deliberations as in the preceding problem, we can construct a hysteresis loop, which has the shape shown in Fig. 71.

The area of the hysteresis loop is equal to:

$$\Psi = \frac{2R^3 J(\operatorname{ctg}\beta + \operatorname{tg}\beta)}{Ebc^3\gamma(\operatorname{ctg}^2\beta - J)}\left[\left(\frac{\operatorname{ctg}\beta - J}{\operatorname{tg}\beta + J}P\right)^2 - \left(\frac{\operatorname{ctg}\beta + J}{\operatorname{tg}\beta - J}rP\right)^2\right]. \quad (12.37)$$

[Footnotes]

Manuscript Page No.

107 Figure 62d does not show tangential stresses in the strip's cross sections; these stresses, variable along the length (arising according to the pairing property of tangential stresses), create a self-balanced system in each section and will not enter the equations that are subsequently formulated.

111 A more detailed analysis shows that no rigid coupling on a segment of the strip length is possible during unloading.

Part Two

SYSTEMS WITH ELASTIC-FRICTIONAL COUPLINGS

Chapter 5

RIVETED JOINTS

§13. AN ELEMENTARY SYSTEM

To clarify the basic qualitative peculiarities of the deformation of systems with elastic frictional character of interaction between parts, let us consider the elementary system represented in Fig. 75a.

The system consists of an elastic strip, pressed to a rigid undeformable foundation; it differs from the system considered in § 1 by the presence of couplings elastically resisting slippage of the strip along the foundation. Therefore, not only frictional forces but also tangential forces of interaction which have an elastic character, arise between the strip and the foundation. The number of elastic couplings is assumed to be sufficiently great so that it is possible to replace discrete couplings by a continuous elastic layer; furthermore, the tangential interaction forces between the strip and the foundation will be assumed to be distributed along the entire length of the strip.

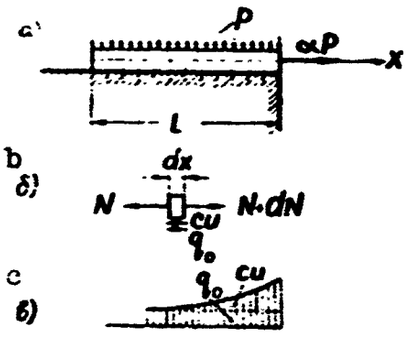

Fig. 75

The peculiarities of the distribution of frictional forces between the strip and foundation pointed out in Section 1 remain valid in this case; frictional forces are equal to zero at segments where slip is absent; where slip is present, these forces are equal to q_0. Let us add to this that the reactions of elastic couplings arise only in those

regions where the strip slips along the foundation; the elastic reactions thus arise only in those regions where frictional forces are present. The intensity of the reaction of elastic couplings will be determined by the dependence

$$q = -cu, \tag{13.1}$$

where c (kg/cm^2) is the rigidity coefficient of the couplings and u, as above, the displacement of the current section in the direction of the x-axis; this displacement will be denoted by the indices 1, 2 and 3, corresponding to the three stages of the process.

The first stage. Fig. 75b illustrates an element of the strip isolated in its deformation zone, and also forces acting on this element. The equilibrium equation

$$N' - q_0 - cu_1 = 0 \tag{13.2}$$

after the substitution

$$N = EFu_1' \tag{13.3}$$

is reduced to the differential equation

$$u_1'' - \beta^2 u_1 = \frac{q_0}{EF}, \tag{13.4}$$

where

$$\beta = \sqrt{\frac{c}{EF}}. \tag{13.5}$$

The solution of Eq. (13.4) has the form

$$u_1 = A_1 e^{\beta x} + B_1 e^{-\beta x} - \frac{q_0}{c}. \tag{13.6}$$

For determination of the quantities A_1 and B_1 and also of the size of the deformation zone, we will utilize the following three boundary conditions:

$$u_1(l - a_1, a) = 0; \quad u_1'(l - a_1, a) = 0; \tag{13.7}$$

$$u_1'(0, \alpha) = \frac{\alpha P}{EF}. \qquad (13.7)$$

Here a_1 is the length of the slip region corresponding to the given value of α. It is assumed that force N is not too great, so that $a_1 < l$ even for $\alpha = 1$. The first two conditions thus pertain to the left boundary of the slip segment, where it is the displacement and the longitudinal force N, proportional to the derivative u_1', which are equal to zero; the last condition pertains to the right end of the strip. Utilizing (13.7), we will get

$$A_1 = \frac{\alpha\beta P}{2c\varepsilon^{\beta l}}\left[\sqrt{1+\left(\frac{q_0}{\alpha\beta P}\right)^2}+1\right],$$
$$B_1 = \frac{\alpha\beta P\varepsilon^{\beta l}}{2c}\left[\sqrt{1+\left(\frac{q_0}{\alpha\beta P}\right)^2}+1\right], \qquad (13.8)$$
$$a_1 = \frac{1}{\beta}\ln\left[\frac{\alpha\beta P}{q_0}\left(\sqrt{1+\left(\frac{q_0}{\alpha\beta P}\right)^2}+1\right)\right].$$

The distribution of tangential forces of interation between the strip and the foundation in the process of the first loading is shown in Fig. 75c.

The second stage. During the second stage a reverse slip zone appears near to the end; the equation for this zone will be written in the form

$$u_2'' - \beta^2 u_2 = -\frac{q_0}{EF}. \qquad (13.9)$$

The solution of this equation should satisfy the boundary conditions

$$u_2(l-a_2, \alpha) = u_1(l-a_2, 1),$$
$$u_2'(l-a_2, \alpha) = u_1'(l-a_2, 1), \qquad (13.10)$$
$$u_2'(l, \alpha) = \frac{\alpha P}{EF}.$$

The first two conditions pertain to the boundary between the direct and reverse slip zones, when the solutions of Eqs. (13.4) and (13.9) should

coincide with the first derivatives of these solutions.

The solution of Eq. (13.9) has the form

$$u_2 = A_2 e^{\beta x} + B_2 e^{-\beta x} + \frac{q_0}{c}. \tag{13.11}$$

where

$$\begin{aligned} A_2 &= \frac{\beta P}{2ce^{\beta l}}\left[\sqrt{1+\left(\frac{q_0}{\beta P}\right)^2} - \sqrt{(\alpha-1)^2+\left(\frac{2q_0}{\beta P}\right)^2} + \alpha\right], \\ B_2 &= \frac{\beta P e^{\beta l}}{2c}\left[\sqrt{1+\left(\frac{q_0}{\beta P}\right)^2} - \sqrt{(\alpha-1)^2+\left(\frac{2q_0}{\beta P}\right)^2} - \alpha\right]. \end{aligned} \tag{13.12}$$

The length of the reverse slip zone is determined by the formula

$$a_2 = \frac{1}{\beta}\ln\left[\frac{\beta P}{2q_0}\sqrt{(\alpha-1)^2+\left(\frac{2q_0}{\beta P}\right)^2} - \alpha + 1\right]. \tag{13.13}$$

<u>The third stage</u>. The load increases again. For the end segment when direct slip is renewed, the equation again acquires the previous form (13.4), so that the solution will be written in the form

$$u_3 = A_3 e^{\beta x} + B_3 e^{-\beta x} - \frac{q_0}{c}. \tag{13.14}$$

Boundary conditions

$$\begin{aligned} u_3(l-a_3, \alpha) &= u_2(l-a_3, r), \\ u'_3(l-a_3, \alpha) &= u'_2(l-a_3, r), \\ u'_3(l, \alpha) &= \frac{\alpha P}{EF}. \end{aligned} \tag{13.15}$$

serve for the determination of the length of the end zone a_3 and of the quantities A_3 and B_3. Utilizing (13.15), we will find

$$\begin{aligned} a_3 &= \frac{1}{\beta}\ln\left[\frac{\beta P}{2q_0}\sqrt{(\alpha-r)^2+\left(\frac{2q_0}{\beta P}\right)^2} + \alpha - r\right], \\ A_3 &= \frac{\beta P}{2ce^{\beta l}}\left[\sqrt{1+\left(\frac{q_0}{\beta P}\right)^2} - \sqrt{(1-r)^2+\left(\frac{2q_0}{\beta P}\right)^2} + \right. \\ &\quad \left. + \sqrt{(\alpha-r)^2+\left(\frac{2q_0}{\beta P}\right)^2} + \alpha\right], \\ B_3 &= \frac{\beta P e^{\beta l}}{2c}\left[\sqrt{1+\left(\frac{q_0}{\beta P}\right)^2} - \sqrt{(1-r)^2+\left(\frac{2q_0}{\beta P}\right)^2} + \right. \\ &\quad \left. + \sqrt{(\alpha-r)^2+\left(\frac{2q_0}{\beta P}\right)^2} - \alpha\right]. \end{aligned} \tag{13.16}$$

Utilizing Expressions (13.6), (13.11) and (13.14) for u_1, u_2 and u_3, we can construct a hysteresis loop for any given combination of the system's parameters. The general character of the loop coincides with that illustrated in Fig. 14. The area of the loop is determined by Formula (1.32) and is equal to

$$\Psi = \frac{2q_0(1-r)P}{c} + \frac{2q_0^2}{\beta c}\ln\frac{r-1+\sqrt{(1-r)^2+\left(\frac{2q_0}{\beta P}\right)^2}}{1-r+\sqrt{(1-r)^2+\left(\frac{2q_0}{\beta P}\right)^2}}. \qquad (13.17)$$

Substituting here, as above, $P(1-r) = 2P_v$, we will get

$$\Psi = \frac{2P_0^2}{q_0 E f}\left[2\gamma^2 + \gamma^3\ln\frac{\sqrt{1+\gamma^2}-1}{\sqrt{1+\gamma^2}+1}\right], \qquad (13.18)$$

where the parameter

$$\gamma = \frac{q_0}{\beta P_0} \qquad (13.19)$$

characterizes the role of frictional forces in relation to the foundation. For a vanishingly small rigidity of couplings we can assume that $\beta = 0$ and the expression in parentheses will become indeterminate. After the indeterminate function has been evaluated, we find that it is equal to 1/3; furthermore, Solution (1.34) coincides with Solution (13.18) obtained above for the case when elastic couplings are absent. For vanishingly small frictional forces $q_0 = 0$ and the entire expression (13.18) becomes zero.

Figure 76 shows the dependence of the area of the hysteresis loop Ψ on the dimensionless parameter γ. The ratio of Ψ to the value of Ψ_0 calculated by Formula (1.34) and corresponding to the case when elastic couplings are absent is laid off along the ordinate axis.

As can be seen from the graph, already for $\gamma > 2$ the difference between Ψ and Ψ_0 becomes insubstantial and it is possible to approximately estimate energy dissipation disregarding the role of elastic

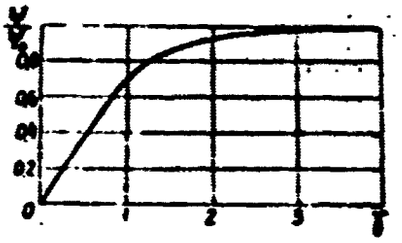

Fig. 76

couplings.

The solution here presented can without difficulty be extended to the case when slip takes place along the entire length of the strip for large values of P.

§14. JOINING TWO STRIPS BY COVER PLATES

Let us now consider two strips joined by cover plates by means of rivets (Fig. 77). If the number of rivets is sufficiently great we can assume that the intensity of tangential forces of interaction in the slip zone is equal to

$$q = q_0 + c(u_1 - u_2), \tag{14.1}$$

where u_1 is the displacement of the current section of the strip and u_2 is the displacement of the current section of the cover plates.

The intensity of the reaction of the elastic couplings

$$s = c(u_1 - u_2). \tag{14.2}$$

Figure 78 shows the loading of the elements of the joint at the end of the first loading stage (it is assumed that the value of force P is insufficient for the relative displacements to propagate over the entire mating surface).

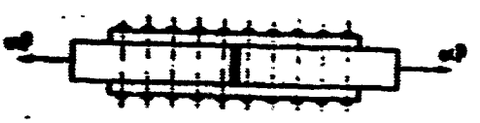

Fig. 77

Let us consider the equilibrium of an end segment of the strip, on which slip takes place. This segment has a length a_1 and is subjected to the action of forces αP, q and $k\alpha P$, as this is shown in Fig. 79a. The magnitude of force $k\alpha P$ is determined from the condition of equality of the displacements of the strip and the cover plates at the boundary of the segment and is

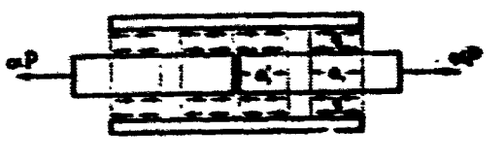

Fig. 78

equal to

$$k\alpha P = \frac{k_1}{k_1 + k_2}\alpha P, \tag{14.3}$$

i.e.,

$$k = \frac{k_1}{k_1 + k_2}, \tag{14.4}$$

where k_1 is the rigidity of the strip's section and k_2 is the total rigidity of the cover plates' sections.

Denoting the normal forces in the current sections of the strip and the cover plates by N_1 and N_2, we will write the condition for the equilibrium of the strip element (Fig. 79d)

$$N_1' - c(u_1 - u_2) = q_0. \tag{14.5}$$

Differentiating Eq. (14.5) in respect to $\underline{x}$ and keeping in mind that $N_1 = k_1 u'_1$ and $u_2' = \frac{\alpha P}{k_2} - u_1' \frac{k_1}{k_2}$ (since $N_2 = \alpha P - N_1$ in any section), we will get the equation

$$u_1''' - \beta^2 u_1' = -\frac{\alpha P c}{k_1 k_2}, \tag{14.6}$$

where

$$\beta^2 = c\left(\frac{1}{k_1} + \frac{1}{k_2}\right). \tag{14.7}$$

As follows from load systems on the element during the second and third loading stages (Fig. 79b and $\underline{c}$), Eq. (14.6) is valid also for these stages.

Assigning to $\underline{u}$ additional indices, corresponding to the stage numbers, we will write the boundary conditions for each stage.

The first stage:

$$\begin{aligned} u_{11}(a, 0) &= 0, \\ u_{11}'(a, 0) &= \frac{k\alpha P}{k_1}, \end{aligned} \tag{14.8}$$

$$u'_{11}(\alpha, a_1) = \frac{\alpha P}{k_1},$$
$$u''_{11}(\alpha, 0) = \frac{q_0}{k_1} \qquad (14.8)$$

The second stage:

$$u_{12}(\alpha, a_2) = u_{11}(1, a_2) - \frac{(1-\alpha)Pa_2}{k_1 + k_2},$$
$$u'_{12}(\alpha, a_2) = u'_{11}(1, a_2) - \frac{(1-\alpha)P}{k_1 + k_2},$$
$$u''_{12}(\alpha, a_2) = u''_{12}(1, a_2) - \frac{2q_0}{k_1}, \qquad (14.9)$$
$$u'_2(\alpha, a_1) = \frac{\alpha P}{k_1}.$$

The third stage:

$$u_{13}(\alpha, a_3) = u_{12}(r, a_3) + \frac{(\alpha - r)Pa_3}{k_1 + k_2},$$
$$u'_{13}(\alpha, a_3) = u'_{12}(r, a_3) + \frac{(\alpha - r)P}{k_1 + k_2},$$
$$u''_{13}(\alpha, a_3) = u''_{12}(r, a_3) + \frac{2q_0}{k_1}, \qquad (14.10)$$
$$u'_{13}(\alpha, a_1) = \frac{\alpha P_0}{k_1}.$$

Subjecting the solution of Eq. (14.6) successively to the boundary conditions (14.8), (14.9) and (14.10), we will obtain the following expression for determination of the displacement of the right end section.

During the first stage:

$$u_{11} = \frac{q_0}{\beta^2 k_1}\left\{\sqrt{\left[\frac{(1-k)\alpha\beta P}{q_0}\right]^2 + 1} - 1\right\} + \frac{\alpha P a_1}{k_1 + k_2}, \qquad (14.11)$$

where

$$a_1 = \frac{1}{\beta}\ln\left\{\frac{P(1-k)\beta}{q_0} + \sqrt{\left[\frac{P\beta(1-k)}{q_0}\right]^2 + 1}\right\}. \qquad (14.12)$$

During the second stage:

$$u_{12} = \frac{q_0}{\beta^2 k_1}\left\{\sqrt{\left[\frac{P\beta(1-k)}{q_0}\right]^2 + 1} - \right. \qquad (14.13)$$

$$-2\sqrt{\left[\frac{(1-\alpha)(1-k)\beta P}{2q_0}\right]^2+1}-1\Bigg\}+\frac{\alpha P a_1}{k_1+k_2}. \qquad (14.13)$$

During the third stage:

$$u_{13}=\frac{q_0}{\beta^2 k_1}\left\{\sqrt{\left[\frac{P\beta(1-k)}{q_0}\right]^2+1}-2\sqrt{\left[\frac{(1-r)P(1-k)\beta}{2q_0}\right]^2+1}+\right.$$
$$\left.+2\sqrt{\left[\frac{(\alpha-r)P(1-k)\beta}{2q_0}\right]^2+1}-1\right\}+\frac{\alpha P a_1}{k_1+k_2}. \qquad (14.14)$$

The graph of the dependence of the displacement of the right end section of the strip on the force αP is similar to that illustrated

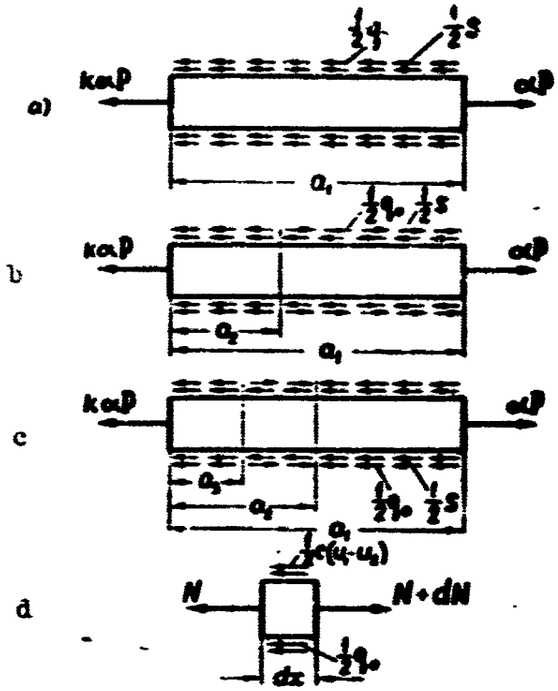

Fig. 79

in Fig. 14.

Finding, as before the area of the hysteresis loop, we will obtain the value of the energy dissipated in the considered part of the joint:

$$\Psi=\frac{4P_0^2(1-k)^2}{q_0k_2}\left(\gamma_1^2-\gamma_1^2\operatorname{Arsh}\frac{1}{\gamma_1}\right), \qquad (14.15)$$

where

$$\gamma_1=\frac{q_0}{P_0(1-k)\beta};\qquad P_0=\frac{1-r}{2}P. \qquad (14.16)$$

To determine the energy dissipated on the internal segments of the mating surface (segment a_1' in Fig. 78), it is sufficient to interchange the positions of k_1 and k_2 in Expression (14.15). Then we will obtain the following expression for the total dissipated energy:

$$\Psi^* = \frac{4P_*^3}{q_0}\left[\left(\gamma_1^2 - \gamma_1^3 \operatorname{Arsh}\frac{1}{\gamma_1}\right)\frac{(1-k)^2}{k_1} + \left(\gamma_2^2 - \gamma_2^3 \operatorname{Arsh}\frac{1}{\gamma_2}\right)\frac{k^2}{k_2}\right], \qquad (14.17)$$

where

$$\gamma_2 = \frac{q_0}{P_* \beta k}. \qquad (14.18)$$

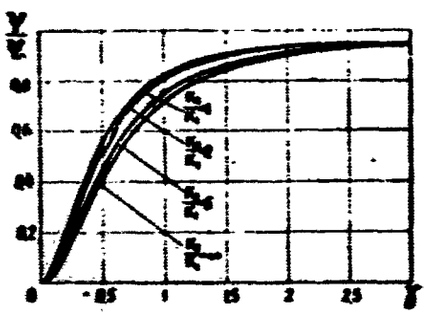

Fig. 80

Figure 80 illustrates the dependence of the area of the hysteresis loop on the parameter $\gamma = \frac{q_0}{P_*}\sqrt{\frac{k_1}{c}}$ for different ratios $k_2 : k_1$. The ratio of Ψ to the value of Ψ_0 corresponding to a purely frictional coupling is, as before, laid off on the ordinate axis. Value $k_2 : k_1 = 1$ corresponds to the maximal energy dissipation, the value $k_2 : k_1 = \infty$ – to minimal dissipation. The curve for $k_2 : k_1 = \infty$ coincides with that shown in Fig. 76, since in this case Formula (14.17) is transformed into (13.18). As can be seen from the graphs, the simpler Formula (13.18) can be utilized for an approximate estimate, and Formula (1.34) – for $\gamma > 2$.

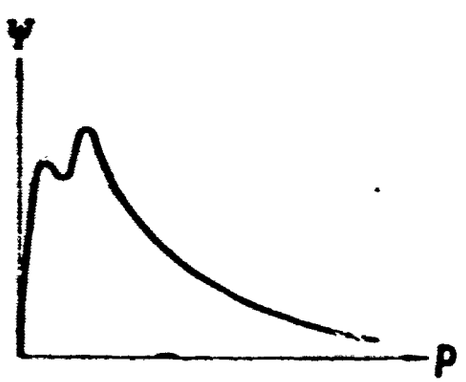

Fig. 81

The character of the dependence of the area of the hysteresis loop Ψ on the frictional force q_0 is shown in Fig. 81. In the general case, the curve has two maxima, corresponding to the maxima of energy dissipated in two different ends of the mating surface.

§15. PURE BENDING OF A BEAM WITH COVER PLATES

Figure 82 shows the beam with cover plates which is considered here, loaded by two bending moments. The cover plates are joined to the beam by rivets; the external moment is applied only to the beam. This scheme is similar to that considered in Section 4.

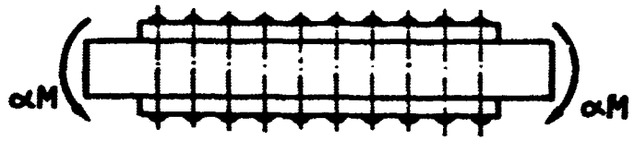

Fig. 82

Slip of the cover plate relative to the external fiber of the beam occurs at the beam's ends for any value of αM. The intensity of the tangential forces of interaction between the cover plates and the beam will be written as before in the form

$$q = c(u_1 - u_2) + q_0 \qquad (15.1)$$

where u_1 is the displacement of a point of the extreme beam layer and u_2 is the displacement of the corresponding point on the cover plate.

It is assumed in the subsequent calculations that the cover plates are sufficiently thin and their rigidity in bending is not taken into account.

Figure 83 shows the beam loading during the three loading stages (the cover plates are taken off). Let us separate a differential element of the segment where slip took place (Fig. 84) and, denoting the bending moment in the beam section by M_0, let us write the condition for the element's equilibrium

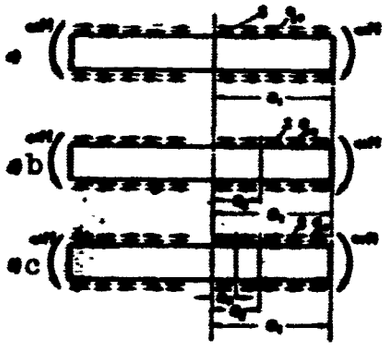

Fig. 83

$$\frac{dM_0}{dx} - qh = 0, \qquad (15.2)$$

where h is the height of the beam.

Utilizing also the equation for the equilibrium of the end segment of the beam (Fig. 85)

$$aM = M_0 + EFu_2' \tag{15.3}$$

and the relationship

$$M_0 = \frac{2EJ_0}{h} u_1', \tag{15.4}$$

where F is the cross-sectional area of the cover plates and J_0 is the moment of inertia of the beam section without the cover plates, we will obtain the equation

$$u_1''' - \frac{cJ}{EJ_0F} u_1' = -\frac{aMch}{2E^2J_0F}. \tag{15.5}$$

where J is the moment of inertia of the cross section of the beam with the cover plates.

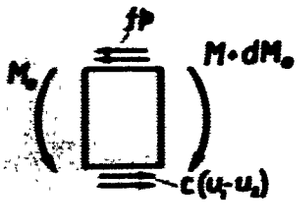

Fig. 84

The form of Eq. (15.5) is similar to Eq. (14.6). Similar to the manner in which it was done in the preceding paragraph, we can obtain the following expression for the energy dissipated during the beam's loading cycle:

$$\Psi = \frac{M_0^2h^2F^2}{EJ^2J_0q_0}\left(\gamma^2 - \gamma^2 \operatorname{Arsh}\frac{1}{\gamma}\right), \tag{15.6}$$

where

$$\gamma = \frac{q_0h}{M_0}\sqrt{\frac{EJF}{cJ_0}}. \tag{15.7}$$

It is obvious that also in this case it is possible to approximately determine, for $\gamma > 2$, the dissipated energy by Formula (4.15), obtained for a purely frictional joint.

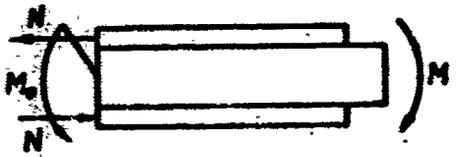

Fig. 85

If the slip regions are propagated over the entire mating surface, the hys-

teresis loop has the shape shown in Fig. 21. In this case a successive analysis of the five loading stages results in the following formula for the area of the loop:

$$\Psi = \frac{8q_0^2 J}{EFJ_0\beta^3}\left[\frac{1}{\gamma}\left(1-\frac{1}{ch\beta l}\right)+\operatorname{th}\beta l-\beta l\right], \qquad (15.8)$$

where $\beta^2 = \frac{cJ}{EFJ_0}$; and $2\underline{l}$ is the length of the cover plate.

The boundary of applicability of Formulas (15.7) and (15.9)[sic] is determined by the amplitude of the moment

$$M_0 = \frac{2q_0 J \operatorname{sh}\beta l}{\beta hF}. \qquad (15.9)$$

Formula (15.6) is valid for smaller amplitudes and Formula (15.8) for larger ones.

The applicability of the dependencies obtained above for determination of energy dissipation of actual riveted joints operating in the dynamic mode was verified by experiment.

The experimental specimen constituted a steel beam with a rectangular cross section (Fig. 86) fabricated together with the

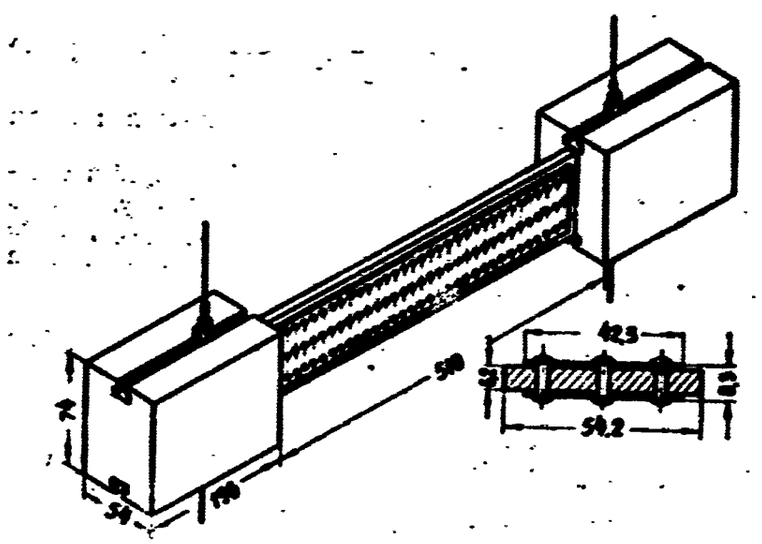

Fig. 86

end masses as a single entity. The cover plates were fastened to the

beam by steel rivets. To ensure a sufficiently uniform pressi. ıe cover plates to the beam and to improve filling of the holes, the ‹et heads were formed by pressing the rivets using the same force for each of them.

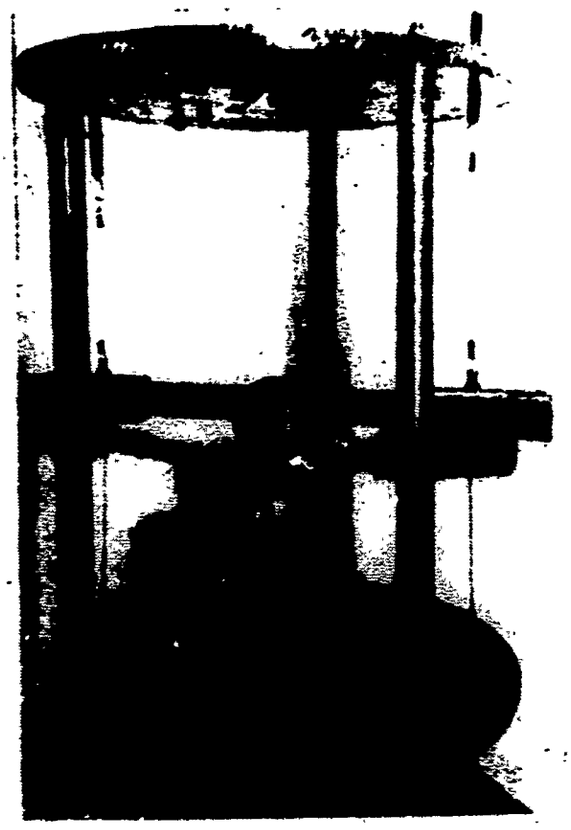

Fig. 87

The general view of the experimental installation is shown in Fig. 87. The beam was suspended by vertical wires to massive plates and was brought into resonance by an electromagnet oscillator, fed by variable-frequency AC. Of the two possible bending-vibration modes, (Fig. 88), we induced the first. The amplitude of the disturbing force could be changed and the amplitude controlled by varying the distance between the oscillator and the beam. After the given amplitude has been set, the oscillator was shut off and the oscillogram of free vibrations was recorded. The recording was made off a tensometer utilizing the UD-3M (IMASh AN SSSR) amplifier and the MPO-2

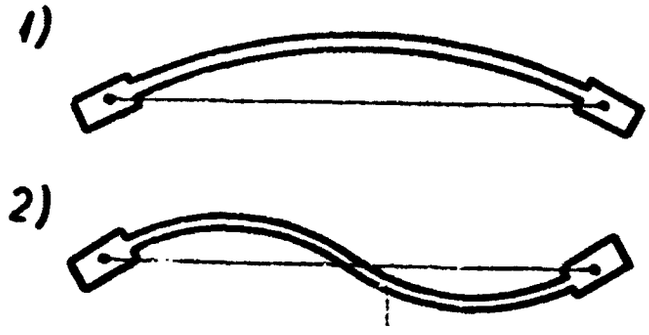

Fig. 88

oscillograph.

The energy dissipated during one cycle was determined by the formula

$$\Psi = \frac{k}{2}(\varphi_i^2 - \varphi_{i+1}^2), \qquad (15.10)$$

where k is the rigidity of the beam, i.e., the torque creating a relative angle of twist of the end masses equal to one radian and φ_1 is the angle of relative twist of the end masses.

The determination of the beam's rigidity and calibration of the oscillograms were performed under static conditions.

A linear relationship between the deformation on one hand and the torque and angle of twist on the other was assumed in the interpretation of the oscillograms.

The results of the experiment were compared with the theoretical, calculated by Formula (15.7) transformed to the form

$$\Psi = \frac{M_0^2 k^2 f^2}{2J^2 J_0 E f p n}\left(2\pi\gamma^2 + \pi^{\frac{3}{2}}\gamma^2 \ln\frac{\sqrt{\pi\gamma^2+1}-1}{\sqrt{\pi\gamma^2+1}+1}\right). \qquad (15.12)$$

Here

$$\gamma = \frac{2fp}{M_0 k}\sqrt{\frac{EJJ_0}{cF}}.$$

where fp is the frictional force corresponding to one rivet, c is the

rigidity of one rivet and n is the number of rivets per unit length of the cover plates.

The number of rivets n and the frictional force fp were varied in the course of the experiments; the latter was achieved by changing the force with which the rivet heads were pressed.

Special specimens (Fig. 89), consisting of two plates joined by cover plates by four or six rivets, the heads of which were pressed by the same force as was used in the assembly of the beam, were fabricated for the determination of numerical values of quantities c and fp. Thin graduation lines were made in the polished side surfaces of the specimen; the specimen was stretched in a special fixture and the relative displacements of the graduation lines on loading and unloading were measured under a microscope with 280x magnification (MIM-6). Graphs of the dependence of the stretching force Q on the mean relative displacement δ had the shape shown in Fig. 90. The values of fp and c were taken as equal to:

$$fp = \frac{Q_0}{2n}; \qquad c = \frac{tg\varphi}{2n},$$

where n is the number of rivets on the specimen. It was found that the frictional force fp is equal to 25 and 60 kg respectively for a head pressing force of 1000 and 3000 kg. The mean rigidity c on changing the pressing force from 1000 to 3000 remained constant and was equal to 6.10^4 kg/cm. Deviation from the mean values did not exceed 25%.

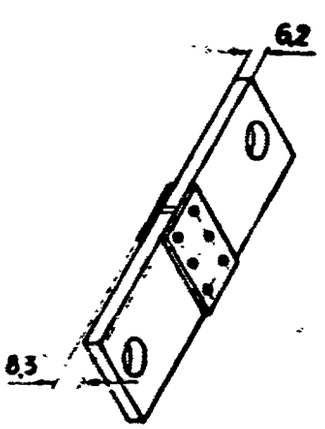

Fig. 89

The frictional force was determined by still another method. A slot from the middle rivet hole to the edge was cut in one of the specimen's plates (Fig. 91).

The cover plates were joined to this plate by one rivet put into the slot. The frictional force was assumed to be equal to half of the tearing capacity of the plate. Results measured by the first and second methods gave the same mean value of the quantity fp.

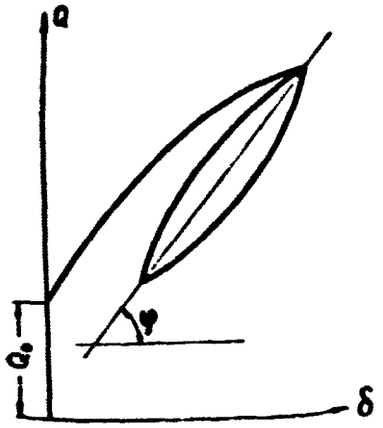

Fig. 90

Graphs showing the dependence of energy dissipated during one cycle on the amplitude of the torque and the experimental points corresponding to them are shown in Figs. 92 and 93. The experimental results fully verify the validity of the theoretical relationships. A curve corresponding to the case c = 0 (purely frictional joint) is shown in Fig. 93 by a dashed line. The two curves almost coincide, which verifies the previously drawn conclusion as to the applicability of Formula (4.15) for approximate calculations of energy dissipation in elastic-frictional joints (for large values of parameter γ).

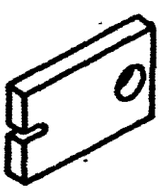

Fig. 91

§16. TRANSVERSE BENDING OF A CANTILEVER

We shall consider Goodman's and Klamp's problem

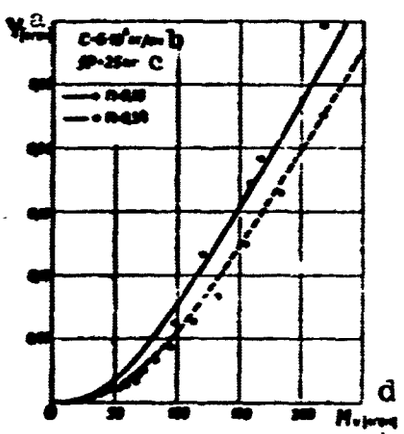

Fig. 92. a) Kg-cm; b) kg/cm; c) kg; d) kg-cm.

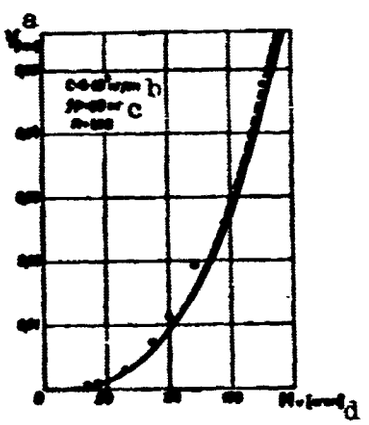

Fig. 93. a) Kg-cm; b) kg/cm; c) kg; d) kg-cm.

presented in Section 5 on the assumption that not only tangential frictional forces, but elastic resistance forces (for example, due to a rivet or bolt system) can act on the mating surface of two beam layers.

During the first stage, as in the Goodman and Klamp problem, both halves of the cantilever deform together and the end deflection is determined by Formula (5.2) up to the value $\alpha_0 = 4/3\ q_0 h$; here the tangential forces along the mating surface of the parts are realized only in the form of frictional forces.

After the tangential forces reach the value q_0, simultaneous slip will occur over the entire mating surface. The load system on a half of the cantilever during the second stage is shown in Fig. 94. The intensity of the distributed tangential load q is determined by the dependence

$$q = q_0 + 2cu, \tag{16.1}$$

where u is the displacement in the current section along the mating plane.

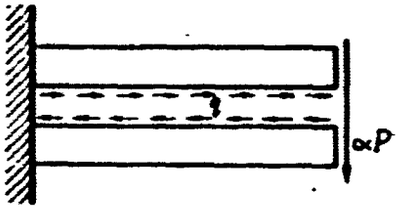

Fig. 94

For determination of the displacement u let us consider the conditions for the equilibrium of an element isolated at a distance x from the free end (Fig. 95):

$$M' + (2cu + q_0)\frac{h}{2} - Q = 0, \tag{16.2}$$

$$N' - (2cu + q_0) = 0, \tag{16.3}$$

where M, N and Q are the bending moment, the normal and shear forces in one layer of the cantilever.

From the condition of equilibrium of the cut-off part of the cantilever (Fig. 96) we will get

$$Nh + 2M = \alpha P x. \tag{16.4}$$

Hooke's law for the beam's contact surface can be written in the form

$$\frac{N}{bh} - \frac{6M}{bh^2} = Eu'. \tag{16.5}$$

Utilizing Dependencies (16.2), (16.3), (16.4) and (16.5), we will get the equation

$$u'' - \beta^2 u = -\frac{3(\alpha - \alpha_0)P}{Ebh^2}, \tag{16.6}$$

where

$$\beta^2 = \frac{8c}{Ebh}. \tag{16.7}$$

The boundary conditions of our problem have the following form:

$$u(l) = 0, \quad u'(l) = 0. \tag{16.8}$$

Determining u and thus clarifying the value of the distributed moment load, equal to qh/2, we will find the displacement of the cantilever's end during the second stage:

$$x_2 = \frac{Pl^3}{24EJ}\left[(4\alpha - 3\alpha_0) - 9(\alpha - \alpha_0)\left(\frac{1}{3} - \frac{1}{\beta^2 l^2} + \frac{\operatorname{th}\beta l}{\beta^3 l^3}\right)\right]. \tag{16.9}$$

The two halves again deform together during the third stage and the deflection of the cantilever's end is equal to:

$$y_2 = y_2 - \frac{(1-\alpha)Pl^3}{24EJ} \tag{16.10}$$

or

$$y_2 = \frac{Pl^3}{24EJ}\left[\alpha + 9(1-\alpha_0)\left(\frac{1}{\beta^2 l^2} - \frac{\operatorname{th}\beta l}{\beta^3 l^3}\right)\right]. \tag{16.11}$$

Without dwelling on the subsequent [processes], let us note that in the given case the hysteresis loop is similar to that presented in Fig. 29. Calculating the area of the loop by Formula (5.16), we will get

$$\Psi = \frac{8q_0 l^2}{Ebh^2}(3l - 4q_0 h)\left(\frac{1}{\beta^2 l^2} - \frac{\operatorname{th}\beta l}{\beta^3 l^3}\right). \tag{16.12}$$

Figure 97 illustrates the dependence of the ratio $\Psi : \Psi_0$ (Ψ_0 is calculated by Formula (5.17)) upon the parameter $1/\beta l$. The graph coincides with that shown in Fig. 76. The ratio Ψ/Ψ_0 differs very little from zero for the value $1/\beta l > 2$, i.e., the role of elastic couplings becomes insignificant. The dependence of the dissipated energy on the frictional forces can be illustrated by graphs (see Fig. 81), by changing the scale of the ordinate axis by a ratio of

$$3\left(\frac{1}{\beta^2 l^2} - \frac{\operatorname{th}\beta l}{\beta^3 l^3}\right)$$

Let us present the final results of the solution of the problem of bending of a cantilevered beam with pressure plates (see Fig. 10).

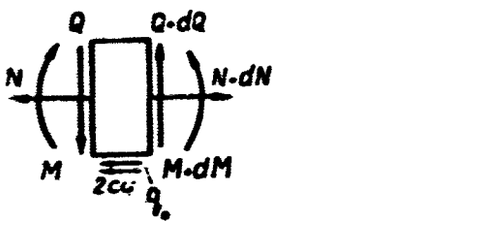

Fig. 95

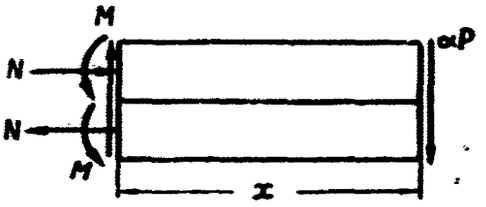

Fig. 96

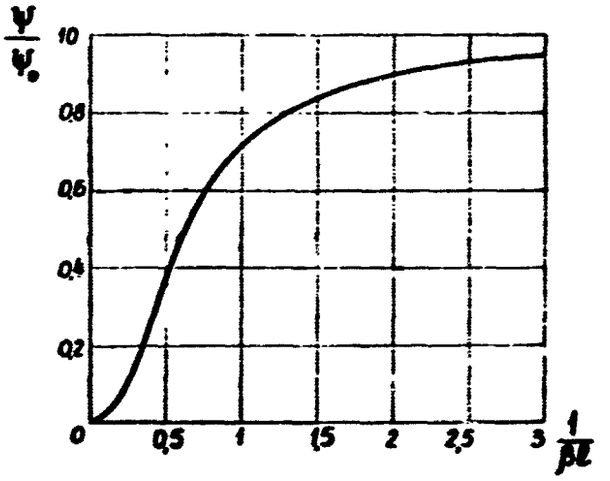

Fig. 97

Pian [36] has solved a similar problem on the assumption that the interaction between the cover plates and the beam carries an elastic-frictional character, and has obtained the following formula for the energy dissipated during one beam loading cycle:

$$\Psi = \frac{4EJ_0 qk^2}{cJ^2\gamma}(\gamma l - A\operatorname{rsh}\gamma l). \qquad (16.13)$$

Here

$$\gamma = \frac{P_0 Fh}{2Jq_0 + P_0 Fh}\sqrt{\frac{cJ}{EJ_0}}.$$

Formula (5.29) is obtained for $\underline{c} = 0$ as a particular result of Formula (16.13).

The experiment set up by Pian has as its goal checking the dependence of dissipated energy on the amplitude of the force. The experimental beam is shown in Fig. 98. The pressure plates were fastened to the beam by special threaded joints, consisting of dowels with two nuts. The design of the joints ensured transmission of the elastic forces from the beam to the pressure plates. It has been established by special

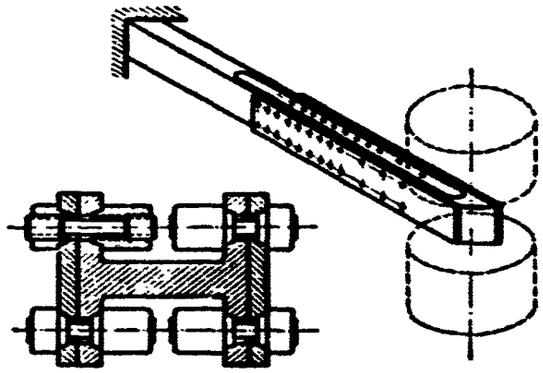

Fig. 98

measurements that the rigidity of the elastic couplings amounts on the average to 7400 kg/cm^2, and the frictional force per unit length of the pressure plate is related to the nut tightening torque M in the following manner:

$$q_0 = 20M.$$

The value of the dissipated energy was calculated by the oscillograms of free damped vibrations. Figure 99 shows theoretical and experimental dependencies of the dissipated energy on twice the load amplitude, obtained by Pian.

As can be seen, the experimental data verify the theory very well.

§17. STRUCTURAL DAMPING IN A RIVETED THIN-WALLED BEAM

Earlier (§ 7) we have considered the purely frictional scheme of

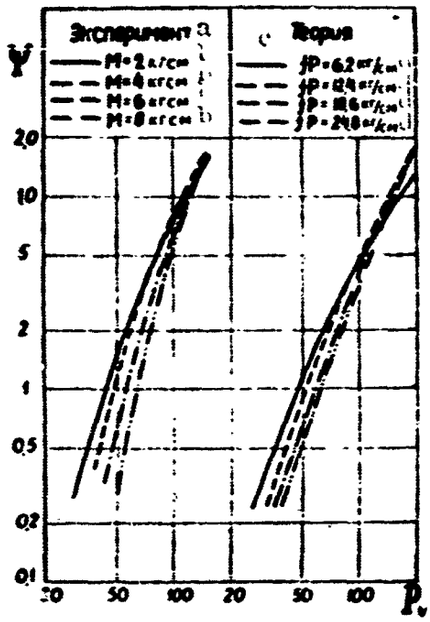

Fig. 99. a) Experiment; b) kg-cm; c) theory; d) kg/cm.

the structural damping problem in a thin-walled beam. It was assumed there that the rivets connecting the web to the rods (standards and flanges) only ensure pressing the web to the rods and do not resist relative slip of the web and the rods due to the fact that the rivet blanks are seated in the holes with a positive allowance.

In the present section we will approximately take into account the elastic resistance force which is exerted by the rivets on the displacements of the wall relative to the rods. As in the preceding sections, we will assume that a homogeneous elastic layer between the joined elements has replaced the rivets. This layer exerts a resistance to the slip of the joined components, proportional to the relative displacements.

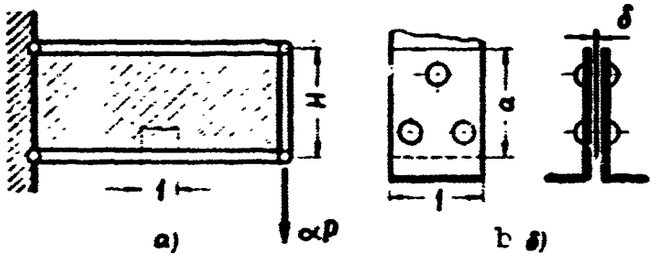

Fig. 100

Let us consider a single-panel thin-walled beam shown in Fig. 100a. Since all the seams are subject to the same conditions, it is sufficient to consider a seam element of unit length (Fig. 100b). As can be seen, the contact region where the web is compressed between

the angle bars forming the flange is of width a.

The tangential forces q in the beam web are determined by the formula

$$q = \frac{\alpha P}{h}. \qquad (17.1)$$

If the beam is multi-panelled and several forces αP act on one side of the section under consideration, then the transverse shear force should be substituted into Formula (17.1).

The tangential forces in the web increase with an increasing load. As a result, shear takes place also in that section of the web which is compressed between the rods. This shear results in slip of the web relative to the rods. If we discuss Fig. 100b, then slip starts in the upper part of the contact region and is propagated downward.

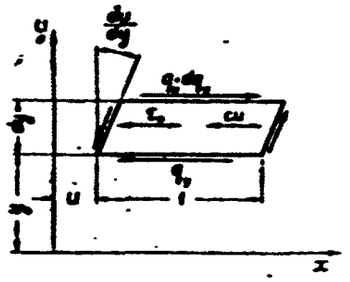

Fig. 101

Let us consider the equilibrium and deformations of a web element (Fig. 101), isolated in the slip zone. The element is subject to the action of: tangential forces q_y in the section where y = const., frictional forces and elastic rivet reaction forces. Let us refer the frictional forces τ_0 and the rivet reaction forces cu to unit contact surface. The quantity c is the rigidity coefficient of the plastic layer which replaced the rivets. Projecting the forces applied to the element on the x-axis, we will get

$$\frac{dq_y}{dy} = 2\tau_0 + cu. \qquad (17.2)$$

The multiplier 2 of τ_0 takes into account the two-sided contact between the web and the flange and u is the displacement of the web

relative to the flanges in the contact zone.

The shearing strain in the web is equal to $\gamma_{xy} = du/dy$. Utilizing Hooke's law, we will get

$$\frac{du}{dy} = \frac{q_y}{G\delta}. \tag{17.3}$$

Here δ is the web thickness and G is the shear modulus. From (17.2) and (17.3) we will obtain the differential equation

$$\frac{d^2u}{dy^2} - \beta^2 u = \frac{2\tau_0}{G\delta}, \tag{17.4}$$

where

$$\beta^2 = \frac{c}{G\delta}. \tag{17.5}$$

The solution of Eq. (17.4) has the form:

$$u = A_1 \operatorname{ch} \beta y + B_1 \operatorname{sh} \beta y - \frac{2\tau_0}{c}. \tag{17.6}$$

Then from (17.3):

$$q_y = G\delta \frac{du}{dy} = \beta G\delta (A_2 \operatorname{sh} \beta y + B_1 \operatorname{ch} \beta y). \tag{17.7}$$

Let us turn to the first loading stage when α varies from zero to unity. Let, for a certain value of the coefficient α_1, when the tangential forces in the web reach the value q_1, the slip have spread to the width a_1 (Fig. 102a). The x-axis will be directed along the lower boundary of the slip zone. Then u = 0 and $q_{1y} = 0$

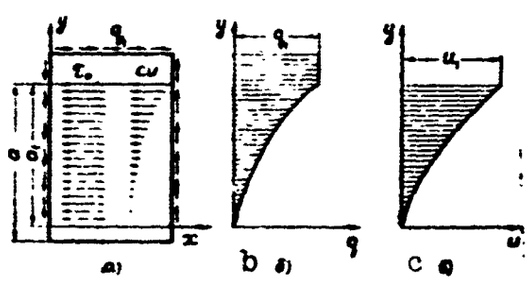

Fig. 102

for y = 0. Under these boundary conditions we will find from (17.6)

and (17.7)

$$A_1 = \frac{2\tau_0}{c}; \qquad B_1 = 0.$$

Consequently, the displacements and tangential forces in the slip region are, during the first loading, determined by the formulas

$$u_{1y} = \frac{2\tau_0}{c}(\operatorname{ch}\beta y - 1), \tag{17.8}$$

$$q_{1y} = \frac{2\tau_0}{\beta}\operatorname{sh}\beta y. \tag{17.9}$$

The diagrams of quantities q_{1y} and u_{1y} are shown in Fig. 102b and c. For $y = a_1$ the tangential forces $q_{1y} = q_1$. From this condition and from Formula (17.9) we can find the width a_1 of the slip zone:

$$\operatorname{sh}\beta a_1 = \frac{\beta q_1}{2\tau_0}. \tag{17.10}$$

In particular, the displacement of the upper edge of the contact region will be determined from (17.8) if we set $y = a_1$. We will get

$$u_1 = \frac{2\tau_0}{c}(\operatorname{ch}\beta a_1 - 1). \tag{17.11}$$

For $a_1 = a$ the slip will spread to the entire width of the contact surface. We subsequently assume that the load coefficient $\alpha = 1$ corresponds to this case.

Let us now consider the unloading stage, when the force in the web changes from q_1 to q_2. As the load decreases, slip will occur in a direction opposite to that of the loading stage. This slip will also start from the top and will spread downward. For q_2 the width of the reverse slip zone will be a_2 (Fig. 103a). Dependencies (17.6) and (17.7) remain valid in the reverse slip zone, it is only necessary to change the sign of τ_0, i.e.,

$$\begin{aligned} u_{2y} &= A_2 \operatorname{ch}\beta y + B_2 \operatorname{sh}\beta y + \frac{2\tau_0}{c}, \\ q_{2y} &= \beta G\delta (A_2 \operatorname{sh}\beta y + B_2 \operatorname{ch}\beta y). \end{aligned} \tag{17.13}$$

In these equalities $a_1 - a_2 \leq y \leq a_1$.

The constants of integration A_2 and B_2 are determined from the conditions that the displacements are $u_{2y} = u_{1y}$ and the tangential forces $q_{2y} = q_{1y}$ at the edge $y = a_1 - a_2$ separating the first and second slip zones. Performing the necessary calculations, we will get

$$A_2 = \frac{2\tau_0}{c}[1 - 2\operatorname{ch}\beta(a_1 - a_2)],$$
$$B_2 = \frac{4\tau_0}{c}\operatorname{sh}\beta(a_1 - a_2). \tag{17.14}$$

Consequently, in the reverse slip zone

$$u_{2y} = \frac{2\tau_0}{c}[1 + \operatorname{ch}\beta y - 2\operatorname{ch}\beta(a_1 - a_2 - y)], \tag{17.15}$$

$$q_{2y} = \frac{2\tau_0}{c}[\operatorname{sh}\beta y + 2\operatorname{sh}\beta(a_1 - a_2 - y)]. \tag{17.16}$$

The width a_2 of the reverse slip zone will be found from (17.16) and the condition that $q_{2y} = q_{02}$ [sic] for $y = a_1$. Taking into account Equality (17.10), this gives

$$\operatorname{sh}\beta a_2 = \frac{1}{2}\left(\operatorname{sh}\beta a_1 - \frac{\beta q_2}{2\tau_0}\right) = \frac{\beta(q_1 - q_2)}{4\tau_0}. \tag{17.17}$$

If $a_2 = a$, then reverse slip will embrace the entire width of the contact region. $\alpha = -1$ corresponds to this case.

The displacement of the upper edge of the contact region, where $y = a_1$, during the unloading stage, will be

$$u_1 = \frac{2\tau_0}{c}(1 + \operatorname{ch}\beta a_1 - 2\operatorname{ch}\beta a_2). \tag{17.18}$$

As can be seen, on full unloading, when $q_2 = 0$, the system does not return to its original state. The residual displacements at the upper edge will be

$$u_1(0) = \frac{2\tau_0}{c}\left(1 + \operatorname{ch}\beta a_1 - 2\sqrt{1 + \frac{\beta^2 q_{01}^2}{16\tau_0^2}}\right).$$

Let the load, having reached a certain smallest value, for which

the force in the web is equal to q_2, begin to increase anew. Together with the increase in the load slip of the web will occur in the same direction as during the first loading. Referring to Fig. 100b, this slip, starting from the top, will spread downward, When the force in the web reaches a certain value q_3 the width of slip reaches the value a_3 (Fig. 104a).

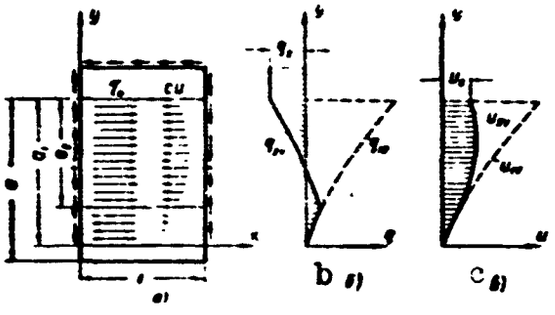

Fig. 103

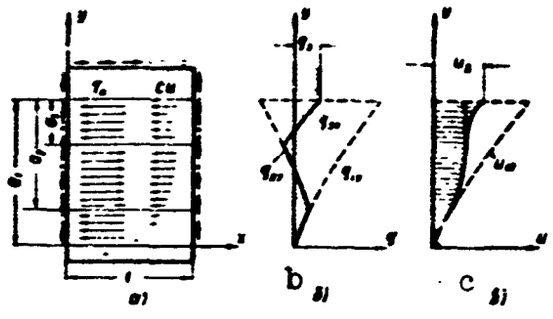

Fig. 104

Dependencies (17.5) and (17.6) remain valid in the secondary slip zone, i.e.,

$$u_{3y} = A_3 \operatorname{ch} \beta y + B_3 \operatorname{sh} \beta y - \frac{2\tau_0}{c},$$

$$q_{3y} = \beta G \delta (A_3 \operatorname{sh} \beta y + B_3 \operatorname{ch} \beta y).$$

Constants A_3 and B_3 will be found from the conditions that $u_{2y} = u_{3y}$ and $q_{2y} = q_{3y}$ for $y = a_1 - a_3$. Performing the necessary calculations, we will find

$$A_3 = \frac{2\tau_0}{c} [1 + 2 \operatorname{ch} \beta (a_1 - a_3) - 2 \operatorname{ch} \beta (a_1 - a_2)],$$

$$B_3 = \frac{4\tau_0}{c} [\operatorname{sh} \beta (a_1 - a_2) - \operatorname{sh} \beta (a_2 - a_3)].$$

Then the displacements and the forces in the web sections in the zone $y \geq a_1 - a_3$ will be

$$u_{3y} = \frac{2\tau_0}{c} [-1 + \operatorname{ch} \beta y + 2 \operatorname{ch} \beta (a_1 - a_2 - y) - 2 \operatorname{ch} \beta (a_1 - a_2 - y)], \qquad (17.19)$$

$$q_{3y} = \frac{2\tau_0}{\beta} [\operatorname{sh} \beta y - 2 \operatorname{sh} \beta (a_1 - a_2 - y) + 2 \operatorname{sh} \beta (a_1 - a_2 - y)]. \qquad (17.20)$$

Diagrams of the quantities q_{3y} and u_{3y} are shown in Fig. 104b and c. These same figures show the character of the force and displacements distributions in the slip zone, when the tangential forces in the web vary within the limits $q_1 > q_3 > q_2$.

The width a_3 of the secondary slip zone will be found from the condition that $q_{3y} = q_3$ for $y = a_1$. Utilizing Equalities (17.10) and (17.17), we will get

$$\operatorname{sh} \beta a_3 = \frac{\beta (q_3 - q_2)}{4\tau_0}. \qquad (17.21)$$

The displacements at the upper edge of the contact region ($y = a_1$) are determined by the formula

$$u_3 = \frac{2\tau_0}{e}(-1 + \operatorname{ch} \beta a_1 + 2 \operatorname{ch} \beta a_3 - 2 \operatorname{ch} \beta a_2). \qquad (17.22)$$

It can be easily seen that for $a_3 = 0$ Equality (17.22) coincides with (17.15). If $a_3 = a_2$ then the reverse slip zone disappears and Equality (17.8) is obtained from (17.22).

A hysteresis loop the area of which is proprotional to the energy irreversibly absorbed by unit seam element during one loading cycle is presented in Fig. 105. The displacements of the upper edge of the contact region are laid off on the abscissa axis and the load coefficient α – on the ordinate axis. Curve 1 corresponds to the first loading and represents Dependence (17.11), curve 2 corresponds to the unloading stage and Equality (17.18), curve 3 describes the displacements on the renewed loading stage, determined by Formula (17.22).

The energy absorbed by unit seam element during one loading cycle, when the load coefficient varies between the limits $r \leq \alpha \leq 1$, is calculated by the formula

$$\Psi = \frac{P}{H} \int_r^1 (u_2 - u_3)\, d\alpha.$$

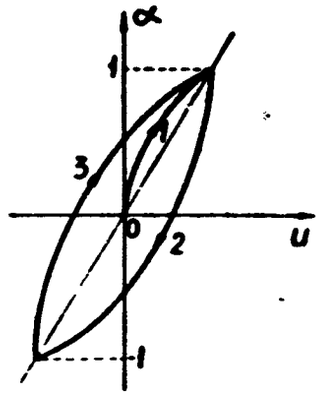

Fig. 105

Substituting here u_2 from (17.11) and u_3 from (17.22) and performing the necessary calculations, we will get:

$$\Psi_1 = \frac{16\tau_*^2}{\beta^2 G\delta}\left\{\gamma P_* - \ln\left[\gamma P_* + \sqrt{1+\gamma^2 P_*^2}\right]\right\}, \quad (17.23)$$

where

$$\gamma = \frac{\beta}{2\tau_* H}. \quad (17.24$$

Energy absorbed by a seam element of length l_{sh} will be obtained by multiplying Ψ_1 by l_{sh}.

Manuscript Page No.

[List of Transliterated Symbols]

140 ИМАШ АН СССР = IMASh AN SSSR = USSR Academy of Sciences Institute of Machine Building

Chapter 6

THREADED AND SLOTTED JOINTS

§18. THE ELEMENTARY PROBLEM

In order to analyze the energy dissipation attendant to the loading of a threaded joint, it is first necessary to consider the following auxiliary problem. A thin disk, bounded by two parallel planes and two conic surfaces (Fig. 106), is loaded by a system of normal stresses σ_x and $\sigma_x + \Delta\sigma_x$, uniformly distributed along the disk base.

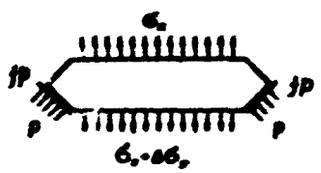

Fig. 106

The following simplified assumptions will be utilized in the subsequent analysis of the deformations and displacements; their convenience and nature will become clear below, when we will speak about the deformation of a bank of similar disks. We shall assume that the disk is pressed only to the lower conical rim surface; the normal reactions p and the tangential frictional forces fp, which are assumed to be uniformly distributed along the entire bearing surface, arise along this surface. We shall further assume that the disk does not bend and, therefore, disk bases which were plane before loading will remain plane also after loading. Finally, we shall assume that the system of support reactions results in compression of the disk in the radial direction constant along its entire thickness; it is understood that the normal stresses, given at the disk base, will also exert an influence on this compression.

Reactions p are determined from the condition of equilibrium of the entire disk

$$p = \frac{\Delta\sigma_x}{\Delta x} \frac{2r_0}{tg\beta + f}, \qquad (18.1)$$

where r_0 is the mean radius of the tapered surface of the disk. The average stress along the disk thickness, σ_r, amounts to

$$\sigma_r = -\frac{1}{2} p (1 - f \operatorname{tg} \beta). \tag{18.2}$$

Let us now find the disk's radial deformation, caused both by the stress σ_r as well as by the stress σ_x:

$$\varepsilon_r = \frac{\sigma_r (1-\mu)}{E} - \frac{\mu \sigma_x}{E} = -\frac{p (1 - f \operatorname{tg} \beta)(1-\mu)}{2E} - \frac{\mu \sigma_x}{E}. \tag{18.3}$$

The mean radius of the disk changes as a result of the radial deformation; the absolute value of this change

$$\Delta r_0 = -\varepsilon_r r_0 = \frac{p r_0 (1 - f \operatorname{tg} \beta)(1-\mu)}{2E} + \frac{\mu r_0 \sigma_x}{E}. \tag{18.4}$$

This lessening of the disk radius, in turn, is the factor causing the disk to be displaced in the direction of the x-axis:

$$u = \frac{\Delta r_0}{\operatorname{tg} \beta} = \frac{p r_0 (1 - f \operatorname{tg} \beta)(1-\mu)}{2E \operatorname{tg} \beta} + \frac{\mu r_0 \sigma_x}{E \operatorname{tg} \beta}. \tag{18.5}$$

It should be noted that the displacement of the disk depends on the value of σ_x (the second component), as well as on the value of $\Delta\sigma_x$ (the first component), in the terms of which the pressure p is expressed in accordance with Formula (18.1).

Let us now consider the disk's unloading process. The beginning of this process is quite unique. As soon as the external load on the disk begins to decrease, a decrease of the frictional forces along the bearing surface will also occur. Since the new values of the frictional forces are smaller than the limiting value fp, slip of the disk becomes impossible and rigid coupling of the disk with the rim will occur. The change of external forces during this loading stage is not accompanied by any displacements of the disk. This is shown in Fig. 107. The frictional forces are here smaller than the limiting value fp and are related to the reactions p by the condition of con-

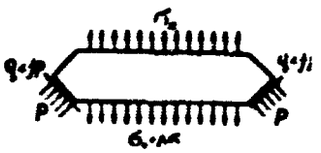

Fig. 107

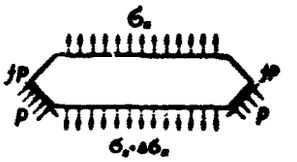

Fig. 108

stancy of the disk's radial deformation.

As the load is decreased, the frictional forces will also decrease, change their sign and, finally, will again reach their limiting value fp, which will signal the beginning of reverse slip; the loads on the disk during this new stage are shown in Fig. 108. The following group of expressions, replacing Relationships (18.1) – (18.5) of the first loading stage, corresponds to this stage:

$$p = \frac{\Delta\sigma_z}{\Delta x} \cdot \frac{r_0}{\operatorname{tg}\beta - f}; \tag{18.6}$$

$$\sigma_r = -\frac{p}{2}(1 + f\operatorname{tg}\beta); \tag{18.7}$$

$$\varepsilon_r = -\frac{p(1 + f\operatorname{tg}\beta)(1-\mu)}{2E} - \frac{\mu\sigma_z}{E}; \tag{18.8}$$

$$\Delta r_0 = \frac{pr_0(1 + f\operatorname{tg}\beta)(1-\mu)}{2E} + \frac{\mu r_0\sigma_z}{E}; \tag{18.9}$$

$$u = \frac{pr_0(1 + f\operatorname{tg}\beta)(1-\mu)}{2E\operatorname{tg}\beta} + \frac{\mu r_0\sigma_z}{E\operatorname{tg}\beta}. \tag{18.10}$$

The expressions presented above can be obtained from Relationships (18.1) – (18.5) by simple change of signs of the friction coefficient f.

Having solved this elementary problem, we can pass on to the solution of the basic problem of the present section about energy dissipation in a threaded joint (Fig. 109). This joint can be regarded as an ensemble of a large number of disks, situated in an elastic rim nut; here each disk will represent a simplified schematic of one turn

of the bolt thread. For a quite large number of turns it is natural to make a limit transition and to regard the threading as consisting of an infinitely large number of infinitesimally thin disks: this approach has received widespread application in threaded joint calculations (see, for example, the Reference by I.A. Birger [3])*. For the sake of simplification of our calculations we will assume that the nut is completely rigid, which will make it possible to most clearly expose all the substantial peculiarities of the problem's solution. The case when the elasticity of the bolt, as well as the nut, is taken into account is considered in Article [15].

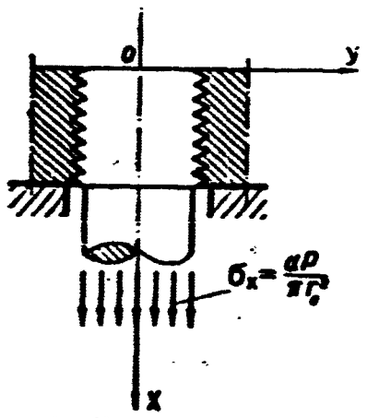

Fig. 109

Making a limit transition, we will obtain instead of (18.1)

$$p = \frac{d\sigma_z}{dx}\frac{r_0}{\operatorname{tg}\beta + f}. \qquad (18.11)$$

Tnen Expression (18.5) will take on the form

$$u = \frac{r_0^2(1 - f\operatorname{tg}\beta)(1-\mu)\sigma_z'}{2E\operatorname{tg}\beta(\operatorname{tg}\beta + f)} + \frac{\mu r_0 \sigma_z}{E\operatorname{tg}\beta}. \qquad (18.12)$$

Correspondingly, the derivative of u in respect to x is

$$u' = \frac{r_0^2(1 - f\operatorname{tg}\beta)(1-\mu)\sigma_z''}{2E\operatorname{tg}\beta(\operatorname{tg}\beta + f)} + \frac{\mu r_0 \sigma_z'}{E\operatorname{tg}\beta}. \qquad (18.13)$$

On the other hand, we should also have

$$u' = \varepsilon_z = \frac{\sigma_z}{E} - \frac{2\mu\sigma_r}{E} = \frac{\sigma_z}{E} + \frac{\mu p(1 - f\operatorname{tg}\beta)}{E} = \frac{\sigma_z}{E} + \frac{\mu r_0(1 - f\operatorname{tg}\beta)\sigma_z'}{E(\operatorname{tg}\beta + f)}. \qquad (18.14)$$

Equating (18.13) and (18.14) we will obtain the fundamental equation of the problem for the first loading stage:

$$\sigma_z'' + a\sigma_z' - b\sigma_z = 0. \qquad (18.15)$$

The notations used here are:

$$a = -\frac{2\mu f(1+\operatorname{tg}^2\beta)}{r_0(1-f\operatorname{tg}\beta)(1-\mu)}, \tag{18.16}$$

$$b = -\frac{2\operatorname{tg}\beta(\operatorname{tg}\beta+f)}{r_0^2(1-f\operatorname{tg}\beta)(1-\mu)}. \tag{18.17}$$

The solution of this equation, subjected to the boundary conditions

$$\sigma_x = 0 \quad \text{for} \quad x = 0,$$

$$\sigma_x = \frac{\alpha P}{\pi r_0^2} \quad \text{for} \quad x = H,$$

has the form

$$\sigma_x = \frac{\alpha P}{\pi r_0^2}\frac{e^{-\frac{ax}{2}}\operatorname{sh}\frac{x}{2}\sqrt{a^2+4b}}{e^{-\frac{aH}{2}}\operatorname{sh}\frac{H}{2}\sqrt{a^2+4b}}. \tag{18.18}$$

Substituting (18.18) into Expression (18.12) and then setting x = H, we will find the displacement of the end section as a function of the applied force

$$u = \frac{\alpha P}{\pi E\operatorname{tg}\beta}\left[\frac{(1-f\operatorname{tg}\beta)(1-\mu)}{4(\operatorname{tg}\beta+f)}\left(\frac{\sqrt{a^2+4b}}{\operatorname{tg}\frac{H}{2}\sqrt{a^2+4b}}-a\right)+\frac{\mu}{r_0}\right]. \tag{18.19}$$

Expression (18.19) describes the joint's loading process; this process is illustrated by the straight line 1 in Fig. 110. The displacement u at the beginning of the loading process remains constant up to the time when the frictional forces change sign and reach the limiting value fp (see segment 2 in Fig. 110). The subsequent process will be described by new equations, which can be obtained as before by a limit transition in Expressions (18.6) and (18.10). We will then obtain the previous Expression (18.15), but with different values of the coefficients

$$a_1 = -\frac{2\mu f(1+\operatorname{tg}^2\beta)}{r_0(1+f\operatorname{tg}\beta)(1-\mu)}, \tag{18.20}$$

$$b_1 = \frac{2\operatorname{tg}\beta(\operatorname{tg}\beta-f)}{r_0^2(1+f\operatorname{tg}\beta)(1-\mu)}. \tag{18.21}$$

These expressions can be obtained directly from Relationships (18.16) and (18.17) by changing the sign of the friction coefficient f. Continuing further in the same manner, we will arrive at a new expression for u which differs from (18.19) only by the sign of f. Ray 3 in Fig. 110 illustrates the last stage of the loading process. The triangular hysteresis loop, formed by segments 1, 2 and 3, pertains to a pulsating cycle. The area of this loop is equal to

$$\Psi = \frac{P^2\mu}{2\pi E r_0 \operatorname{tg}\beta}\,|1 + m(f)|\cdot\left[1 - \frac{1 + m(f)}{1 + n(f)}\right]. \qquad (18.22)$$

where

$$m(f) = \frac{r_0(1 - f\operatorname{tg}\beta)(1-\mu)}{\mu(4\operatorname{tg}\beta + f)}\left(\frac{\sqrt{a^2+4b}}{\operatorname{tg}\frac{H}{2}\sqrt{a^2+4b}} - a\right).$$

$$n(f) = \frac{r_0(1 + f\operatorname{tg}\beta)(1-\mu)}{\mu(4\operatorname{tg}\beta + f)}\left(\frac{\sqrt{a_1^2+4b_1}}{\operatorname{tg}\frac{H}{2}\sqrt{a_1^2+4b_1^2}} - a_1\right). \qquad (18.23)$$

The center line in Fig. 110 corresponds to the case when no hysteresis losses exist in the system.

Consideration of a cycle with any other asymmetry characteristic will not present any fundamental difficulty.

§19. THREADED JOINTS

The preceding section was devoted to the consideration of a simplified scheme of a threaded joint, with the nut regarded as absolutely rigid. Here we consider typical threaded joints and we take into account the finite rigidity of the nut. Figure 111 shows three schemes of threaded joints: bolt – nut, bolt – turnbuckle and bolt – sleeve. The most widespread type of a threaded joint is the bolt – nut joint (see Fig. 111a), and we shall therefore clarify the peculiarities of the cyclical loading process of a threaded joint with triangular threads on an example of this joint type.

The displacement of an infitesimally thin disk can be determined if limit transition is performed in Expression (18.6) of the preceding

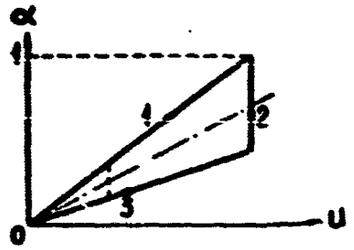

Fig. 110

section, i.e., if expression $\Delta\sigma_{1x}/\Delta x$ is replaced by its derivative $d\sigma_{1x}/dx$. This approach, obviously, does not make it possible to take into account the effect of the local bending deformation of the thread profile on the force distribution between the threads.

After limit transition is performed, the displacement of the bolt section which is removed from the origin of coordinates by the distance $\underline{x}$ (Fig. 112), for the loading stage, can be determined by a formula, following from (18.12):

$$u = \left(\frac{\mu_1\sigma_{1x}}{E_1} + \frac{\mu_2\sigma_{2x}}{E_2}\right)\frac{r_0}{\operatorname{tg}\beta} - \frac{r_0^2 mk}{2\operatorname{tg}\beta}\frac{d\sigma_{1x}}{dx}, \qquad (19.1)$$

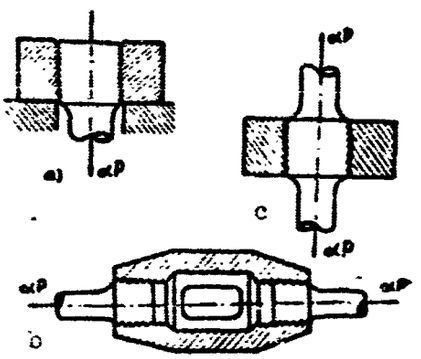

Fig. 111

where $m = \frac{f\sin\beta - \cos\beta}{f\cos\beta + \sin\beta}$, $k = \frac{1-\mu_1}{E_1}$, σ_{1x} and σ_{2x} are the normal stresses in the $\underline{x}$ section of the bolt and the nut, μ_1, μ_2, E_1 and E_2 are constants of the bolt and nut materials and r_0 is the mean radius of the thread.

The normal forces in the bolt and nut sections will be equal, respectively, to $\sigma_{1x}F_1$ and $\sigma_{2x}F_2$. We find from the condition of equilibrium of that part of the joint situated between the origin of coordinates and the given section, that

$$\sigma_{1x}F_1 = \sigma_{2x}F_2. \qquad (19.2)$$

Expressing the cross-sectional areas of the bolt and the nut in terms of the known thread diameters and of the equivalent nut diameter, we will obtain a relationship between the stresses in the bolt and nut sections in the form

$$\sigma_{2x} = \frac{r_0^2}{r_0^2 - r_0^2}\sigma_{1x}, \qquad (19.3)$$

where r_e is the equivalent nut radius. Relationship (19.1) for the loading stage will now take on the form

$$u = \frac{r_0 l}{\operatorname{tg}\beta}\sigma_{1z} - \frac{r_0^2 km}{2\operatorname{tg}\beta}\frac{d\sigma_{1z}}{dx}, \qquad (19.4)$$

where

$$l = \frac{\mu_1}{E_1} + \frac{r_0^2}{r_0^2 - r_0^2}\frac{\mu_2}{E_2}.$$

The displacement of this section for the unloading stage will be determined by the formula

$$u = \frac{r_0 l}{\operatorname{tg}\beta}\sigma_{1z} - \frac{r_0^2 kn}{2\operatorname{tg}\beta}\frac{d\sigma_{1z}}{dx}, \qquad (19.5)$$

where

$$n = \frac{f\sin\beta + \cos\beta}{f\cos\beta - \sin\beta}.$$

The above expressions for u should be transformed in such a manner as to obtain the dependencies of the displacement on the current value of the load αP, which are of interest to us. For this it is necessary to take into account the fact that relationship

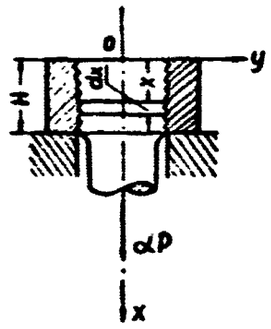

Fig. 112

$$\varepsilon_{1z} = \frac{\sigma_{1z}}{E_1} - 2\sigma_r\frac{\mu_1}{E_1}. \qquad (19.6)$$

where

$$\sigma_r = p(f\sin\beta - \cos\beta) = \frac{1}{2}r_0 m\frac{d\sigma_z x}{dx}. \qquad (19.7)$$

exists between the stresses and the longitudinal deformation of the bolt.

Keeping in mind that $\varepsilon_{1x} = du/dx$, we will obtain, according to (19.4), for the loading stage

$$\varepsilon_{1z} = \frac{r_0 l}{\operatorname{tg}\beta}\frac{d\sigma_{1z}}{dx} - \frac{r_0^2 km}{2\operatorname{tg}\beta}\frac{d^2\sigma_{1z}}{dx^2}.$$

Replacing now σ_r in the right-hand side of (19.6) by its expression (19.7), we will, after limit transition, obtain the basic equation of the problem for the loading stage

$$\sigma_x'' - a\sigma_x' + b\,\varepsilon_x = 0, \tag{19.8}$$

where

$$a = \frac{2\,(lE_1 + \mu_1 m \operatorname{tg}\beta)}{mlr_0E_1}, \quad b = \frac{2\operatorname{tg}\beta}{ml r_0^2 E_1}. \tag{19.9}$$

Under the boundary conditions $\sigma_x(0) = 0, \sigma_x(l) = \frac{\alpha P}{\pi r_0^2}$ the solution of this equation will take on the form

$$\sigma_x(x) = \frac{\alpha P}{\pi r_0^2} \cdot \frac{e^{-\frac{ax}{2}} \operatorname{sh} \frac{x}{2}\sqrt{a^2+4b}}{e^{-\frac{aH}{2}} \operatorname{sh} \frac{H}{2}\sqrt{a^2+4b}}. \tag{19.10}$$

Here H is the length of the engaged parts of the bolt and the nut threads (the height of the nut). Relationship (19.10) determines the normal stress distribution along the bolt sections during the loading process. It should be noted that this distribution is substantially dependent on the friction coefficient f; this circumstance is important not only in the determination of hysteresis losses, but also in strength calculations of threaded joints.

Utilizing (19.4) and (19.10), we will obtain the displacement of any section as a function of the load:

$$u(x,x) = \alpha P \frac{mk}{4\pi \operatorname{tg}\beta} \frac{\left(a \operatorname{sh}\frac{x}{2}\sqrt{a^2+4b} - \sqrt{a^2-4b}\operatorname{ch}\frac{x}{2}\sqrt{a^2+4b}\right)e^{-\frac{ax}{2}}}{e^{-\frac{aH}{2}} \operatorname{sh}\frac{H}{2}\sqrt{a^2+4b}} + \\ + \alpha P \frac{l}{\pi r_0 \operatorname{tg}\beta} \frac{e^{-\frac{ax}{2}} \operatorname{sh}\frac{x}{2}\sqrt{a^2+4b}}{e^{-\frac{aH}{2}} \operatorname{sh}\frac{H}{2}\sqrt{a^2+4b}}. \tag{19.11}$$

Substituting here x = H, we will find the dependence of the displacement of the section to which the load is applied on the dimensionless load

parameter in which we are interested:

$$u(\alpha, H) = \frac{\alpha P k m}{4\pi \operatorname{tg}\beta}\left(a - \sqrt{a^2+4b}\operatorname{ctg}\frac{H}{2}\sqrt{a^2+4b}\right) + \frac{\alpha P l}{\pi r_0 \operatorname{tg}\beta} \qquad (19.12)$$

Let us note that the displacement of the section $x = 0$, to which no load is applied, is not equal to zero, i.e., $u(\alpha, 0) \neq 0$. This means that, for any as small as desired value of the load, the bolt and nut interaction is realized simultaneously along the entire length of the engaged part of the thread.

The basic solution of this problem for the unloading stage, when reverse slip between the thread turns appears, can be obtained from Eq. (19.8) by changing the sign of the friction coefficient f. The coefficients of the new equation

$$c = \frac{2(lE_1 + \mu_1 n \operatorname{tg}\beta)}{E_1 n r_0 k}, \qquad d = \frac{2\operatorname{tg}\beta}{r_0^2 E_1 n k}. \qquad (19.13)$$

The dependence of the displacement on the loading for this stage

$$u(r, x) = \alpha P \frac{nk}{4\pi \operatorname{tg}\beta} \frac{\left(c \operatorname{sh}\frac{x}{2}\sqrt{c^2+4d} - \sqrt{c^2+4d}\operatorname{ch}\frac{x}{2}\sqrt{c^2+4d}\right)e^{-\frac{cx}{2}}}{e^{-\frac{cH}{2}}\operatorname{sh}\frac{H}{2}\sqrt{c^2+4d}} +$$

$$+ \alpha P \frac{l}{\pi r_0 \operatorname{tg}\beta} \frac{e^{-\frac{cx}{2}}\operatorname{sh}\frac{x}{2}\sqrt{c^2+4d}}{e^{-\frac{cH}{2}}\operatorname{sh}\frac{H}{2}\sqrt{c^2+4d}}. \qquad (19.14)$$

The displacement of the bolt's end section with the coordinate $x = H$ (the load is applied to this section) is determined by the formula

$$u(\alpha, H) = \frac{\alpha P n k}{4\pi \operatorname{tg}\beta}\left(c - \sqrt{c^2+4d}\operatorname{cth}\frac{H}{2}\sqrt{c^2+4d}\right) + \frac{\alpha P l}{\pi r_0 \operatorname{tg}\beta}. \qquad (19.15)$$

The displacement of section $x = H$ when the bolt is loaded by a pulsating load is thus described by three different analytic expressions:

1) by Dependence (19.12) during loading;

2) by the dependence u(α, H) = const immediately after the commencement of unloading, as long as rigid coupling between the bolt and nut threading takes place;

3) by Dependence (19.15) in the subsequent unloading stage. The graph of this dependence coincides with that presented in Fig. 110. It can be seen from this figure that the shape of the hysteresis loop is triangular; the area of the loop is equal to:

$$\Psi = \frac{P^2}{4\pi r_0^2 \operatorname{tg}\beta}\left[nkr_0\sqrt{c^2+4d}\operatorname{ctg}\frac{H}{2}\sqrt{c^2+4d} - \right.$$
$$\left. - mkr_0\sqrt{a^2+4b}\operatorname{ctg}\frac{H}{2}\sqrt{a^2+4b} - \frac{2f\mu_1\operatorname{tg}\beta}{E_1(\sin^2\beta - f^2\cos^2\beta)}\right] \times$$
$$\times \frac{kmr_0\sqrt{a^2+4b}\operatorname{cth}\frac{H}{2}\sqrt{a^2+4b} + \frac{\mu_1}{E_1}m\operatorname{tg}\beta + l}{knr_0\sqrt{c^2+4d}\operatorname{cth}\frac{H}{2}\sqrt{c^2+4d} + \frac{\mu_1}{E_1}n\operatorname{tg}\beta + l}. \qquad (19.16)$$

The hysteresis loop for a cycle with the arbitrary characteristic $r = P_{min}/P_{max}$ has the form of a trapezoid. The commencement of the renewed loading is accompanied by rigid coupling of the thread turns along the contact surface; therefore the beginning of this stage on the force – displacement graph (see Fig. 110) also appears as a vertical segment (dashed line). The area of the hysteresis loop is determined by the formula

$$\Psi = \frac{A}{B}P^2(B^2 - r^2). \qquad (19.17)$$

where

$$A = \frac{k}{4\pi\operatorname{tg}\beta}\left(n\sqrt{c^2+4d}\operatorname{cth}\frac{H}{2}\sqrt{c^2+4d} - \right.$$
$$\left. - m\sqrt{a^2+4b}\operatorname{cth}\frac{H}{2}\sqrt{a^2+4b} + ma - nc\right), \qquad (19.18)$$
$$B = \frac{m\sqrt{a^2+4b}\operatorname{cth}\frac{H}{2}\sqrt{a^2+4b} - am + \frac{2l}{kr_0}}{n\sqrt{c^2+4d}\operatorname{cth}\frac{H}{2}\sqrt{c^2+4d} - cn + \frac{2l}{kr_0}}.$$

The dependence of the area of the hysteresis loop on the friction coefficient f for a pulsating cycle is shown in Fig. 113.

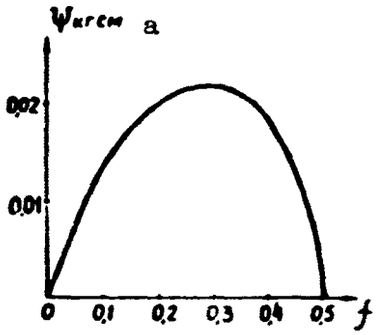

Fig. 113. a) Kg-cm.

The calculations were performed for a steel bolt with an M20 metric thread for a nut of normal height. The maximal value of the load was taken as being P = 1000 kg. It can be seen from the graph that there exists an optimal value of the friction coefficient for which the energy dissipation is greatest. There is little dissipation for small values of f, since the frictional forces are not great; jamming of the threads (rigid coupling) takes place for large values of the friction coefficient.

The bolt – turnbuckle nut joint is another type of a threaded joint. The schematic of the bolt – turnbuckle nut joint is shown in Fig. 114. The bolt and the turnbuckle nut expand under the action of the load. The condition for the equilibrium of that part of the joint which is situated between the origin of coordinates and the given section will, in this case, be written in the form

$$F_1\sigma_{1x} + F_2\sigma_{2x} = \alpha P, \qquad (19.19)$$

where $F_1\sigma_{1x}$ and $F_2\sigma_{2x}$, respectively, are the normal forces in the bolt and turnbuckle nut sections.

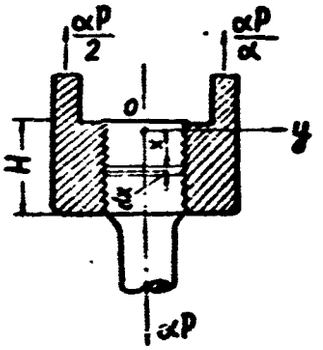

Fig. 114

The equilibrium condition (19.19) makes it possible to establish a relationship between the stresses σ_{1x} and σ_{2x}. Expressing the areas in terms of the mean thread diameter and the equivalent turnbuckle nut radius, we will get

$$\sigma_{2x} = \frac{\alpha P - \pi r_0^2 \sigma_{1x}}{\pi (r_*^2 - r_0^2)}. \qquad (19.20)$$

The basic solution of the problem for the loading stage is written also in the form of (19.8), however; the equation's coefficients should be calculated by the formulas

$$a = \frac{2}{r_0 mk}\left(\frac{\mu_1}{E_1}\frac{\sin 2\beta + f\cos 2\beta}{(f\cos\beta + \sin\beta)\cos\beta} - \frac{\mu_2}{E_2}\frac{r_0^2}{r_e^2 - r_0^2}\right);\ b = \frac{2\operatorname{tg}\beta}{E_1 k m r_0^2}. \qquad (19.21)$$

These coefficients can be obtained for the unloading stage by a simple change of the sign of friction coefficient f. The solution of Eq. (19.8), satisfying the boundary conditions

$$\sigma_{1x}(0) = 0 \text{ and } \sigma_{1x}(H) = \frac{\alpha P}{\pi r_0^2},$$

is written in the form of (19.10).

Utilizing (19.4), it is not too difficult to set up an expression for the displacement of an arbitrary section

$$u(\alpha, x) =$$

$$= \frac{\alpha P}{4\pi\operatorname{tg}\beta}\frac{e^{-\frac{ax}{2}}\left(a\operatorname{sh}\frac{x}{2}\sqrt{a^2+4b} - \sqrt{a^2+4b}\operatorname{ch}\frac{x}{2}\sqrt{a^2+4b}\right)}{e^{-\frac{aH}{2}}\operatorname{sh}\frac{H}{2}\sqrt{a^2+4b}} +$$

where

$$+ \frac{\alpha P r_0 \mu_2}{\pi E_2 (r_e^2 - r_0^2)\operatorname{tg}\beta} + \frac{\alpha P s}{\pi r_e \operatorname{tg}\beta}\frac{e^{-\frac{ax}{2}}\operatorname{sh}\frac{x}{2}\sqrt{a^2+4b}}{e^{-\frac{aH}{2}}\operatorname{sh}\frac{H}{2}\sqrt{a^2+4b}}, \qquad (19.22)$$

$$s = \frac{u_1}{E_1} - \frac{r_0^2}{r_e^2 - r_0^2}\frac{\mu_2}{E_2}.$$

The displacement of the end section to which the load is applied

$$u(\alpha, H) = \frac{\alpha P m k}{4\pi\operatorname{tg}\beta}\left(a - \sqrt{a^2+4b}\operatorname{cth}\frac{H}{2}\sqrt{a^2+4b}\right) +$$
$$+ \frac{\alpha P r_0 \mu_2}{\pi E_2 (r_e^2 - r_0^2)\operatorname{tg}\beta} + \frac{\alpha P s}{\pi r_e \operatorname{tg}\beta}. \qquad (19.23)$$

The hysteresis loop for cyclical loading with a cycle having an arbitrary characteristic has the shape of a trapezoid, the sides of which are formed by two ray segments and two inclined segments parallel to one another (Fig. 115). The parallel segments correspond to the initial phases of the loading and secondary loading cycles, when rigid

coupling occurs at the contact surfaces. We disregard the inclination of the parallel segments in the calculation of the hysteresis loop area, and then the area of the trapezoid LQRS is determined by Formula (19.17), in which coefficients A and B are expressed by the following formulas:

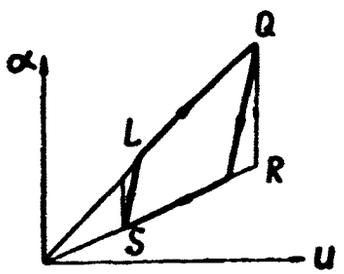

Fig. 115

$$A=\frac{1}{4\pi r_0 \operatorname{tg}\beta}\left[r_0 nk\sqrt{c^2+4d}\operatorname{cth}\frac{H}{2}\sqrt{c^2+4d}-\right.$$

$$\left.-r_0 mk\sqrt{a^2+4b}\operatorname{cth}\frac{H}{2}\sqrt{a^2+4b}-\frac{2\mu_1 f\operatorname{tg}\beta}{E_1(\sin^2\beta-f^2\cos^2\beta)}\right]; \quad (19.24)$$

$$B=\frac{r_0 mk\sqrt{a^2+4b}\operatorname{cth}\frac{H}{2}\sqrt{a^2+4b}+\frac{\mu_2}{E_2}\frac{r_0^2}{r_0^2-r_0^2}+\frac{\mu_1}{E_1}\frac{f}{(\sin\beta+f\cos\beta)\cos\beta}}{r_0 nk\sqrt{c^2+4d}\operatorname{cth}\frac{H}{2}\sqrt{c^2+4d}+\frac{\mu_2}{E_2}\frac{r_0^2}{r_0^2-r_0^2}-\frac{\mu_1}{E_1}\frac{f}{(\sin\beta-f\cos\beta)\cos\beta}}. \quad (19.25)$$

The bolt – sleeve joint is illustrated in Fig. 116. The bolt expands under the action of the external load and the sleeve expands with it. The computational scheme of this joint is similar to that of the bolt – turnbuckle nut scheme; however, certain substantial peculiarities do appear in the dissipation-characteristic calculation for this joint. The basic equation of the problem is written in the form of (19.8); the coefficients of the sought function and its derivatives are determined by Formulas (19.21). The solution of the basic equation for the boundary conditions

$$\sigma_{1z}(0)=-\frac{\alpha P}{\pi r_0^2},$$

$$\sigma_{1z}(2H)=\frac{\alpha P}{\pi r_0^2}$$

has the form

$$\sigma_{1z}=De^{-\frac{\alpha z}{2}}\operatorname{sh}\left(\frac{z}{2}\sqrt{a^2+4b}+\varphi\right). \quad (19.26)$$

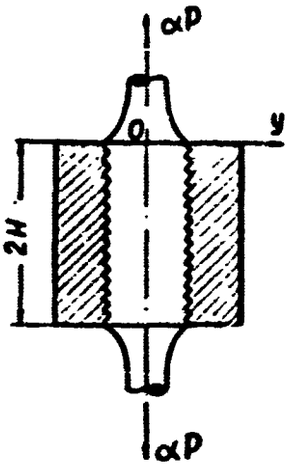

Fig. 116

Constants D and φ for the loading stage are determined by formulas

$$D = \frac{\alpha P}{\pi r_0^2} \frac{\sqrt{e^{2Ha} + 2e^{Ha} \operatorname{ch} H\sqrt{a^2 + 4b} + 1}}{\operatorname{sh} H\sqrt{a^2 + 4b}},$$

$$\operatorname{sh} \varphi = -\frac{\operatorname{sh} H\sqrt{a^2 + 4b}}{\sqrt{e^{2Ha} + 2e^{Ha} \operatorname{ch} H\sqrt{a^2 + 4b} + 1}}. \qquad (19.27)$$

and the coefficients a and b – by Formulas (19.21). Formulas (19.27) for the unloading stage are obtained by replacing f with – f.

Now, on the basis of (19.4) it is not difficult to obtain the dependence of the displacement on the load

$$u(\alpha, x) = -\frac{\pi l r_0^2 D}{4 \operatorname{tg} \beta} \left[\sqrt{a^2 + 4b} \operatorname{ch}\left(\frac{x}{2}\sqrt{a^2 + 4b} + \varphi\right) - a \operatorname{sh}\left(\frac{x}{2}\sqrt{a^2 + 4b} + \varphi\right)\right] e^{-\frac{ax}{2}} + \frac{\alpha P r_0 \mu_2}{E_2 (r_0^2 - r_0^2) \operatorname{tg} \beta} + \frac{D r_0 s}{\operatorname{tg} \beta} e^{-\frac{ax}{2}} \operatorname{sh}\left(\frac{x}{2}\sqrt{a^2 + 4b} + \varphi\right). \qquad (19.28)$$

Relative displacement of bolt sections situated on the planes of the nut ends, u = u(α, 2H) – u(α, 0) will be determined for the loading stage by formula

$$u = \frac{2\alpha P s}{\pi r_0 \operatorname{tg} \beta} + \frac{\alpha P k m}{2\pi \operatorname{tg} \beta}\left(a + \frac{\sqrt{a^2 + 4b} \operatorname{sh} Ha}{\operatorname{sh} H\sqrt{a^2 + 4b}}\right). \qquad (19.29)$$

and for the unloading stage – by formula

$$v = \frac{2\alpha P s}{\pi r_0 \operatorname{tg} \beta} + \frac{\alpha P l n}{2\pi \operatorname{tg} \beta}\left(c + \frac{\sqrt{c^2 + 4d} \operatorname{sh} Hc}{\operatorname{sh} H\sqrt{c^2 + 4d}}\right). \qquad (19.30)$$

The hysteresis loop for a bolt and sleeve loaded by a cyclical load with an arbitrary cycle characteristic has the shape of a trapezoid (see Fig. 115). The area of the hysteresis loop is determined by (19.17); however, constants A and B have new values:

$$A = \frac{1}{2\pi r_0 \operatorname{tg}\beta}\left[\frac{mkr_0\sqrt{a^2+4b}\,\operatorname{sh}Ha}{\operatorname{sh}H\sqrt{a^2+4b}} - \frac{nkr_0\sqrt{c^2+4d}\,\operatorname{sh}Hc}{\operatorname{sh}H\sqrt{c^2+4d}} \quad \frac{2\mu_1 f\operatorname{tg}\beta}{E_1(\sin^2\beta - f^2\cos^2\beta)}\right] \tag{19.31}$$

$$B = \frac{\dfrac{mkr_0\sqrt{a^2+4b}\operatorname{sh}Ha}{\operatorname{sh}H\sqrt{a^2+4b}} + \dfrac{\mu_2 r_0^2}{E_2(r_*^2 - r_0^2)} - \dfrac{\mu_1 f}{E_1(\sin\beta + f\cos\beta)\cos\beta}}{\dfrac{nkr_0\sqrt{c^2+4d}\operatorname{sh}Hc}{\operatorname{sh}H\sqrt{c^2+4d}} + \dfrac{\mu_2 r_0^2}{E_2(r_*^2 - r_0^2)} + \dfrac{\mu_1 f}{E_1(\sin\beta - f\cos\beta)\cos\beta}}. \tag{19.32}$$

Formula (19.17) for the area of the hysteresis loop, for the corresponding values of quantities A and B entering it, determines the intensity of structural damping per cycle in the above three types of threaded joints.

§20. SLOTTED CONNECTIONS

(a simplified system)

The problem of energy dissipation in slotted joints arises, for example, in conjunction with vibrations of turbine buckets with an attachment of the "fir-tree" type (Fig. 117); similar joints are used in fastening of gas and steam turbine buckets and also for fastening of axial compressor buckets. We shall subsequently consider the problem of a bucket attachment acted upon by a variable bending moment only. It is assumed for the sake of simplification that longitudinal forces are absent. It is obvious that this consideration can provide us with only the most general theoretical basis for the calculation of energy dissipation in actual turbine bucket attachments. Let us consider the following auxiliary problem. A thin plate, rectangular in plan, with side dimensions 2a x b and thickness Δx is loaded along planes parallel to the median plane by stresses σ_x and $\sigma_x + \Delta\sigma_x$, independent of the

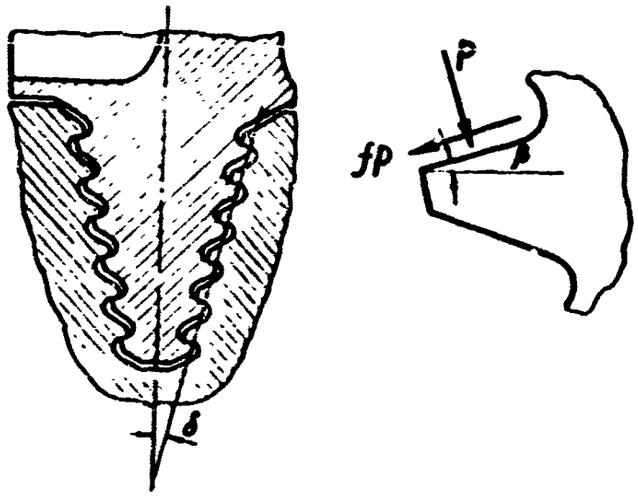

Fig. 117

z-coordinate and varying linearly along the y-axis. This stress system is statically equivalent to two couples with moments M_x and $M_x + \Delta M_x$. The plate is supported on two absolutely rigid bearing surfaces along its two side faces, parallel to the z-axis; these faces form an angle

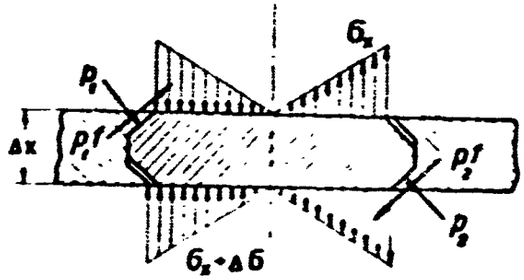

Fig. 118

β with the median surface. The two other sides of the plate are not loaded (Fig. 118). Normal reactions p_1 and p_2 and also tangential frictional forces $p_1 f$ and $p_2 f$, uniformly distributed along the bearing surfaces, will arise on the bearing surfaces. It follows from the conditions of equilibrium that $p_1 = p_2$; consequently, the limiting frictional forces are also equal. We shall assume that surfaces of the plate, plane before the load has been applied, remain plane also under the action of the external forces and that the system of the support reactions results in an uniform compression of the plate in the direction

of the y-axis; deformation of the plate in the direction of the z-axis is taken as equal to 0. It is obvious that stresses on the end surfaces of the plate also exert an influence on the plate's deformation.

Reactions p are determined from the condition that the plate is in equilibrium and are equal to

$$p = \frac{1}{2ab(\cos\beta - f\sin\beta)} \frac{\Delta M}{\Delta x}. \tag{20.1}$$

The limiting frictional force T at the support surfaces has the units of a force per unit length of the loop contour, and is equal to

$$T = fp = \frac{f}{2ab(\cos\beta - f\sin\beta)} \frac{\Delta M}{\Delta x}. \tag{20.2}$$

Average stresses σ_y along the plate thickness amount to

$$\sigma_y = \frac{\operatorname{tg}\beta - f}{2ab(1 - f\operatorname{tg}\beta)} \cdot \frac{\Delta M}{\Delta x}. \tag{20.3}$$

Average stresses σ_z along the plate thickness are determined by Hooke's law from the condition $\varepsilon_z = 0$. Then the relative deformation ε_y brought about by the stress components σ_x, σ_y and σ_z will be determined by the formula

$$\varepsilon_y = \frac{1}{E}[\sigma_y(1-\mu^2) - \mu(1+\mu)\sigma_x], \tag{20.4}$$

where E and μ are the modulus of elasticity and Poisson's ratio for the plate material.

The absolute deformation of the plate in the direction of the y-axis is influenced only by the stresses σ_y; therefore

$$\Delta a = \int_{-a}^{+a} \varepsilon_y\, dy = \frac{1-\mu^2}{bE} \cdot \frac{\operatorname{tg}\beta - f}{1 - f\operatorname{tg}\beta} \cdot \frac{\Delta M}{\Delta x}. \tag{20.5}$$

As a result of the fact that the plate is compressed in the direction of the y-axis it becomes possible for the plate to turn relative to the base as a rigid body. Slip over bearing surfaces between the

plate and the base occurs during this rotation.

The angle of rotation of the median plane of the plate on loading is determined by the formula

$$\varphi = \frac{\operatorname{tg}\beta}{a}\Delta a = \frac{1-\mu^2}{E}\cdot\frac{\operatorname{tg}\beta - f}{2ab(1-f\operatorname{tg}\beta)}\cdot\frac{\Delta M}{\Delta x}. \qquad (20.6)$$

Let us note that this angle depends only on the increment of the bending moment and is independent of its absolute value.

Let us now consider the unloading process, the commencement of which is quite peculiar: as soon as the external load applied to the plate begins to decrease, a decrease in the pressure at the bearing surface takes place and the limiting value of the frictional forces is decreased. However, the actual value of the frictional force during the beginning of unloading still remains smaller than the limiting [value] fp; this makes it impossible for slip to occur, since rigid coupling between the plate and the base takes place. The change in external forces during this unloading stage is not accompanied by any displacements of the plate.

As the load is further decreased, the actual value of the frictional forces becomes equal to the limiting and slip again begins on the bearing surfaces. Slip and frictional forces have directions opposite to those which they had during the loading stage. The following group of expressions corresponds to the plate's unloading during this new stage under consideration:

$$p = \frac{1}{2ab(\cos\beta + f\sin\beta)}\frac{\Delta M}{\Delta x}, \qquad (20.7)$$

$$\tau_y = \frac{\operatorname{tg}\beta + f}{2ab(1 + f\operatorname{tg}\beta)}\frac{\Delta M}{\Delta x}, \qquad (20.8)$$

$$\varphi_p = \frac{1-\mu^2}{2abE}\cdot\frac{\operatorname{tg}\beta + f}{(1 + f\operatorname{tg}\beta)}\cdot\frac{\Delta M}{\Delta x}. \qquad (20.9)$$

The beginning of the new loading is again accompanied by rigid

coupling. Only after the actual value of the frictional force will become equal to the limiting and slip will again appear on the bearing surfaces will the loading process be accompanied by rotation of the plate. All the stages of this process are repeated successively with a cyclically varying load.

In solving the problem of energy dissipation in a slotted joint of the "fir tree" joint type it is natural to consider the slotted root as an assembly of plates. In the case of a sufficiently large number of small plates it is natural to consider the joint as consisting of infinitely large number of infinitesimally thin plates. This approach has come into widespread use in threaded-joint calculations and was already utilized by us in §§ 18 and 19.

For the sake of simplicity, let us first consider a slotted joint in which the root constitutes an elastic prismatic body and the base is absolutely rigid. Making a limit transition, we will obtain instead of (20.1)

$$p = \frac{1}{2ab\,(\cos\beta - f\sin\beta)} \cdot \frac{dM}{dx}. \qquad (20.10)$$

where a and b are the dimensions of the root cross section, M is the bending moment in section x and E and μ are the modulus of elasticity and Poisson's ratio of the root material.

As a result of the limit transition, Expression (20.6) will take on the form

$$\varphi = \frac{1-\mu^2}{E} \cdot \frac{\operatorname{tg}\beta - f}{2ab\,(1 - f\operatorname{tg}\beta)} \cdot \frac{dM}{dx}, \qquad (20.11)$$

where φ is the angle of rotation of the current root section. The moment M is related to the angle φ by the known relationship

$$\frac{d\varphi}{dx} = \frac{M(x)}{EJ}, \qquad (20.12)$$

where J is the moment of inertia of the root section. After differentiation of (20.11) in respect to x and substitution of the derivative into (20.12), we will obtain an equation for the moment M

$$\frac{d^2M}{dx^2} - \lambda^2 M = 0, \tag{20.13}$$

where

$$\lambda^2 = \frac{2nb(1 - f\operatorname{tg}\beta)}{J(1-\mu^2)(\operatorname{tg}\beta - f)}. \tag{20.14}$$

The solution of Eq. (20.13), subjected to the boundary conditions

$$\begin{aligned} M(x) &= \alpha M \quad \text{for } x = 0, \\ M(x) &= 0 \quad \text{for } x = h, \end{aligned} \tag{20.15}$$

(h is the root length), has the form

$$M(x, \alpha) = \frac{\operatorname{sh}\lambda(h-x)}{\operatorname{sh}\lambda h}\alpha M. \tag{20.16}$$

Taking a derivative of M(x, α) in respect to x, substituting it into (20.11) and then setting x = 0, we will obtain the angle of rotation of the initial root section during the loading stage

$$\varphi_1(0, \alpha) = \frac{(1-\mu^2)\lambda}{2Eab} \cdot \frac{\operatorname{tg}\beta - f}{1 - f\operatorname{tg}\beta} \operatorname{cth}\lambda h \alpha M. \tag{20.17}$$

Rigid coupling between the root slots and the mating base takes place during the beginning of the loading phase, and therefore the root sections do not rotate, i.e.,

$$\varphi_2(0, \alpha) = \frac{(1-\mu^2)\lambda}{2Eab} \cdot \frac{\operatorname{tg}\beta - f}{1 - f\operatorname{tg}\beta} \operatorname{cth}\lambda h M.$$

The angle of rotation of the first root section after slip has begun anew will be obtained from Expression (20.17) by a simple change of the friction coefficient f and by replacement of the constant λ by ω.

$$\varphi_2(0, \alpha) = \frac{(1-\mu^2)\omega}{2Eab} \cdot \frac{\operatorname{tg}\beta + f}{1 + f\operatorname{tg}\beta} \operatorname{ctn}\omega h \alpha M. \tag{20.18}$$

where

$$\omega^2 = \frac{2ab(1 + f\,\mathrm{tg}\,\beta)}{J(\mathrm{tg}\,\beta + f)(1 - \mu^2)}. \qquad (20.19)$$

The loading and unloading process is illustrated in Fig. 110 by rays 1, 2 and 3.

The area of the hysteresis loop for a pulsating cycle is determined by the formula

$$\Psi = \frac{M^2(1 - \mu^2)\lambda}{4Eab} \cdot \frac{\mathrm{tg}\,\beta - f}{1 - f\,\mathrm{tg}\,\beta} \mathrm{cth}\,\lambda h \left[1 - \frac{\lambda(\mathrm{tg}\,\beta - f)(1 + f\,\mathrm{tg}\,\beta)\,\mathrm{cth}\,\lambda h}{\omega(1 - f\,\mathrm{tg}\,\beta)(\mathrm{tg}\,\beta + f)\,\mathrm{cth}\,\omega h}\right]. \qquad (20.20)$$

§21. A SLOTTED ATTACHMENT OF THE "FIR-TREE" TYPE

Having solved the simplified system, let us pass on to the consideration of the problem of energy dissipation in turbine bucket root attachments. Of all the different forms of slotted root joints we will consider only multi-slotted joints of the "fir-tree" type with the slots having a straight axis. The consideration of slotted joints with a curvilinear axis is more complex, but possible in principle. The design of a fir-tree attachment involves the idea of strength equality. The profile of the slots (see Fig. 117) is similar to the profile of bearing threads and the contour of the root has the shape of a wedge (the vertex angle of the wedge, 2σ [sic], varies in actual turbine bucket designs between the limits 25 – 40°).

Let us consider a bucket root element, formed by two parallel planes normal to the longitudinal root axis and removed from one another by the distance dx.

The differential relationship between the normal pressure p on the element's bearing surface and the current bending moment M(x) has the form of Dependence (20.10) of the preceding section (a and b are the dimensions of the root section), here a(x) depends on the coordinate

of the section and is determined by the dependence

$$a(x) = (H - x)\operatorname{tg}\delta, \tag{21.1}$$

where H is the height of the root wedge (see Fig. 119) and 2δ is the vertex angle of the wedge. The absolute deformation of the bucket root element is determined by the formula

$$\Delta a_a = \frac{1-\mu_a^2}{bE_a} \cdot \frac{\operatorname{tg}\beta - f}{1 - f\operatorname{tg}\beta} \cdot \frac{dM}{dx}, \tag{21.2}$$

where E_1 and μ_1 are the elastic characteristics of the root material and M is the bending moment in the root section.

The angular displacement of an element of the bucket attachment depends not only on the root deformation but also on the deformation of the turbine runner with which it is mated. Regarding a single projection on the runner as a reversed bucket root, loaded by an external bending moment αM in the root section, we will determine the absolute deformation of an element of the projection by a formula similar to (21.2):

$$\Delta c = \frac{1-\mu_a^2}{bE_a} \times \times \frac{\operatorname{tg}\beta - f}{1 - f\operatorname{tg}\beta} \cdot \frac{dM}{dx}, \tag{21.3}$$

where E_d and μ_d are the elastic constants of the disk material and $2c$ is the width of the current element of the rotor's projection. The relationship between the quantity $c(x)$ and the design dimensions of the attachment has the form

$$c(x) = l - (H - x)\operatorname{tg}\delta.$$

where $2l$ is the spacing at which the buckets are seated along the runner circumference.

The bending moment in the section of the rotor's projection is determined by the formula

$$M_x(x) = aM - M(x). \qquad (21.4)$$

The angle of rotation of a bucket element is determined by the formula

$$\varphi(x, a) = \frac{\Delta a - \Delta c}{a(x)} \qquad (21.5)$$

or

$$\varphi(x, a) = \frac{(\operatorname{tg}\beta - f)\operatorname{tg}\beta}{2a(x)\,b\,(1 - f\operatorname{tg}\beta)} \cdot \left(\frac{1-\mu_x^2}{E_x} + \frac{c(x)}{a(x)} \cdot \frac{1-\mu_x^2}{E_x}\right)\frac{dM}{dx}. \qquad (21.6)$$

If we assume that the differential relationship (20.12) is valid for a wedge-shaped bucket root subject to bending, then we will find the dependence for the change of the bending moment along the root length, which is of interest to us. However, in the utilization of Relationship (20.12) we should keep in mind that the moment of inertia J of the wedge-shaped root depends on the x-coordinate. Differentiating (21.6) once in respect to x, and substituting the value of dφ/dx into (20.12), we will obtain the differential equation

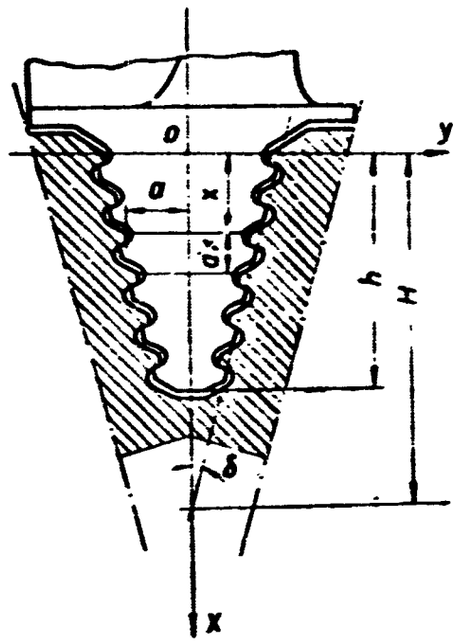

Fig. 119

$$z\left[\frac{1-\mu_3^2}{E_3} + \frac{1-\mu_x^2}{E_x}(l-a)\right]\frac{d^2M}{dz^2} - \left[\frac{1-\mu_3^2}{E_3} + \frac{1-\mu_x^2}{E_x}(2l-z)\right] \cdot \frac{dM}{dz} = \frac{3(1-f\operatorname{tg}\beta)M}{E_x \operatorname{tg}^2\beta(\operatorname{tg}\beta - f)\operatorname{tg}\beta}. \qquad (21.7)$$

into which the new independent variable

$$z = a = (H - x)\operatorname{tg}\delta. \qquad (21.8)$$

has been introduced. The just obtained equation can be solved by classical methods. However, of practical interest is the case when the elastic properties characteristics of the rotor and bucket materials are

the same, $E_1 = E_d$ and $\mu_1 = \mu_d$. Equation (21.7) is considerably simplified in this case and is transformed to the form

$$z\frac{d^2M}{dz^2} + 2\frac{dM}{dz} - \lambda M = 0, \tag{21.9}$$

where

$$\lambda = -\frac{3(1 - f\operatorname{tg}\beta)}{\mu^2\delta\operatorname{tg}\rho(\operatorname{tg}\beta - f)(1 - \mu^2)l}.$$

The general solution of the last equation will be written in the form

$$M = z^{-\frac{1}{2}}\left[C_1 I_3(2\sqrt{\lambda z}) + C_2 K_3(2\sqrt{\lambda z})\right], \tag{21.10}$$

where I_3 and K_3 are the Bessel functions of the imaginary argument and C_1 and C_2 are constants of integration which will be determined from the boundary conditions

$$M(z) = \alpha M \quad \text{for } z = H\operatorname{tg}\delta, \tag{21.11}$$

$$M(z) = 0 \quad \text{for } z = (H - h)\operatorname{tg}\delta$$

in the form

$$C_1 = \frac{(H\operatorname{tg}\delta)^{-\frac{3}{2}} K_3(2\sqrt{\lambda(H-h)\operatorname{tg}\delta})\,\alpha M}{I_3(2\sqrt{\lambda H\operatorname{tg}\delta})K_3(2\sqrt{\lambda(H-h)\operatorname{tg}\delta}) - I_3(2\sqrt{\lambda(H-h)\operatorname{tg}\delta})K_3(2\sqrt{\lambda H\operatorname{tg}\delta})}$$

$$C_2 = \frac{-(H\operatorname{tg}\delta)^{-\frac{3}{2}} I_3(2\sqrt{\lambda(H-h)\operatorname{tg}\delta})\,\alpha M}{I_3(2\sqrt{\lambda H\operatorname{tg}\delta})K_3(2\sqrt{\lambda(H-h)\operatorname{tg}\delta}) - I_3(2\sqrt{\lambda(H-h)\operatorname{tg}\delta})K_3(2\sqrt{\lambda H\operatorname{tg}\delta})} \tag{21.12}$$

The angle of rotation of the current section x is, on the basis of Expression (21.6) determined by the formula

$$\varphi_1(x, \alpha) = \frac{1 - \mu^2 E(\operatorname{tg}\rho - f)\operatorname{tg}\rho}{2Ea(x)b(1 - f\operatorname{tg}\rho)} \cdot \frac{c(x) + a(x)}{a(x)}\frac{dM}{dx}, \tag{21.13}$$

and the angle of rotation of the first section — by the formula

$$\varphi_1(0, \alpha) = \frac{(1 - \mu^2)l}{2bH^2\operatorname{tg}^2\delta} \cdot \frac{(\operatorname{tg}\beta - f)\operatorname{tg}\rho}{(1 - f\operatorname{tg}\beta)}\left.\frac{dM}{dx}\right|_{x=0}, \tag{21.14}$$

where

$$\left.\frac{dM}{dx}\right|_{x=0} = -3\operatorname{tg}\delta\sqrt{H\operatorname{tg}\delta}\left[C_1 I_3\left(2\sqrt{\lambda H\operatorname{tg}\delta}\right) + C_2 K_3\left(2\sqrt{\lambda H\operatorname{tg}\delta}\right)\right] -$$
$$- H^2\operatorname{tg}^2\delta\sqrt{\lambda}\left[C_1 I_2\left(2\sqrt{\lambda H\operatorname{tg}\delta}\right) - C_2 K_2\left(2\sqrt{\lambda H\operatorname{tg}\delta}\right)\right]. \tag{21.15}$$

Taking into account that constants C_1 and C_2 are determined by Formula (21.12), let us note that the displacement $\varphi(0, \alpha)$ is linearly dependent on the parameter α.

Formula (21.13) establishes a relationship between the external load and the displacement during the loading stage. A similar relationship for the unloading stage will be obtained by simply changing the sign of the friction coefficient f

$$\varphi_2(0, \alpha) = \frac{l(\operatorname{tg}\beta + f)\operatorname{tg}\beta}{2H^2 b\operatorname{tg}^2\delta(1 + f\operatorname{tg}\beta)} \cdot \frac{1-\mu^2}{E}\left.\frac{dM}{dx}\right|_{x=0}, \tag{21.16}$$

where $\left.\frac{dM}{dx}\right|_{x=0}$ has a new value

$$\left.\frac{dM}{dx}\right|_{x=0} = -3\operatorname{tg}\delta\sqrt{H\operatorname{tg}\delta}\left[D_1 I_3\left(2\sqrt{\omega H\operatorname{tg}\delta}\right) + D_2 K_3\left(2\sqrt{\omega H\operatorname{tg}\delta}\right)\right] -$$
$$- H^2\operatorname{tg}^2\delta\sqrt{\omega}\left[D_1 I_2\left(2\sqrt{\omega H\operatorname{tg}\delta}\right) - D_2 K_2\left(2\sqrt{\omega H\operatorname{tg}\delta}\right)\right]; \tag{21.17}$$

here

$$D_1 = \frac{(H\operatorname{tg}\delta)^{-\frac{3}{2}} K_3\left(2\sqrt{\omega(H-h)\operatorname{tg}\delta}\right)\alpha M}{I_3\left(2\sqrt{\omega H\operatorname{tg}\delta}\right)K_3\left(2\sqrt{\omega(H-h)\operatorname{tg}\delta}\right) - I_3\left(2\sqrt{\omega(H-h)\operatorname{tg}\delta}\right)K_3\left(2\sqrt{\omega H\operatorname{tg}\delta}\right)},$$

$$D_2 = \frac{(H\operatorname{tg}\delta)^{-\frac{3}{2}} I_3\left(2\sqrt{\omega(H-h)\operatorname{tg}\delta}\right)\alpha M}{I_3\left(2\sqrt{\omega H\operatorname{tg}\delta}\right)K_3\left(2\sqrt{\omega(H-h)\operatorname{tg}\delta}\right) - I_3\left(2\sqrt{\omega(H-h)\operatorname{tg}\delta}\right)K_3\left(2\sqrt{\omega H\operatorname{tg}\delta}\right)},$$

$$\omega = \frac{3(1 + f\operatorname{tg}\beta)}{\operatorname{tg}^2\delta\operatorname{tg}\beta(\operatorname{tg}\beta + f)l(1-\mu^2)}. \tag{21.18}$$

The loading and unloading process for a pulsating loading cycle is illustrated by rays 1 and 3 (see Fig. 110), the beginning of the unloading process – by segment 2. This stage is characterized by a complete absence of rotation of the section

$$\varphi_2(0, \alpha) = \varphi_1(0, 1).$$

The triangular hysteresis loop formed by segments 1, 2 and 3 pertains to a pulsating cycle. The area of the hysteresis loop is determined by the formula

$$\psi = \frac{1}{2}\varphi_1(0, 1)\left[1 - \alpha\frac{\varphi_1(0, 1)}{\varphi_2(0, \alpha)}\right]. \qquad (21.19)$$

Consideration of a cycle with an arbitrary characteristic does not present any special difficulty.

As a more particular case of the problem we can consider energy dissipation in a bucket attachment with a prismatic root. The displacement of the current section when the root and the runner are made from the same material is determined by the formula

$$\varphi(x, \alpha) = \frac{(1-\mu)^2 l}{2Ea^2 b}\cdot\frac{(\operatorname{tg}\beta - f)\operatorname{tg}\beta}{(1 - f\operatorname{tg}\beta)}\frac{dM}{dx}, \qquad (21.30)$$

where a, b and l are the design dimensions of the joint. The basic solution of the problem will be written in the form of (20.13); however, λ now has the new value

$$\lambda^2 = \frac{2a^2 b}{(1-\mu^2)lJ}\cdot\frac{1 - f\operatorname{tg}\beta}{(\operatorname{tg}\beta - f)\operatorname{tg}\beta}. \qquad (21.21)$$

The general solution of the basic equation subjected to the boundary conditions (20.15) is, for the new value of λ, written in the form of (20.16).

Let us determine the angle of rotation of the first root section, to which the external load is applied. On loading

$$\varphi_1(0, \alpha) = \frac{\lambda l(1-\mu^2)}{2a^2 bE}\cdot\frac{(\operatorname{tg}\beta - f)\operatorname{tg}\beta}{1 - f\operatorname{tg}\beta}\operatorname{cth}\lambda h \cdot \alpha M. \qquad (21.22)$$

The angle of rotation of the same first section during the unloading process is determined by the formula

$$\varphi_2(0, \alpha) = \frac{\omega l(1-\mu^2)}{2a^2 bE}\cdot\frac{(\operatorname{tg}\beta + f)\operatorname{tg}\beta}{1 + f\operatorname{tg}\beta}\operatorname{cth}\omega h \cdot \alpha M. \qquad (21.23)$$

where

$$\omega^2 = \frac{2a^2b}{(1-\mu^2)IJ} \cdot \frac{1+f\operatorname{tg}\beta}{(\operatorname{tg}\beta+f)\operatorname{tg}\beta}.$$

The area of the hysteresis loop of a pulsating cycle is determined by Formula (21.19), into which Expressions (21.21) and (21.23) should be substituted with the corresponding values of the arguments:

$$W = \frac{\lambda l(1-\mu^2)}{4a^2bE} \cdot \frac{(\operatorname{tg}\beta - f)\operatorname{tg}\beta}{1-f\operatorname{tg}\beta} \operatorname{cth}\lambda h \cdot \left(1 - \frac{\lambda}{\omega} \cdot \frac{\operatorname{tg}\beta - f}{1-f\operatorname{tg}\beta} \cdot \frac{1+f\operatorname{tg}\beta}{\operatorname{tg}\beta+f} \cdot \frac{\operatorname{cth}\lambda}{\operatorname{ctn}\omega}\right) M^2. \quad (21.24)$$

After appropriate transformations this formula fully coincides with the similar formula for the hysteresis loop obtained for the case of a rigid base.

[Footnote]

Manuscript Page No.

159 The problem of force distribution along the thread loops was first solved by N.E. Zhukovskiy [5].

Manuscript Page No.

[List of Transliterated Symbols]

162 э = e = ekvivalentnyy = equivalent

178 л = l = lopatka = bucket

178 д = d = disk = disk

CONCLUSION

The entire preceding presentation has solved in substance a series of static problems, devoted to the problem of the operation of elastic-frictional systems. Naturally, the question can be raised as to the degree and manner in which the above results can be applied to the solution of dynamic problems.

To give an answer to this question, let us dwell on the following essential circumstances.

1. The assumed simplified concepts about the nature of forces of dry friction make it possible to assume that energy dissipation attendant to vibrations is independent of the rate of the process. In this sense, the rate of change of external forces acting on the joint becomes indifferent.

2. In all the problems with relatively weak damping (i.e., in those cases when intensive drainage of the hydraulic damper type is absent) energy dissipation plays a noticeable role only in the immediate proximity of resonance. Therefore the consideration of friction losses in joints has a practical sense only in the analysis of resonance modes.

3. The complex problem of the form of forced vibrations of systems with several degrees of freedom for arbitrary periodic disturbances becomes relatively simple, if any of the resonance modes is considered. Actually, here:

a) even when the disturbing force is multi-harmonic it is permissible to take into account only the resonance harmonic; by virtue of the same fact it is possible to consider a single-harmonic vibratory pro-

cess simply assuming all the nonresonance harmonics as being absent; b) the mode of forced vibrations under the above conditions of weak damping can be regarded as coinciding with the mode of free undamped vibrations corresponding to the resonance frequency under consideration.

The above circumstances make it possible to designate the following practical scheme for calculation of resonance amplitude of vibrations for systems with weak damping.*

1. The frequencies and modes of free vibrations of the given system are determined on the assumption that friction losses are absent.

Let, for example X(x), the fundamental function for the case of a vibrating beam, be normalized in such a manner that the deflection of any characteristic section is equal to unity. Then the deflections in the state of greatest deflection of a system performing forced vibrations will be described by the dependence

$$Y = AX(x), \tag{22.1}$$

where A is the amplitude of vibrations of the above section.

2. The work of the disturbing load per one vibratory cycle is determined. If the resonance harmonic of the disturbing force is given in the form

$$P(x, t) = P_0(x) \sin \omega t, \tag{22.2}$$

then the sought work amounts to:

$$W = \pi A \int_0^l P_0(x) X(x)\, dx. \tag{22.3}$$

This expression is a generalization of a formula, determing the work of a concentrated disturbing force

$$P(t) = P_0 \sin \omega t \tag{22.4}$$

on resonance vibrations according to the relationship

$$y(t) = A\cos\omega t \qquad (22.5)$$

($y(t)$ is the displacement of the point of application of force P); as we know, the work of the disturbing force per one vibratory cycle is in this case equal to $\pi P_0 A$.

3. The energy dissipation Ψ in the damping element per one vibratory cycle is determined, but not as a function of the amplitude of the force applied to the element, but of the amplitude of its displacement; the latter is expressed by A and the dependence

$$\Psi = \Psi(A). \qquad (22.6)$$

is thus established.

4. The work of the disturbing load (22.3) is equated to the energy (22.6) and the simple algebraic equation thus obtained is then solved.

The operations by which the resonance amplitude is calculated thus make it unnecessary to formulate and integrate complex nonlinear differential equations; let us note that the nonlinearity inherent to the systems under consideration influences also the recommended order of calculations, but this only in the last stage of solution of the above algebraic equation.

As an elementary problem, let us consider the determination of resonance amplitudes for the Goodman and Klamp problem (§ 5), assuming that a mass m is attached to the end of the cantilever and is so great that it is possible to disregard the mass of the beam proper. Let us assume that a disturbing force $P_0 \sin \omega t$ is applied to this mass. The amplitude of resonance vibrations can be found from the energy balance equation: the work of the external force $\pi P_0 A$ per one cycle is equal to the dissipated energy $\Psi(A)$, which is measured by the area of the hysteresis loop, i.e.,

$$\pi P_0 A = \Psi(A). \qquad (22.7)$$

The area of the hysteresis loop in this equation must be written as a function of the amplitude of the displacement A of the point of application of the external force. For this we shall substitute into Formula (5.17) the expression for P from Formula (5.7); then we will obtain instead of (5.17)

$$\Psi(A) = 4q_0 A - \frac{2q_0^2 k^2 P}{9EJ}, \qquad (22.8)$$

where the quantity A coincides with the quantity $u_2(1)$ in Expression (5.7). Here Eq. (22.7) becomes linear; however, even for nonlinear dependencies $\Psi(A)$, as this takes place in the majority of structural damping problems, the solution does not encounter serious difficulty. Solving Eq. (22.7) for A, we will get

$$A = \frac{2q_0^2 k^2 P}{9EJ(4q_0 k - \pi P_0)}. \qquad (22.9)$$

This expression makes sense only under the condition that the frictional forces are sufficiently great $\left(q_0 k > \frac{\pi}{4} P_0\right)$: in the opposite case the vibratory amplitudes become infinite. This coincides with the known result, according to which dry friction absorbers are capable of limiting the amplitude of resonance vibrations only for sufficiently large frictional forces.

Expression (22.9) also makes possible the determination of the optimal value of compression of beam layers.

It is obvious that the above computation procedure is not always possible. Absorber systems of the tapered rings type, i.e., systems with quite intensive energy dissipation, require a more exact analysis. Luckily, it is namely in these cases that the hysteresis loop is formed by straight line segments and it is possible to perform segment by segment solution, as for separate linear systems, utilizing the [curve]

fitting method.

We shall not dwell on the details of this problem, or on certain other problems of solution of dynamic problems, bearing in mind that the main goal of the present book is to obtain estimates of structural damping in different types of systems, since the unavailability of precisely these estimates has resulted in specific difficulties in the formulation of dynamic problems.

[Footnote]

Manuscript Page No.

185 These recommendations obviously retain their validity also for other cases of weak damping, for example, in problems on vibrations of systems with internal friction in the material.

REFERENCES

1. Babayev, N.N. O vnutrennikh soprotivleniyakh, vosnikayushchikh pri kolebanii korpusa korablya [Internal Resistances Arising in Vibrations of Ship Hulls], Tr. nauchn.-tekhn. soveshchaniya po dempfirovaniyu kolebaniy [Trans. Scientific-Technical Conference on Vibration Damping]. Izd-vo AN Ukr. SSR [Publishing House of the Academy of Sciences UkrSSR], 1960.
2. Biderman, V.L. Raschet listovykh ressor [Calculations for Leaf Springs]. In book entitled: Raschety na prochnost' v mashinostroyenii [Strength Calculations in Machine Building], Vol. I, Under the General Editorship of S.D. Ponomarev, Mashgiz [State Scientific-Technical Press for Machine Construction Literature], 1957.
3. Birger, I.A. Raschet rez'bovykh soyedineniy [Calculations for Threaded Joints]. Oborongiz [State Scientific and Technical Publishing House of the Defense Industry], 1951.
4. Debrivniy, I.Ye. Rozsiyannya yenergiy v stalevikh kanatakh pri asimetrichnomu tsikli napruzhennya [Dissipation of Energy in Steel Cables in an Asymmetric Loading Cycle]. Dopovidi AN URSR [Proc. Acad. Sci. UkrSSR], 1959, 11.
5. Zhukovskiy, N.Ye. Raspredeleniye davleniy mezhdu vitkami [Distribution of Pressure Between Turns]. Complete Collected Works, VIII. Moscow, 1937.
6. Kalinin, N.G. and Lebdev, Yu.A. Konstruktsionnoye dempfirovaniye v tonkostennoy balke [Structural Damping in a Thin-Webbed Beam]. Izv. AN Latv. SSR [Bull. Acad. Sci. Latvian SSR], 1959, 12.

7. Karpachev, N.F. Issledovaniye listovogo torsiona [Investigation of Sheet Torsion]. Collection entitled Raschet na prochnost' elementov konstruktsiy [Strength Calculations for Structural Elements], 11, Mashgiz [State Scientific-Technical Press for Machine Construction Literature], Moscow-Sverdlovsk, 1957.

8. Kats, A.M. Teoriya uprugosti [Elasticity Theory]. GITTL [State Publishing House for Technical and Theoretical Literature], Moscow, 1956.

9. Kovalenko, A.D. Issledovaniye dempfirovaniye pri vibratsii paketov lopatok parovykh trubin [Study of Damping for Vibration of Steam-Turbine Bucket Banks]. Sb. dokladov po dinamicheskoy prochnosti detaley mashin [Collection of Papers on the Dynamic Strength of Machine Parts], Izd-vo AN SSSR [Publishing House of the Academy of Sciences USSR], 1946.

10. Krasavin, I.V. Issledovaniye treniye v ressornom podveshivanii [Study of Friction in a Spring Suspension]. Avtorev. diss. na soisk. uch. st. kand. tekhn. nauk. [Author's Abstract of Dissertation in Competition for Academic Degree of Candidate of Technical Sciences]. Leningradskiy institut inzhenerov zhel.-dor. transporta [Leningrad Institute of Railroad Transportation Engineers], Leningrad, 1956.

11. Lebedev, Yu.A. Konstruktsionnoye dempfirovaniye v zaklepochnykh soyedineniyakh [Structural Damping in Riveted Joints]. Izv. Latv. SSR, 1959, 12.

12. Lebedev, Yu.A. Kharakteristiki dempfirovaniya amortizatorov s kol'tsevymi pruzhinami [Damping Characteristics of Shock Absorbers with Annular Springs]. Collection entitled "Voprosy dinamiki i prochnosti" [Problems of Dynamics and Strength], VI, Izd-vo AN Latv. SSR [Publishing House of the Academy of Sciences of the Lat-

vian SSR], 1959.

13. Lebedeva, V.I. Konstruktsionnoye dempfirovaniya vo friktsionnykh muftakh pri tsiklicheskom nagruzhenii [Structural Damping in Friction Clutches Under Cyclic Loading]. Izv. AN Latv. SSR, 1959, 11.

14. Panovko, Ya.G. Gol'tsev, D.I. and Strakhov, G.I. Elementarnyye zadachi konstruktivnogo gisterezisa [Elementary Problems of Structural Hysteresis]. Collection entitled "Voprosy dinamiki i prochnosti" [Problems of Dynamics and Strength], V, Izd-vo AN Latv. SSR, 1958.

15. Panovko, Ya.G. and Strakhov, G.I. Konstruktsionnoye dempfirovaniye v rez'bovykh soyedineniyakh [Structural Damping in Threaded Joints]. Izv. AN Latv. SSR, 1959, 12.

16. Parkhilovskiy, I.G. Avtomobil'nyye listovyye ressory [Automobile Leaf Springs]. Mashgiz, 1954.

17. Poznyak, E.L. Issledovaniye kolebaniy valov [Study of Shaft Vibrations]. Collection entitled "Problemy prochnosti v mashinostroyenii" [Strength Problems in Machine Building], I, Izd-vo AN SSSR, 1958.

18. Ponomarev, S.D. Rascheti vitykh pruzhin [Calculations for Coil Springs]. In book entitled: Rashcheti na prochnost' v mashinostroyenii [Strength Calculations in Machine Building], I, Under the General Editorship of S.D. Ponomarev, Mashgiz, 1957.

19. Rabinovich, I.M. Nekotoryye soobrazheniya o svyazi mezhdu sostoyaniyem metallicheskogo prcletnogo stroyeniya i ego kolebaniyami [Certain Delibrations on the Relationship Between the State of Metallic Span Structures and Their Vibrations]. 11th sb. otdela inzhenernykh issledovaniy [Eleventh Symposium of the Engineering Research Division], Transpechat' [Administration for the Distribu-

tion and Dispatch of Printed Matter of the State Publishing House for Railroad Transportation Literature (Transzheldorizdat)], Moscow, 1927.

20. Reshetov, D.N. and Levina, Z.M. Dempfirovaniye kolebaniy v soyedineniyakh detaley mashin [Vibration Damping in the Joints of Machine Components]. Vestnik mashinostroyeniya [Herald of Machine Building], 1956, 12.

Reshetov, D.N. and Levina, Z.M. Dempfirovaniye kolebaniy v detalyakh stankov [Vibration Damping in Machine-Tool Components]. Mashgiz, 1958.

Reshetov, D.N. and Levina, Z.M. Vozbuzhdeniye i dempfirovaniye kolebaniy v stankakh [Excitation and Damping of Vibrations in Machine Tools]. Mashgiz, 1958.

21. Soyfer, A.M. O dinamicheskom podobii v nekotorykh mekhanicheskikh dissipativnykh kolebatel'nykh sistemakh [Dynamic Similitude in Certain Dissipative Mechanical Oscillatory Systems]. Tr. Kuybyshevskogo aviatsionnogo instituta [Transactions of the Kuybyshev Aviation Institute], VI, 1958.

22. Soyfer, A.M. Konstruktorskiye zadachi povysheniya nadezhnosti gazoturbinnykh aviatsionnykh dvigateley [Designers' Problems in Improving the Realiability of Aviation Gas-Turbine Engines]. Tr. Kuybyshevskogo aviatsionnogo instituta [Transactions of the Kuybyshev Aviation Institute], VI, 1958.

23. Soyfer, A.M. Izyskaniye metodov konstruktivnogo dempfirovaniya vibratsiy detaley gasoturbinnykh dvigateley [Search for Methods for Structural Damping of Vibration in Gas-Turbine Engine Components], Tr. nauchno-tekhnicheskogo soveshchaniya po izucheniyu rasseyaniya energii pri kolebaniyakh uprugikh tel [Transactions of Scientific-Technical Conference on Dissipation of Energy in Vibrations of

Elastic Bodies]. Izd-vo AN Ukr. SSR, 1958.

24. Soyfer, A.M. and Filekin, V.P. Konstruktivnoye dempfirovaniye kolebaniy tonkostennykh obolochek tipa korpusnykh detaley GTD [Structural Damping of Vibrations of Thin-Walled Shells of the Type Found in Housing Components of Gas-Turbine Engines]. Izv. VUZov MVO SSSR [Bull. Higher Educ. Insts., Ministry of Higher Education of the USSR], 1, series "Aviatsionnaya tekhnika" ["Aviation Engineering"], 1958.

25. Strakhov, G.I. Konstruktsionnyy gisterezis v pressovom soyedinenii pri rastyazhenii - szhatii [Structural Hysteresis in the Press-Fitted Joint Under Tension/Compression]. Izv. AN Latv. SSR, 1958, 5.

26. Strakhov, G.I. Konstruktsionnyy gisterezis v amortizatorakh rezino-metallicheskogo tipa [Structural Hysteresis in Rubber-and Metal Shock Absorbers]. Collection entitled "Voprosy dinamiki i prochnosti" [Problems of Dynamics and Strength], VI, Izd-vo AN Latv. SSR, 1959.

27. Strakhov, G.I. Kharakteristika dempfirovaniya v dvukhlistovoy ressore [Damping Characteristics in the Two-Leaf Spring]. Izv. AN Latv. SSR, 1958, 10.

28. Strakhov, G.I. Prosteyshiye zadachi konstruktsionnogo dempfirovaniya [Elementary Problems of Structural Damping]. Dissertation in Competition for the scholarly degree of Candidate of Technical Sciences, Institut mashinovedeniya AN Latv. SSR [Inst. Mech. Engrg. Acad. Sci. Latvian SSR], 1958.

29. Feodos'yev, V.I. Izbrannye zadachi i voprosy soprotivleniya materialov [Selected Problems and questions in Strength of Materials]. GITTL, Moscow, 1950.

30. Filekin, V.P. Konstruktivnyy gisterezis v sostavnoy balke pri

FTD-TT-63-755/1+2

otsutstvii skol'zheniya na kont'sakh [Structural Damping in a Built-Up Beam in the Absence of Slip at the Contacts]. Izvestiya vysshikh uchebnykh zavedeniy MVO SSSR [Bulletin of the Higher Educational Institutions of the USSR Ministry of Education], Series "Aviatsionnaya tekhnika" ["Aviation Engineering"], 1960, 1.

30a. Chayevskiy, M.I. Vliyaniye gisterezisnykh poter' v mestakh sopryazheniya detaley na ustoychivost' dvizheniya gibkogo vala [Influence of Hysteresis Losses at Mating Points Between Components on Motion Stability of Flexible Shaft]. Nauchn. zap. Instituta mashinovedeniya AN Ukr. SSR [Scientific Notes of the Machine-Building Institute of the Academy of Sciences UkrSSR], 6, 1957.

31. Shapiro, G.A. Rabota zaklepochnykh soyedineniy stal'nykh konstruktsiy [The Work of Riveted Joints in Steel Structures]. Stroyvoyenmorixdat [Publishing House of the Ministry for the Construction of Military and Naval Establishments of the USSR], 1949.

32. Di Taranto, R.A. A Blade-Vibration-Damping Device, Its Testibg and a Preliminary Theory of Its Operation. J. Appl. Mech., 1958, 1.

33. Goodman, L.E. and Klamp, I.H. Analysis of Slip-Damping. J. Appl. Mech., 1956, 3.

34. Kumai, T. Damping Factors in the Higher Modes of Ship Vibration. J. Ship Techn. Soc., Oslo, 1958, VII, 1.

35. Meyer, I. Zur Frage der Blattfederreibung und der gunstigsten Federbreite bei Verwendung mit und ohne Stossdämpfer [Problem of Leaf-Spring Friction and the Optimum Spring Width for Use with and without Shock Absorption]. Automobiltechn. Ztschr. [Automotive Engineering Journal], 1956, 1.

36. Pian, T.H.H. Structural Bending of a Simple Built-Up Beam with

Riveted Joints in Bending. J. Appl. Mech., 1957, 1.

37. Pian, T.H.H. Structural Bending of a Simple Built-Up Beam with Riveted Joints in Bending. Paper, Amer. Soc. Mech. Engrs., 1956, A-2.

38. Pian, T.H.H. and Hallowell, F.C. Structural Damping in a Simple Built-Up Beam. Ir., Proc. First U.S. Nat. Congr. Appl. Mech., ASME, 1952, 97-102.

39. Taylor, I.L. Vibration of Ships. Trans. INA, 1930.

40. Yamada, Yoshikazu On the Vibrational Damping of Structural Steel Beams. Mem. Fac. Engng., Kyoto Univ., 1957, 1.

41. Yu. A. Vibration Damping of Stranded Cable. Proc. Soc. Exp. Stress, Anal., 1952, 9, 2.

42. Structural Damping. Papers Presented at a Colloquium on Structural Damping Held at the ASME Annual Meeting in Atlantic City, N.J., XII, 1959.